Distribution Agreement

In presenting this thesis or dissertation as a partial fulfillment of the requirements for an advanced degree from Emory University, I hereby grant to Emory University and its agents the non-exclusive license to archive, make accessible, and display my thesis or dissertation in whole or in part in all forms of media, now or hereafter known, including display on the world wide web. I understand that I may select some access restrictions as part of the online submission of this thesis or dissertation. I retain all ownership rights to the copyright of the thesis or dissertation. I also retain the right to use in future works (such as articles or books) all or part of this thesis or dissertation.

Signature:

_____ _____

Christopher D. Makinson Date

Role of the Voltage Gated Sodium Channel *Scn8a* in Epilepsy

By

Christopher D. Makinson
Doctor of Philosophy

Graduate Division of Biological and Biomedical Sciences
Neuroscience

Andrew P. Escayg, Ph.D
Advisor

Raymond Dingledine, Ph.D
Committee Member

Ellen Hess, Ph.D
Committee Member

Stephen Traynelis, Ph.D
Committee Member

David Weinshenker, Ph.D
Committee Member

Accepted:

Lisa A. Tedesco, Ph.D.
2013

Role of the Voltage Gated Sodium Channel *Scn8a* in Epilepsy

By

Christopher D. Makinson
B.S., Wake Forest University 2007

Advisor: Andrew P. Escayg, Ph.D

An abstract of
A dissertation submitted to the Faculty of the
James T. Laney School of Graduate Studies of Emory University
in partial fulfillment of the requirements for the degree of
Doctor of Philosophy
Graduate Division of Biological and Biomedical Sciences
Neuroscience
2013

Abstract

Role of the Voltage Gated Sodium Channel *Scn8a* in Epilepsy

By Christopher D. Makinson

Voltage gated sodium channels (VGSCs) are critical regulators of neuronal excitability and synchrony. Alterations in the function of the CNS VGSCs are associated with susceptibility to epilepsy, cognitive impairment, and emotional disturbances. Mice with mutations in the VGSC *Scn8a* exhibit increased resistance to induced seizures; however, interestingly, *Scn8a* mutant mice also experience frequent spontaneous absence seizures. Epilepsy-causing mutations in the human *SCN8A* gene were recently identified but little is currently known about the mechanisms by which altered *SCN8A* function leads to epilepsy, or perhaps can confer seizure protection.

Using genetic approaches we probed the developmental and brain-region dependence of *Scn8a*-mediated seizure protection in order to establish the feasibility of achieving seizure protection by selectively targeting *Scn8a* during adulthood. We assessed induced hippocampal bursting properties throughout postnatal development in *Scn8a* mutant mice. We also established that increased resistance to induced seizures is achieved when *Scn8a* is inactivated in the adult mouse and we further demonstrated that selective targeting of *Scn8a* in the hippocampus via either lentiviral-delivered *Cre* or adeno-associated viral-delivered *Scn8a* shRNA is sufficient to confer seizure resistance.

In order to provide a more complete understanding of the consequences of altering *Scn8a* function, we investigated the seizure, behavioral, and electrophysiological effects of a novel mutation in the *Scn8a* gene, R1627H. Analysis of *Scn8a*-R1627H channels in *Xenopus oocytes* revealed a depolarizing shift in the voltage dependence of activation, increased recovery from inactivation and increased persistent current. To establish the *in vivo* effects of this mutation, it was knocked into the mouse *Scn8a* gene. Interestingly, heterozygous $Scn8a^{RH/+}$ mutants exhibited increased resistance to induced seizures, but this was not observed in homozygous $Scn8a^{RH/RH}$ mutants. $Scn8a^{RH/RH}$ mice were also susceptible to audiogenic seizures and displayed a recessive movement disorder.

Lastly, we propose a cellular mechanism to explain the paradoxical seizure outcomes that arise from loss of *Scn8a* activity. *Scn8a* conditional knockout mice were crossed to cell-type specific *Cre* transgenic lines to selectively delete a floxed *Scn8a* allele. Electrocorticogram (EEG) analysis and seizure thresholds were used to evaluate the contribution of *Scn8a* in different cell types to seizure phenotypes. We found that selective reduction of *Scn8a* expression in excitatory neurons results in increased seizure resistance without the generation of absence seizures. We

were also able to elevate seizure thresholds to normal levels in *Scn1a* mutant mice by reducing *Scn8a* expression in excitatory cells. In contrast, the deletion of *Scn8a* in interneurons leads to spontaneous absence seizures but does not influence seizure thresholds. Furthermore, *Scn8a* immunoreactivity and electrophysiological recordings raise the possibility that *Scn8a* expression in the thalamic reticular nucleus is important for the generation of absence seizures.

In conclusion this work 1) provides fundamental information about the development of *Scn8a*-related seizure phenotypes 2) expands upon the known seizure and behavioral phenotypes associated with altered *Scn8a* function, and 3) identifies critical cell-types mediating increased seizure resistance and absence seizure generation in *Scn8a* mutant animals.

Role of the Voltage Gated Sodium Channel *Scn8a* in Epilepsy

By

Christopher D. Makinson
B.S., Wake Forest University 2007

Advisor: Andrew P. Escayg, Ph.D

A dissertation submitted to the Faculty of the
James T. Laney School of Graduate Studies of Emory University
in partial fulfillment of the requirements for the degree of
Doctor of Philosophy
Graduate Division of Biological and Biomedical Sciences
Neuroscience
2013

Acknowledgements

Completing this dissertation has been an immensely challenging and rewarding endeavor. Without the support of my advisor, my committee members, and my friends and family, the work presented here would not have been possible.

I would especially like to thank my dissertation advisor Dr. Andrew Escayg for his steadfast support. Over the past several years Dr. Escayg has encouraged me to improve in all aspects of graduate studies. Dr. Escayg has pushed me when needed but also has provided the space and freedom necessary for me to develop independent ideas. He has been dedicated to my training and maturation as a scientist and also supportive of my interests outside of the laboratory.

I would like to thank the members of my thesis committee, Raymond Dingledine, Ellen Hess, Stephen Traynelis, and David Weinshenker, for their guidance and support throughout my graduate studies. I am also grateful to the students and faculty of the Neuroscience Graduate Program. It has been a privilege to study and work with such talented individuals.

Lastly, I would like to thank my friends and family for their unwavering support. In particular, I would like to thank my fiancé, Stefanie Ritter. She is one of the most thoughtful and inquisitive scientist and one of the most caring and decent people I have ever met. She has both made me a better scientist and a better person.

Table of Contents

CHAPTER 1: Introduction and Background

Figure Index

Tables

CHAPTER 1

INTRODUCTION AND BACKGROUND

1.1. Voltage Gated Sodium Channel Structure and Function

1.1.A. Overview

Voltage gated sodium channels (VGSCs) mediate the voltage-dependent passage of sodium (Na^+) across cellular membranes. Membrane channels that allow for the voltage-dependant passage of sodium ions were first described in a seminal series of papers by Hodgkin and Huxley on the action potential of the squid giant axon (Hodgkin and Huxley, 1952d, c, a, b). They found that depolarization activates an inward Na^+ current that further depolarizes the cell. This current was found to quickly inactivate, within a few milliseconds, and was followed by an outward K^+ current that repolarizes the cell. The timing and direction of these currents, sodium flowing into the cell followed by potassium flowing out, were found to provide the basis of the action potential. More recently, disruptions in VGSC activity have emerged both as major risk factors in many neurological disorders, and as a targets for the treatment of these disorders.

1.1.B. Molecular Organization of VGSCs

The identification and molecular characterization of VGSCs have been an active subject of research since the discovery of voltage-dependent sodium currents (Hodgkin and Huxley, 1952d). Characteristics of VGSC ion selectivity, gating, and inactivation were intensively studied throughout the 1970s. These experiments established many fundamental principles of VGSC function. Ion selectivity was found to involve Na^+ dehydration through interaction with a selectivity pore followed by rehydration in the luminal space and escape into the larger intracellular environment (Hille, 1971, 1972, 1975). Although Hodgkin and Huxley first proposed the existence of a charged voltage sensing subunit which is coupled to gating of the channel, this principle was established by Armstrong and Bezanilla (Armstrong and Bezanilla, 1973, 1977) using detailed electrophysiological recordings in the squid giant axon in the presence and absence of tetrodotoxin (TTX). Additionally, Armstrong and Bezanilla established basic mechanisms of

VGSC inactivation, including the existence of an intracellular component that moves to block the channel pore and thus ion conduction (inactivation gate) (Armstrong and Bezanilla, 1973, 1977; Bezanilla and Armstrong, 1977) (Figure 1.1).

VGSC proteins were first purified in the laboratory of Dr. William Catterall (Beneski and Catterall, 1980; Tamkun and Catterall, 1981) establishing that these proteins are composed of a large α subunit (260 kDa) associated with smaller β subunits (30-40 kDa) (Figure 1.1). Cloning of the VGSC genes provided important insights into the structure and function of VGSCs. Based on analysis of hydrophobicity and amino-acid sequence, VGSC alpha (α) subunits were predicted to be transmembrane proteins consisting of four homologous domains (DI-IV) arranged around a central ion conduction pore (Noda et al., 1986). Each domain consists of six transmembrane segments (S1-S6) (Noda et al., 1986) (Figure 1.1). The fourth transmembrane segment of each domain serves as a voltage sensor and contains a number of evolutionarily conserved positively charged amino acid residues. Conformational changes of this segment in response to membrane voltage deflections lead to channel transitions from open to closed states (Chanda and Bezanilla, 2002; Goldschen-Ohm et al., 2013) (Figure 1.1). Channel opening triggers a delayed conformational change in the intracellular loop that bridges domain III and IV which inactivates the channel (Catterall, 2000). Recent atomic level resolution, obtained from a crystallized VGSC, revealed previously unidentified interactions with plasma membrane phospholipids, and possible new drug binding targets (Payandeh et al., 2011).

VGSC α subunits complex with one or two beta (β) subunits (Isom et al., 1994; Morgan et al., 2000; Yu et al., 2003). There are five known VGSC β subunits (β1-4 and β1B) (Isom et al., 1992; Isom et al., 1995; Kazen-Gillespie et al., 2000; Morgan et al., 2000; Qin et al., 2003; Yu et al., 2003). The β1B subunit is a secreted protein while the other β subunits are single pass transmembrane glycoproteins (Patino et al., 2011). β1 and β3 subunits bind non-covalently, while β2 and β4 are linked to α subunits via disulfide bonds (Isom et al., 1992; Isom et al., 1995;

Morgan et al., 2000; Yu et al., 2003). β subunits modulate virtually all aspects of VGSC function including voltage dependent gating, kinetics of activation and inactivation, localization to the plasma membrane, and the effects of drugs on the activity of VGSCs (Morgan et al., 2000; Yu et al., 2005; Uebachs et al., 2012; Lacroix et al., 2013; Laedermann et al., 2013).

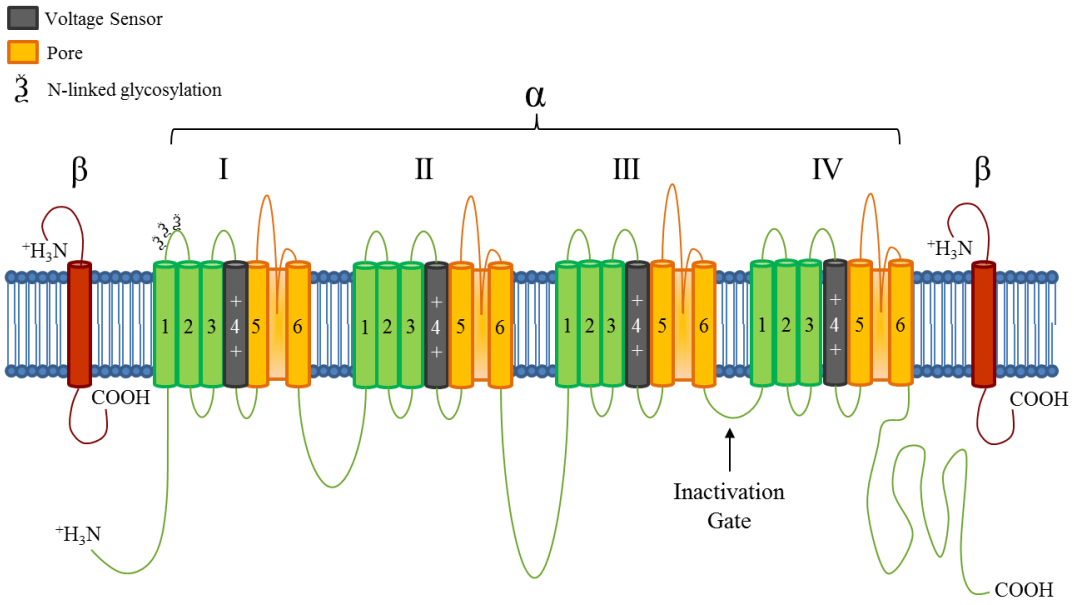

Figure 1.1. Schematic representation of α and β Subunits of a voltage gated sodium channel

VGSC alpha subunits are composed of four domains (I-IV) each consisting of six transmembrane segments. The fourth transmembrane segment of each domain forms the voltage sensor (grey) which contains a large number of positively charged amino-acid residues occurring at every third position. A re-entrant loop between segments 5 and 6 of each domain forms the ion-selectivity filter (yellow). The inactivation gate is formed by the intracellular loop joining domains III and IV. The C- and N- termini are oriented intracellularly. Several N-linked glycosylation sites are located in the extracellular loop spanning segments 1 and 2 of the first domain. β subunits (red) are single-pass transmembrane proteins that influence the activity and localization of VGSCs.

1.2. Genetic Organization of VGSCs

VGSCs are part of an ion channel superfamily that includes structurally, functionally, and genetically similar voltage gated calcium and potassium channels, transient receptor potential (TRP) channels, cyclic nucleotide-gated (CNG), and hyperpolarization-activated cyclic nucleotide-gated (HCN) channels (Yu and Catterall, 2004). The VGSC family of genes is thought to have diverged from ancestral four domain calcium channels (Anderson and Greenberg, 2001; Hille, 2001). The differentiation of VGSCs from calcium channels occurred at about the same time that organisms with specialized neurons appeared (Hille, 2001; Yu and Catterall, 2004). Nine VGSC α subunit genes are expressed in the mammalian genome; *SCN1A*, *SCN2A*, *SCN3A*, *SCN4A*, *SCN5A*, *SCN8A*, *SCN9A*, *SCN10A*, and *SCN11A*, which encode the channel proteins, $Na_v1.1$, $Na_v1.2$, $Na_v1.3$, $Na_v1.4$, $Na_v1.5$, $Na_v1.6$, $Na_v1.7$, $Na_v1.8$, and $Na_v1.9$, respectively (Goldin et al., 2000). Throughout this dissertation the VGSCs will primarily be referred to by their gene names. By convention, human genes are written in uppercase and italics, while non-human gene names are also written in italics but only the first letter is uppercase. *SCN1A*, *SCN2A*, *SCN3A*, and *SCN9A*, are located on chromosome 2 in both humans and rodents. It is likely that *SCN1A*-*SCN3A* arose from duplication events as these channels are clustered and share over 95% amino acid homology. *SCN4A* is located on human chromosome 17 and on rodent chromosome 11. *SCN8A* is located on human chromosome 12 and on rodent chromosome 15. *SCN5A*, *SCN10A*, and *SCN11A* are found on human chromosome 3 and the mouse orthologs are on chromosome 9 (Goldin et al., 2000).

The human β1 gene is found on chromosome 19, while β2 and β3 and β4 are located on human chromosome 11 (Goldin, 2001).

1.3. Distribution of VGSCs

1.3.A. Overview

Of the nine mammalian VGSCs, *SCN1A*, *SCN2A*, *SCN3A*, and *SCN8A* are primarily expressed in the CNS. This section will mainly focus on the expression of the CNS VGSCs, and in particular the rodent *Scn1a* and *Scn8a* genes, as these channels are the major focus of the work presented in this dissertation. However, it is important to appreciate the distinct regional, developmental, cellular, and subcellular expression profiles of the CNS VGSC genes in order to understand the contribution of this gene family to epilepsy.

1.3.B. Distribution of *Scn1a*

In rodents, *Scn1a* is detectable by Western blot analysis and immunocytochemistry after the second postnatal week, reaching adult levels by P24 (Gong et al., 1999). *Scn1a* expression in forebrain interneurons has been extensively demonstrated (Yu et al., 2006; Ogiwara et al., 2007; Dutton et al., 2012; Han et al., 2012b; Papale et al., 2013), with particularly high expression of *Scn1a* in parvalbumin (PV) positive interneurons (Ogiwara et al., 2007). We demonstrated that *Scn1a* colocalizes with inhibitory neuronal markers in the thalamic reticular nucleus, and hypothalamus, as well as serotonergic neurons of the dorsal and median raphe nuclei, cholinergic neurons of the pedunculopontine tegmental nucleus and laterodorsal tegmental nucleus, and orexinergic neurons of the lateral hypothalamus (Papale et al., 2013). *Scn1a* expression has been identified in inhibitory pacemaker neurons of the suprachiasmatic nucleus (Han et al., 2012a). *Scn1a* expression has also been observed in some populations of excitatory hippocampal and cortical neurons (Westenbroek et al., 1989; Yu et al., 2006; Dutton et al., 2012; Ogiwara et al., 2013). We estimate that between 1 and 13% of *Scn1a* positive hippocampal soma colocalize with excitatory cell markers while over 90% of PV cells are *Scn1a* positive (Dutton et al., 2012).

$Na_v1.1$ immunoreactivity has been used to determine the subcellular localization of this channel in the rodent brain. Several studies report abundant somatic expression (Yu et al., 2006; Dutton et al., 2012; Papale et al., 2013) (Fig. 1.2.*A*). Additionally, *Scn1a* is expressed at the axon initial segment (AIS) of PV positive interneurons (Ogiwara et al., 2007) and is specifically enriched at the proximal AIS (Van Wart et al., 2007; Duflocq et al., 2008; Lorincz and Nusser, 2008), raising the possibility that *Scn1a* is important for backpropagation. Expression at the nodes of Ranvier has also been reported, implicating $Na_v1.1$ in axonal conduction (Duflocq et al., 2008) (Fig. 1.2.*A*).

1.3.C. Distribution of *Scn8a*

Scn8a is the most abundant and broadly expressed VGSC gene in the mammalian CNS. Low levels of $Na_v1.6$ channel are detectable by P15 but increasing expression is observed from P20 reaching adult levels by P30 (Liao et al., 2010b).

Scn8a immunoreactivity has been identified at the soma of hippocampal neurons (Blumenfeld et al., 2009), however, most reports have found enrichment of *Scn8a* at the AIS (Lorincz and Nusser, 2008; Feng et al., 2013; Sun et al., 2013) and nodes of Ranvier (Caldwell et al., 2000). Dendritic *Scn8a* expression was also identified, implicating this channel in the propagation of dendritic sodium currents (Lorincz and Nusser, 2010) (Fig. 1.2.*B*).

Scn8a is expressed in almost 90% of ankryn-G positive AISs (Osorio et al., 2010) and at most nodes (Caldwell et al., 2000). *Scn8a* is most highly expressed at the distal AIS, which is in contrast to the enrichment of *Scn1a* and *Scn2a* at the proximal AIS. In agreement with previous reports (Rush et al., 2005), it was discovered that proximal AIS VGSCs (putative *Scn2a* channels) have a higher threshold for activation (~43 mV) than distal VGSCs (~55 mV) (putative *Scn8a* channels) (Hu et al., 2009). It is speculated that this distribution at the AIS is important for the generation of backpropagating action potentials (Fig.1.2*B*). Depolarizing currents at the AIS that

are subthreshold at proximal *Scn2a* channels but are sufficient to activate distal *Scn8a* would produce backpropagating potentials as distal *Scn8a* channel activation will trigger proximal *Scn2a* channels.

1.3.D. Distribution of *Scn2a*

Scn2a expression can be found along most unmyelinated and premyelinated neurons during early development. Later in development, *Scn2a* is primarily found at the proximal axon initial segment (Fig. 1.2.*B*), in a process that follows the formation of the myelin sheath along the axon and the transition from continual to saltatory axonal conduction (Boiko et al., 2001).

1.3.E. Distribution of *Scn3a*

Scn3a is most highly expressed embryonically (Beckh et al., 1989) and during early postnatal development in rodents (Siqueira et al., 2009). *SCN3A* expression decreases during development but is maintained at relatively higher levels during adulthood in humans compared to rodents (Chen et al., 2000). *Scn3a* is expressed in adult dorsal root ganglion neurons following axotomy in rodents (Waxman et al., 1994) and upregulation of *Scn3a* in the hippocampus was observed in *Scn1a* knockout mice, indicating that under certain conditions reemergence of *Scn3a* expression can occur.(Yu et al., 2006). Electrophysiological analysis of neurons from *Scn1a* knockout mice indicate that upregulation of *Scn3a* can restore a small portion of the lost *Scn1a* sodium currents in hippocampal neurons (Yu et al., 2006).

1.3.F. Glial Expression of VGSCs

VGSC expression has also been identified in non-neuronal cells in the brain and spinal cord of rodents (Korotzer and Cotman, 1992; Schmidtmayer et al., 1994) and humans (Norenberg et al., 1994). *Scn1a*, *Scn5a*, and *Scn8a* are the primary VGSCs expressed in microglia (Black et

al., 2009). Microglia are CNS immune cells that are responsible for removing cellular debris and pathogens (Aloisi, 2001). Reducing sodium channel activity either genetically or pharmacologically inhibits many of the functions of microglia including phagocytosis, migration, activation, and release of proinflammatory cytokines (Craner et al., 2005; Black et al., 2009). Upregulation of *Scn1a*, *Scn5a*, and *Scn8a* expression has been observed in microglia following activation by lipopolysaccharide (LPS) treatment and in an experimental autoimmune encephalomyelitis (EAE) model of multiple sclerosis (Craner et al., 2005; Black et al., 2009). Additionally, the *Scn1a*, *Scn2a*, *Scn3a*, *Scn5a*, and *Scn8a* have been identified in rodent astrocytes, particularly under proinflammatory pathological conditions (Ritchie, 1987; Black et al., 1993; Black et al., 1994; Black et al., 1995; Black and Waxman, 1996), and *Scn5a* has been identified in human astrocytes in multiple sclerosis lesions (Black et al., 2010). Upregulation of glial VGSCs in pathological states may help to regulate altered extracellular ion concentration (Black et al., 2010). Additionally, increased glial VGSC expression has been shown to increase proinflammatory cytokine production which may contribute to chronic inflammation in epilepsy.

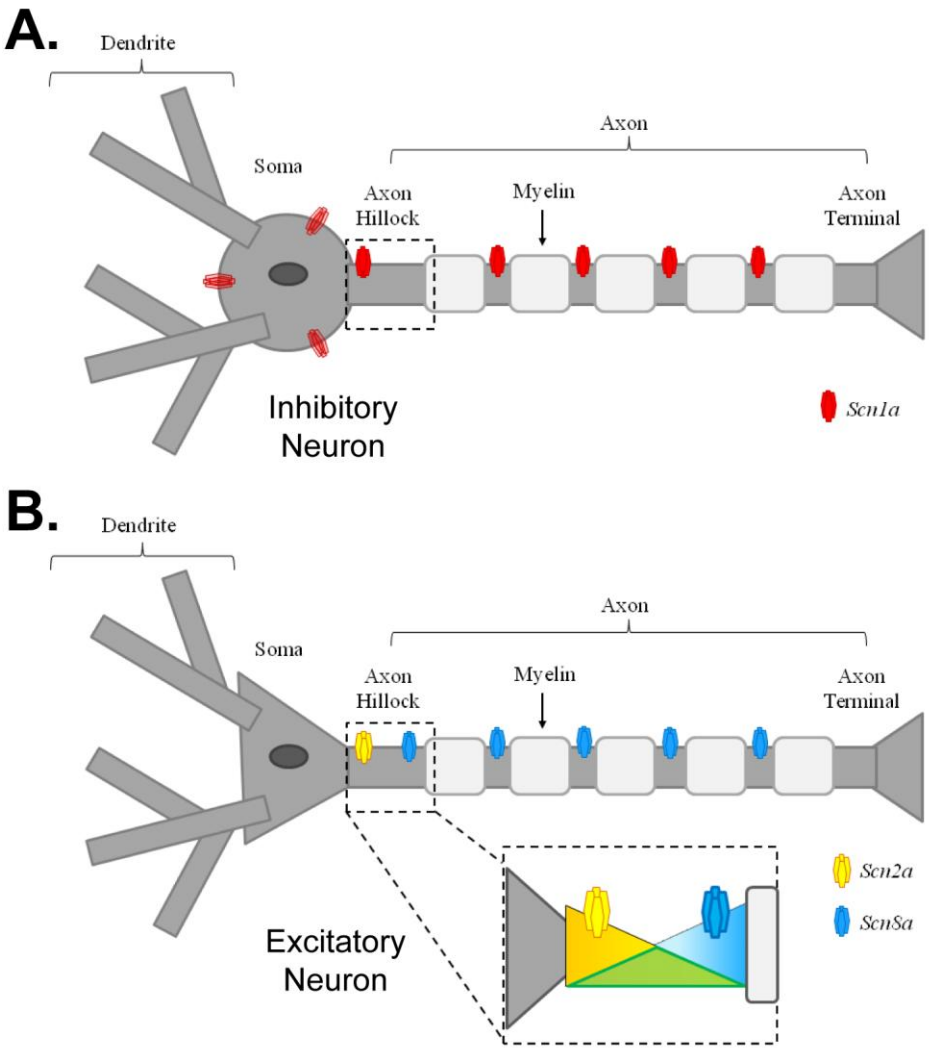

Figure 1.2. Schematic representation of VGSC subcellular Localization

A. Inhibitory neurons are thought to express high levels of *Scn1a* at the soma, axon hillock (axon initial segment) and along the axon at the nodes of Ranvier. ***B.*** *Scn8a* is thought to be highly expressed at the axon hillock and at the nodes of Ranvier in excitatory projection neurons. A proximodistal gradient exists between *Scn2a* and *Scn8a* at the axon hillock (inset) which may be important for back propagation. These models are not meant to represent cells outside of the forebrain and do not include all VGSC subcellular expression.

1.4. Overview of Epilepsy

1.4.A. What is Epilepsy

Epilepsy is defined as a neurological disorder characterized by seizures which are episodes of highly synchronous neuronal activity. Epilepsy is one of the most common neurological conditions, affecting over 50 million people worldwide (Brodie et al., 1997). The prevalence of epilepsy is estimated to be 0.3-1.6% (Begley et al., 2007) and the lifetime risk of diagnosis is estimated to be 2-3% (Browne and Holmes, 2001). Unfortunately, approximately 30% of epileptic patients do not achieve sufficient control of their seizures with currently available treatments (Loscher, 2002) highlighting a continued need to develop novel treatment options.

Epilepsies can be classified by their etiology and presentation. Epilepsies that are thought to be genetic in origin are classified as idiopathic whereas epilepsies in which a precipitating factor is known are classified as symptomatic. Many of the epilepsies are known to have a strong genetic component and heritability can be as high as 70% as has been estimated for partial epilepsy (Kjeldsen et al., 2001). A seizure event is classified as complex if consciousness is lost while simple seizures do not involve loss of consciousness. Seizures involving both hemispheres are classified as generalized while partial seizures only involve one hemisphere. Lastly, absence seizures are non-convulsive events characterized by brief loss of consciousness which are accompanied by three per second spike-and-wave EEG discharges. While seizures can differ substantially in their underlying causes and presentation, a commonality is that they result from aberrant synchronization of neuronal activity.

1.4.B. Idiopathic Epilepsies

Many of the first epilepsy mutations to be identified were found to occur in ion channels and could be considered large effect size variants that often exhibited classic Mendelian

inheritance. Among these channels, the VGSCs and in particular *SCN1A* emerged as important epilepsy risk genes.

The heritability of epilepsy has been very well documented, however, the majority of the genetic causes remain undetermined. The discrepancy between the lack of identified genetic risk factors and the high degree of heritability of the disorder has been observed in many genetic disorders (Manolio et al., 2009) but appears to be particularly high among the epilepsies. This was thought to be a result of the high degree of heterogeneity and complexity of the epilepsies. Most of the first generation of identified epilepsy risk genes are monogenetic and relatively homogeneous. For example, more than 80% of Dravet syndrome cases are caused by mutations in *SCN1A* (Claes et al., 2001; Harkin et al., 2007). In contrast, the majority of idiopathic epilepsies involve rare genetic variants and complex interactions of many genetic risk factors. Only recently, with the advent of whole genome and exome sequencing approaches has it been possible to effectively identify *de novo* disease causing mutations in patients without a family history of the disease (Bamshad et al., 2011; Doherty and Bamshad, 2012; Need et al., 2012; Rauch et al., 2012). Just in the past few years, application of these approaches has revealed a wealth of new epilepsy risk genes (Murdock et al., 2011; Talkowski et al., 2011; Andrade et al., 2012; Cloarec et al., 2012; Elo et al., 2012; Heron et al., 2012; Lemke et al., 2012; Veeramah et al., 2012; Basel-Vanagaite et al., 2013; Jang et al., 2013; Lindgren et al., 2013; Marti-Masso et al., 2013; McDonell et al., 2013; Nakamura et al., 2013; Poulton et al., 2013; Touma et al., 2013; Veeramah et al., 2013). As these approaches continue to reveal new risk genes it will become increasingly possible to understand the complex genetic interactions that lead to many of the epilepsies.

1.5. VGSC Epilepsy Mutations

1.5.A. *SCN1A* Epilepsy Mutations

Currently more epilepsy mutations have been identified in the *SCN1A* gene than in any other epilepsy gene (for databases of *SCN1A* variants see www.molgen.ua.ac.be/SCN1AMutations and www.scn1a.info) (Claes et al., 2009; Lossin, 2009). Missense and in-frame deletions as well as truncation mutations have been identified in virtually every part of the *SCN1A* channel in epileptic patients, including transmembrane spanning segments, intra and extracellular loops, and the C- and N-terminal domains (Catterall et al., 2008).

SCN1A mutations are the leading cause of the childhood encephalopathy, Dravet Syndrome (DS) (Claes et al., 2001). Approximately 70-80% of DS patients carry mutations in the *SCN1A* gene (Marini et al., 2007). Seizures in infants with DS are often initially febrile (fever-induced) early in life (4-8 months of age), and often increase in frequency and severity with age. DS is characterized by cognitive impairment, hyperactivity, photosensitivity, developmental arrest, ataxia, and sleep disturbances. Many children with DS are classified as autistic (Li et al., 2011). DS is often refractory to treatment and premature mortality is estimated to be 15-20% (Genton et al., 2011).

SCN1A mutations are also a major cause of genetic epilepsy with febrile seizures plus (GSFS+) (Escayg et al., 2000). It is estimated that 10% of GEFS+ patients carry *SCN1A* mutations. GEFS+ patients have a heterogeneous epilepsy phenotype but primary characteristics include childhood febrile seizures and afebrile generalized tonic-clonic, absence, atonic, and partial seizures (Scheffer and Berkovic, 1997). *SCN1A* has also been associated with intractable childhood epilepsy with generalized tonic-clonic seizures (Fujiwara et al., 2003) and severe idiopathic generalized epilepsy (Ebach et al., 2005).

Together, these *SCN1A*-related epilepsies encompass a spectrum of phenotypes with overlapping clinical presentations and etiologies that range in severity from relatively benign febrile seizures to the catastrophic DS (Harkin et al., 2007). It is interesting that the most severe *SCN1A* epilepsies often arise from *de novo* loss-of-function mutations and that less severe *SCN1A* epilepsies arise from inherited amino acid substitutions (Catterall et al., 2010; Escayg and Goldin, 2010). This suggests that larger perturbations to channel function lead to more severe types of epilepsy.

1.5.B. *SCN2A* Epilepsy Mutations

Mutations in *SCN2A* are most frequently observed in benign familial neonatal-infantile seizures (BFNIS). BFNIS is characterized by afebrile generalized seizures that begin in the first 3-6 months of life and typically resolve by the end of the first year of life. *SCN2A* mutations have also been identified in a small number of cases of infantile spasms, sporadic neonatal epileptic encephalopathy (Ogiwara et al., 2009), migrating focal seizures of infancy (Dhamija et al., 2013), infantile spasms (Sundaram et al., 2013), and DS (Shi et al., 2009).

1.5.C. *SCN3A*, *SCN8A*, and *SCN9A* Epilepsy Mutations

There is comparatively much less information about the role of the other VGSCs in epilepsy. Gain-of-function *SCN3A* mutations have been identified in five children with partial epilepsy (Holland et al., 2008; Estacion et al., 2010; Vanoye et al., 2013). Very recently, with the application of whole exome and genome sequencing, nine *SCN8A* mutations have been identified in patients with epilepsy (O'Brien and Meisler, 2013). A gain-of-function *SCN8A* mutation was recently discovered in a patient with infantile epileptic encephalopathy and sudden death in epilepsy (SUDEP) (Veeramah et al., 2012). Five additional *SCN8A* mutations linked to epileptic encephalopathies have also been identified (Carvill et al., 2013; Epi et al., 2013), however,

functional analyses of these mutations has not been performed. Three additional unpublished *SCN8A* mutations, identified in patients with epileptic encephalopathy, have been reviewed (O'Brien and Meisler, 2013). *SCN9A* has been linked to FS, GEFS+, and DS, and may be a modifier of *SCN1A*, potentially worsening *SCN1A* epilepsies (Singh et al., 2009; Mulley et al., 2013).

1.5.D. Epilepsy Mutations in VGSC Beta Subunits

VGSC β subunits modulate the properties of VGSC α subunits and also function as cell adhesion molecules that are important for normal brain development. As such, β subunits provide a means by which VGSC activity and brain development can be altered in ways that can lead to epilepsy.

Several epilepsy mutations have been identified in β subunit genes. Mutations in the *SCN1B* (β1) gene have been identified in patients with temporal lobe epilepsy and GEFS+ (Wallace et al., 1998; Scheffer et al., 2007) and DS (Patino et al., 2009; Ogiwara et al., 2012). *SCN1B* knockout mice are ataxic and epileptic (Chen et al., 2004) and exhibit epileptiform burst activity in hippocampal slices and impaired development of the hippocampus (Brackenbury et al., 2013). *SCN2B* (β2) deficiency is not known to cause human epilepsy but β2 null mice are more susceptible to pilocarpine-induced seizures than wild-type littermate controls and have reduced expression of VGSC α subunits and reduced sodium currents in hippocampal neurons (Chen et al., 2002).

1.6. VGSCs and Epilepsy: Mechanisms

Since reducing sodium conduction would be expected to reduce neuronal excitability, it is not surprising that VGSCs are pharmacological targets for the treatment of epilepsy. However,

what is less intuitive is how mutations in a sodium channel can lead to increased excitability and epilepsy.

1.6.A. Mechanisms of *SCN1A* Epilepsies

SCN1A channels have has been shown to be highly expressed in GABAergic inhibitory neurons of the hippocampus and cortex (see 1.3.B. *Scn1a* Distribution) and reduced excitability of these neurons has been observed in *Scn1a* mouse mutants (Yu et al., 2006; Ogiwara et al., 2007; Martin et al., 2010). Cell-type colocalization and electrophysiological analysis of rodent models of *Scn1a* dysfunction lead to the hypothesis that loss of *Scn1a* causes reduced neuronal inhibition and thus increased risk of seizure generation (Yu et al., 2006; Ogiwara et al., 2007). Conditional knockout approaches have been used to probe this hypothesis by selectively inactivating the *Scn1a* gene in different cell types. Work from our lab as well as other investigations have demonstrated that broad loss of *Scn1a* from interneurons (Cheah et al., 2012), or restricted loss of *Scn1a* from parvalbumin interneurons (Dutton et al., 2012; Ogiwara et al., 2013) is sufficient to generate spontaneous seizures and reduce lifespan (Fig. 1.3). Interestingly, conditional inactivation of *Scn1a* in excitatory neurons of the cortex and hippocampal CA1 and dentate granule cell layers was not sufficient to alter latencies to induced seizures (Dutton et al., 2012), but did improve the survival of mice in which *Scn1a* was broadly deleted from interneurons (Ogiwara et al., 2013). These data are consistent with a model in which *Scn1a*-mediated reduction in PV interneuron excitability is primarily driving seizure susceptibility and lethality but the severity of these phenotypes can be either worsened by loss of inhibition from other interneuronal subtypes or lessened to some extent by loss of *Scn1a* from glutamatergic excitatory cells.

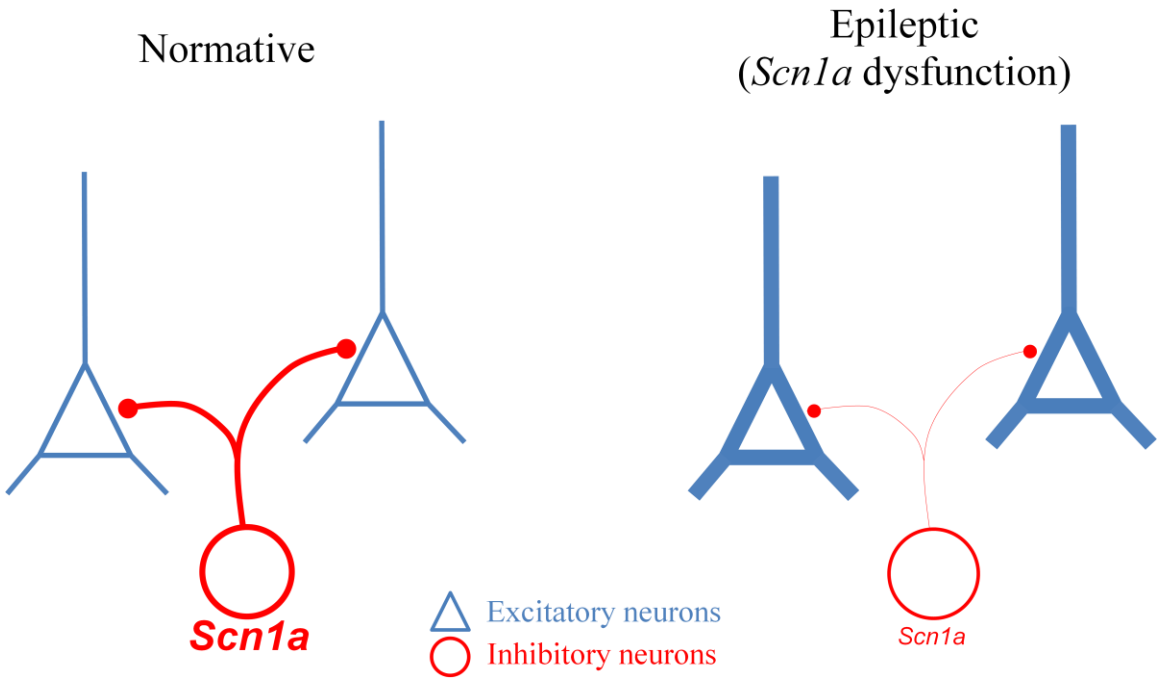

Figure 1.3. Loss of inhibition model of *Scn1a* dysfunction leading to epilepsy

Illustrated are hypothetical cortical parvalbumin positive interneurons (red) synapsing onto two glutamatergic pyramidal neurons (blue) in a normal (left) and epileptic (right) brain. The thickness of the cell body and processes indicates the relative excitability of the cell type. The font size of the VGSC (*Scn1a*) indicates the relative expression level of this channel. In a normal, non-epileptic brain sufficient *Scn1a* expression exists to support interneuronal excitability which suppresses network hyperexcitability. Loss of *Scn1a* expression leads to a reduction in interneuronal function and an overall increase in network activity. This loss of inhibition allows excitatory aspects of the network to enter into hyperexcitable, epileptic states.

1.6.B. Mechanisms of *SCN8A* Epilepsies

A role for *SCN8A* in epilepsy was first investigated in *Scn8a* mouse mutants by determining their susceptibility to induced seizures (Martin et al., 2007; Hawkins et al., 2011). *Scn8a* mutant mice were also crossed to mice carrying *Scn1a* mutations to assess the effect of reduced *Scn8a* activity in DS and GEFS+ epilepsy models (Martin et al., 2007; Hawkins et al., 2011). In contrast to other VGSCs, we found that mutations that reduce the activity of *Scn8a* increase seizure resistance and extend the survival of mouse models of DS and GEFS+ (Martin et al., 2007; Hawkins et al., 2011). These findings identified *Scn8a* as a genetic modifier of *Scn1a* epilepsy phenotypes, and identified *SCN8A* as a possible target for therapeutic intervention.

Loss of function of the mRNA binding protein Celf4 was found to increase the expression of *Scn8a* at the AIS and also increase sodium currents (Sun et al., 2013). Interestingly, Celf4 deficient mice have a complex seizure disorder involving both tonic-clonic seizures and absence seizures (Wagnon et al., 2011). While it is possible that seizures are the result of altered expression of any number of the many other targets of Celf4 (Wagnon et al., 2012), it is tempting to speculate that the increased *Scn8a* expression is responsible for the increased sodium currents and neuronal excitability. Thus alterations that increase *Scn8a* expression may lead to increased neuronal excitability and epilepsy, while mutations that reduce the activity of *Scn8a* increase seizure resistance. In support of this hypothesis, increased *Scn8a* expression was observed in the hippocampus of amygdala-kindled rats (Blumenfeld et al., 2009), and in the entorhinal cortex, a region which provides a major source of excitatory input to the hippocampus, in a hippocampal electrical simulation model of TLE (Hargus et al., 2011). These studies raise the possibility that activity-dependent increases in *Scn8a* expression can lead to increased neuronal activity, initiating a self-reinforcing feedback cycle that promotes the generation of seizures. Additionally, a gain-of-function *SCN8A* mutation, N1768D, was identified in a patient with infantile epileptic encephalopathy and sudden unexplained death in epilepsy (SUDEP) (Veeramah et al., 2012).

Functional analysis of the biophysical properties of mutated *SCN8A* (N1768D) channels revealed a robust increase in persistent sodium current. Given that *Scn8a* is highly expressed in excitatory neurons of the hippocampus and cortex, it seems possible that increased *Scn8a* activity/expression could result in a broad increase in the excitability of excitatory cortical and hippocampal projection neurons, thereby promoting seizure states.

In contrast to the increased seizure resistance associated with *Scn8a* mutations in mice, reduced *Scn8a* activity has also been shown to cause absence epilepsy (Papale et al., 2009). We demonstrated that absence seizure frequency is influenced by genetic background and is suppressed by ethosuximide, a T-type Ca^{++} blocker and first-line treatment for absence epilepsy. Interestingly, absence seizures were observed in the patient with the *SCN8A* N1768D mutation (Veeramah et al., 2012).

1.6.C. Mechanisms of *SCN2A* and *SCN3A* Epilepsies

Mutations in *SCN2A* are most commonly found in children with benign familial neonatal-infantile seizures (BFNIS) (Heron et al., 2002; Herlenius et al., 2007; Liao et al., 2010a). Unlike epilepsies associated with mutations in *SCN1A* and *SCN8A*, which often begin in childhood and worsen over time, BFNIS often resolves by one year of age (Berkovic et al., 2004). This is thought to be a consequence of the normal developmental switch of *SCN2A* with *SCN8A* α subunits, which occurs throughout early development in concert with myelination of maturing neurons (Liao et al., 2010b). In rare cases, *SCN2A* alterations have been identified in more severe intractable childhood epilepsies (Ogiwara et al., 2009) and in GEFS+ (Sugawara et al., 2001) and DS (Shi et al., 2009).

Five *SCN3A* epilepsy mutations have been reported to date; one in a patient with refractory cryptogenic partial epilepsy (Holland et al., 2008) and four in children with focal

epilepsy (Vanoye et al., 2013). Functional analysis of these mutations indicated that they are gain-of-function, leading to increased voltage-dependent sodium currents (Holland et al., 2008).

1.7. VGSC Dysfunction in Cognition and Behavior

1.7.A. *SCN1A* in Cognition and Behavior

Recently, increased attention has been given to the role of VGSCs in cognition and behavior, with a particular emphasis on the behavioral and cognitive comorbidities that have been reported in VGSC epilepsies. While it is clear that seizure activity itself can disrupt cognition, some VGSC mutations have been identified in patients with cognitive and behavioral abnormalities who do not have epilepsy. This suggests that VGSC dysfunction can lead to epilepsy and cognitive-behavioral deficits by separate and/or convergent mechanisms.

SCN1A mutations are often associated clinically with a host of behavioral and cognitive deficits including hyperactivity, attention deficit disorder, sleep disorders, increased anxiety, and impaired social interactions (Mahoney et al., 2009; Brunklaus et al., 2011; Genton et al., 2011; Li et al., 2011). *Scn1a* mutant mice exhibit increased anxiety, hyperactivity, impaired spatial learning, and reduced performance on social tasks (Han et al., 2012b; Ito et al., 2012). Additionally, we have identified sleep abnormalities in a mouse model of GEFS+ (Papale et al., 2013), which may lead to deficits in memory consolidation. In the clinic, behavioral and cognitive dysfunction typically follows the onset of seizures and so it is possible these deficits are the consequence of seizure activity. However, siRNA knockdown of *Scn1a* in the rat basal forebrain was found to interfere with hippocampal oscillations resulting in deficits in spatial memory but not epilepsy (Bender et al., 2013). This finding suggests that at least some *SCN1A* derived cognitive impairments can occur independently of seizures. In addition, *Cre*-mediated deletion of *Scn1a* from interneurons was recently shown to result in autistic-like behaviors in mice (Han et al., 2012a). Surprisingly, acute administration of the gamma-aminobutyric acid

(GABA)-acting benzodiazepine, clonazepam, was capable of transiently abolishing many of these behavioral phenotypes in adult mice (Han et al., 2012b). This finding suggests that 1) many of the behavioral deficits associated with *SCN1A* arise from reduced GABAergic neurotransmission and, 2) that correcting these deficits, even in adulthood, might lead to cognitive and behavioral improvements.

Additionally, disrupted *SCN1A* function has been implicated in the etiology of impaired cognition and the increased incidence of epilepsy that occurs in Alzheimer's disease (AD). The enzyme β-site APP-cleaving enzyme 1 (BACE1), also known as β-secretase 1, is responsible for cleaving amyloid precursor protein (APP) and also the VGSC β2 subunit which is responsible, in part, for inserting *SCN1A* in the plasma membrane (Kim et al., 2011). Thus, elevated BACE1 expression, which often occurs in AD, may lead to cognitive impairment both by increasing Aβ and by reducing *SCN1A* expression in the brain.

1.7.B. *SCN8A* in Cognition and Behavior

SCN8A has been associated with psychiatric disease and cognitive impairment in humans. Human genetic studies have identified an association between *SCN8A* polymorphisms and increased suicidal behavior (Wasserman et al., 2005; Wang et al., 2010), as well as increased risk of bipolar disorder (Wang et al., 2008). An *SCN8A* truncation mutation was also identified in a patient exhibiting cerebellar atrophy, ataxia, and mental retardation, but not epilepsy (Trudeau et al., 2006). In mice, *Cre*-driven inactivation of *Scn8a* in cerebellar Purkinje cells reduces performance in the Morris water maze (Woodruff-Pak et al., 2006). In contrast, no deficits in Morris water maze performance or in a conditioned taste avoidance paradigm were observed in mice carrying a null *Scn8a* mutation; however, increased emotional behaviors were observed (McKinney et al., 2008). We have found that the *Scn8a*-medjo mutation leads to modestly increased spatial memory in a novel object recognition task and alterations to sleep architecture

but not to differences in anxiety or depressive-like phenotypes (Papale et al., 2010). Together, these studies point to a possible role of *SCN8A* in some aspects of cognitive function and behavior.

1.7.C. *SCN2A* and *SCN3A* in Cognition and Behavior

Comparatively little information exists about the possible role of *SCN2A* and *SCN3A* in cognitive processes and behavior. Whole genome sequencing approaches have identified *SCN2A* as a risk gene for autism (Jiang et al., 2013). Furthermore, microdeletions that encompass *SCN2A* and *SCN3A* were identified in a patient with autistic-like features, psychomotor delay, microcephaly, but not epilepsy (Celle et al., 2013) and in an unrelated patient with cognitive and psychiatric impairment (Bartnik et al., 2011). Testing of available rodent models of *Scn2a* and *Scn3a* dysfunction for behavioral abnormalities could potentially be very beneficial to the field.

1.8. VGSCs as Antiepileptic Drug Targets

Pharmacologic targeting of VGSCs has produced some of the most effective and widely used anti-epileptic drugs (AEDs). These drugs include, phenytoin (Kuo and Bean, 1994), lamotrigine, carbamazepine, oxcarbazepine (Schmutz et al., 1994), and zonisamide (Schauf, 1987). Evidence also exists for VGSC targeting by several additional drugs including felbamate (Taglialatela et al., 1996), topiramate (Taverna et al., 1999), and valproate (Van den Berg et al., 1993; Taverna et al., 1998; Xie et al., 2001). Importantly, phenytoin, carbamazepine, and lamotrigine weakly block VGSCs under conditions of normal neuronal activity but increase their potency in a use-dependent fashion in response to sustained depolarization (Rogawski and Loscher, 2004). Therefore, these drugs become maximally effective when they are most required, under conditions of sustained channel activity, which occurs during seizure.

Despite efforts to find compounds that are selective for different VGSC isoforms, few exist. Tetrodotoxin (TTX) and VGSC-acting AEDs non-selectively target these channels, but conceivably targeting specific isoforms could lead to improved seizure suppression with fewer side effects. Moreover, non-selective targeting of VGSCs with lamotrigine can actually worsen some epilepsies that involve an underlying VGSC deficiency such as DS (Guerrini et al., 1998). However, reduced *Scn8a* activity has been shown to normalize seizure thresholds and lifespan in mice with *Scn1a* mutations (Martin et al., 2007; Hawkins et al., 2011), providing proof of concept of the benefits of targeting select VGSC isoforms in epilepsy.

The TTX derivative, 4.9-anhydro-TTX, has been reported to be selective for *Scn8a* (Rosker et al., 2007). IC_{50} values for this compound were evaluated on a combination of human and rodent VGSCs and range from 341±36 nmol/L (*Scn3a*) to 785000±11600 nmol/L (*SCN5A*) compared to 7.8±2.3 nmol/L (*Scn8a*). Unfortunately, *Scn1a* was not evaluated for technical reasons. Without knowing the IC_{50} of this compound for *Scn1a* it is not clear how useful it would be as an experimental tool or a base for developing *SCN8A* selective drugs. Recently, a selective *SCN9A* compound was described with over 32-fold selectivity for *SCN9A* over other VGSC isoforms (Yang et al., 2013). This compound will be useful for the study and treatment of pain but it might also have implications for epilepsy (see the *SCN3A*, *SCN8A*, and *SCN9A* Epilepsy Mutations section). *SCN9A* variants are enriched in DS, however it is not yet clear if these mutations are gain-, reduction- or loss-of-function. If gain-of-function *SCN9A* mutations do contribute to DS, then providing an *SCN9A* selective inhibitor might be beneficial in these patients.

CHAPTER 2

Partial Knockdown of $Na_v1.6$ (*Scn8a*) Sodium Channels in the Hippocampus Confers Seizure Protection

Chapter 2 contains material from the manuscript in preparation: Partial Knockdown of $Na_v1.6$ (*Scn8a*) Sodium Channels in the Hippocampus Confers Seizure Protection, Makinson C.D., Tanaka B., Lamar T., Goldin A. L., Escayg A.

2.1. Summary

SCN1A mutations are the main cause of the epilepsy disorders Dravet syndrome (DS) and genetic epilepsy with febrile seizures plus (GEFS+). Mutations that reduce the activity of the mouse *Scn8a* gene, in contrast, are found to confer seizure resistance and extend the lifespan of mouse models of DS and GEFS+. To investigate the mechanism by which reduced *Scn8a* expression confers seizure resistance, we induced interictal-like burst discharges in hippocampal slices of heterozygous *Scn8a* null mice (*Scn8a*$^{med/+}$) with elevated extracellular potassium. *Scn8a*$^{med/+}$ mutants exhibited reduced epileptiform burst discharge activity after P20, indicating an age-dependent increased threshold for induction of epileptiform discharges. *Scn8a* deficiency also reduced the occurrence of burst discharges in a GEFS+ mouse model (*Scn1a*$^{R1648H/+}$). There was no detectable change in the expression levels of *Scn1a* ($Na_v1.1$) or *Scn2a* ($Na_v1.2$) in the hippocampus of adult *Scn8a*$^{med/+}$ mutants. To determine whether the increased seizure resistance associated with reduced *Scn8a* expression was due to alterations that occurred during development, we examined the effect of deleting *Scn8a* in adult mice. Global *Cre*-mediated deletion of a heterozygous floxed *Scn8a* allele in adult mice was found to increase thresholds to chemically and electrically induced seizures. Knockdown of *Scn8a* gene expression in the adult hippocampus via lentiviral *Cre* injection resulted in a reduction in the number of EEG-confirmed seizures following the administration of picrotoxin. Additionally, knockdown of *Scn8a* expression in the hippocampus of *Scn1a*$^{+/-}$ and WT mice using an adeno-associated viral shRNA was found to increase thresholds to flurothyl-induced seizures. Our results identify the hippocampus as an important structure in the mediation of *Scn8a*-dependent seizure protection and suggest that selective targeting of *Scn8a* activity might be efficacious in patients with epilepsy.

2.2. Introduction

Epilepsy is characterized by unprovoked, recurrent seizures that are manifestations of abnormal neuronal synchrony and excitability. Several genes that are known to cause monogenic forms of epilepsy encode neuronal ion channels, including voltage-gated sodium channels (VGSCs) (Noebels, 2003; Steinlein, 2004). VGSCs are important integrators of synaptic input and are responsible for the initiation and propagation of action potentials in neurons (Gong et al., 1999; Whitaker et al., 2001; Lorincz and Nusser, 2010). Three pore-forming VGSC α-subunit genes are primarily expressed in the adult mammalian central nervous system (CNS): *SCN1A*, *SCN2A*, and *SCN8A*, which encode the $Na_v1.1$, $Na_v1.2$, and $Na_v1.6$ channels, respectively. *SCN1A* has emerged as an important epilepsy gene and is responsible for a number of different epilepsy disorders, including the catastrophic, treatment-resistant childhood encephalopathy Dravet syndrome (DS) and genetic epilepsy with febrile seizures plus (GEFS+) (Escayg et al., 2000; Claes et al., 2001).

Approximately 30% of epileptic patients do not achieve adequate seizure control with currently available anti-epilepsy drugs (AEDs). Moreover, while new AEDs are generally better tolerated, the percentage of patients with treatment-resistant seizures has not changed significantly in the last 40 years, indicating a critical need to identify new treatment options for patients with refractory epilepsy. VGSCs are known targets for several AEDs; however, these drugs are not isoform specific and affect all VGSCs, likely contributing to unwanted side effects. Alternatively, selective targeting of a specific VGSC isoform, may provide improved seizure control with fewer unintended consequences.

We previously demonstrated that thresholds for flurothyl- and kainic acid-induced seizures are elevated in $Scn8a^{med/+}$ and $Scn8a^{medjo/+}$ mutant mice when compared to wild-type (WT) littermates (Martin et al., 2007). Furthermore, the seizure phenotypes of *Scn1a* mutant mice that model DS and GEFS+ were dramatically improved by the co-expression of an *Scn8a*

mutation (Martin et al., 2007; Hawkins et al., 2011). In addition, *Scn8a*-deficient mice are resistant to amygdala kindling, while there is increased *Scn8a* expression in the CA3 region of the hippocampus of amygdala-kindled rats (Blumenfeld et al., 2009). Together, these studies raise the possibility that reduced hippocampal *Scn8a* expression may contribute to the seizure protection observed in *Scn8a*$^{med/+}$ mutants and that the selective targeting of *Scn8a* may be efficacious in some forms of epilepsy. However, a caveat of these earlier experiments is that the relationship between *Scn8a* and seizure resistance was based on the use of *Scn8a* mutant mice, in which the activity of *Scn8a* was reduced throughout brain development. Therefore, whether reduced *Scn8a* activity would confer seizure protection in the adult brain was unknown.

In this study, we examined the effect on seizure susceptibility of reducing *Scn8a* expression in adult mice. In addition to exploring the mechanism of seizure protection associated with altered *Scn8a* function, we used electrophysiological analysis to monitor developmental changes in hippocampal excitability in heterozygous *Scn8a*$^{med/+}$ mutants. Finally, using lentiviral-*Cre* and adeno-asociated viral shRNA strategies, we assessed the effect on seizure phenotypes of reducing *Scn8a* expression in the hippocampus.

2.3. Results

Epileptiform burst discharge activity is reduced in *Scn8a*$^{med/+}$ mutant mice

Since the hippocampus is known to play an important role in seizure generation, we examined temporal changes in the excitability of hippocampal slices from heterozygous *Scn8a* null mutant mice (*Scn8a*$^{med/+}$). Epileptiform burst discharges were induced in the CA3 pyramidal cell layer of the hippocampus by elevating the extracellular potassium concentration (Fig. 1*Aa-c*). Burst discharges were not observed during the initial 5 minutes at physiological potassium concentration (2.5 mM $[K^+]_o$) in hippocampal slices from either WT (Fig. 1*Aa*) or *Scn8a*$^{med/+}$ mutant mice (Fig. 1*B*). However, elevating the extracellular K^+ concentration to 8.5 mM induced

synchronous burst discharge activity in hippocampal slices from most WT mice at all ages (P13-P84) (Fig. 1*A*,*D*). Individual burst discharges were composed of a positive extracellular potential with multiple population spikes (Fig. 1*Ac*). Burst activity continued until the extracellular K^+ was returned to physiological concentration (2.5 mM). Similarly, hippocampal slices from young P13-P20 *Scn8a*$^{med/+}$ mutant mice displayed burst discharges when exposed to elevated potassium (Fig. 1*D*). In contrast, burst discharges were not observed in the majority of slices from *Scn8a*$^{med/+}$ mutant mice older than P20 (Fig. 1*B*,*D*). The lack of activity was not due to poor health of the cells because synaptic connections and neuronal firing remained intact, as determined by stable population spike amplitudes in the CA3 pyramidal layer before and after exposure to elevated potassium (Fig. 1*C*). The frequency of observed epileptiform burst discharges was lower in more mature WT mice (P26 and P70-84), but was still comparably much higher than that observed in slices from *Scn8a*$^{med/+}$ mutant mice (Fig. 1*D*). For example, burst discharges were observed in 86% of slices from adult WT mice, but in only 12% of slices from adult *Scn8a*$^{med/+}$ mice (P70-84).

Latency to burst discharges is increased in *Scn8a*$^{med/+}$ mutant mice

Because $Na_v1.6$ channels are well suited for repetitive firing of action potentials and hence hyperactivity of the neuronal network, we compared the latency to the initiation of burst discharges in slices from *Scn8a*$^{med/+}$ mutants and WT littermates. Latency to the initial burst discharge was measured from the time that elevated potassium ACSF entered the recording chamber. *Scn8a*$^{med/+}$ mutant mice in all 3 age groups tested displayed a significant increase in the latency to the initiation of epileptiform burst activity (Fig. 2.2*A*). However, once burst discharge activity was induced, there were no qualitative differences in the pattern of synchronous activity. To determine whether there were any quantitative differences in burst activity, we analyzed the inter-burst frequency and single burst duration. Because the majority of hippocampal recordings

from *Scn8a*$^{med/+}$ mutant mice did not exhibit burst activity (Fig. 2.1*D*), only hippocampal slices from the few *Scn8a*$^{med/+}$ mutant mice that produced burst discharges were used for this analysis. Inter-burst frequency was measured as the number of burst discharges during a 4-min period, and burst duration was determined from an average of 50 individual bursts (Fig. 2.1*Ac*). There were no significant differences in either the inter-burst frequency or single burst duration between *Scn8a*$^{med/+}$ mutant and WT mice in all 3 age groups examined (Fig. 2.2*B*-*C*).

Reduced *Scn8a* expression decreases the occurrence of burst discharges in *Scn1a*$^{R1648H/+}$ mice

To investigate whether reduced *Scn8a* expression could alter the occurrence of epileptiform burst discharges in a mouse model of GEFS+ (*Scn1a*$^{R1648H/+}$ mice), we generated double heterozygous mutants (*Scn1a*$^{R1648H/+}$/*Scn8a*$^{med/+}$) and quantitatively examined burst activity in hippocampal slices exposed to elevated potassium. Burst occurrence, defined as the number of slices that exhibited bursting, was significantly lower in slices from *Scn8a*$^{med/+}$ and double heterozygous mice compared to WT (Table 1). Burst occurrence was also significantly reduced in double heterozygous mice compared to *Scn1a*$^{R1648H/+}$ mice (Table 1). While burst occurrence was comparable in slices from *Scn1a*$^{R1648H/+}$ mutants and WT littermates, burst latency was significantly shorter in *Scn1a*$^{R1648H/+}$ mice. An increase in inter-burst frequency was also observed in slices from *Scn1a*$^{R1648H/+}$ mutants compared to WT; however, this difference was not statistically significant. It was not possible to statistically evaluate burst latency or frequency in slices from *Scn8a*$^{med/+}$ mice (with or without the *Scn1a*$^{R1648H/+}$ mutation) because of the low percentage of hippocampal slices that demonstrated burst activity. However, increased latencies to bursting and decreased inter-burst frequencies were observed in *Scn8a*$^{med/+}$ slices (with or without the *Scn1a*$^{R1648H/+}$ mutation) compared to *Scn1a*$^{R1648H/+}$ slices in the few instances in which bursting occurred.

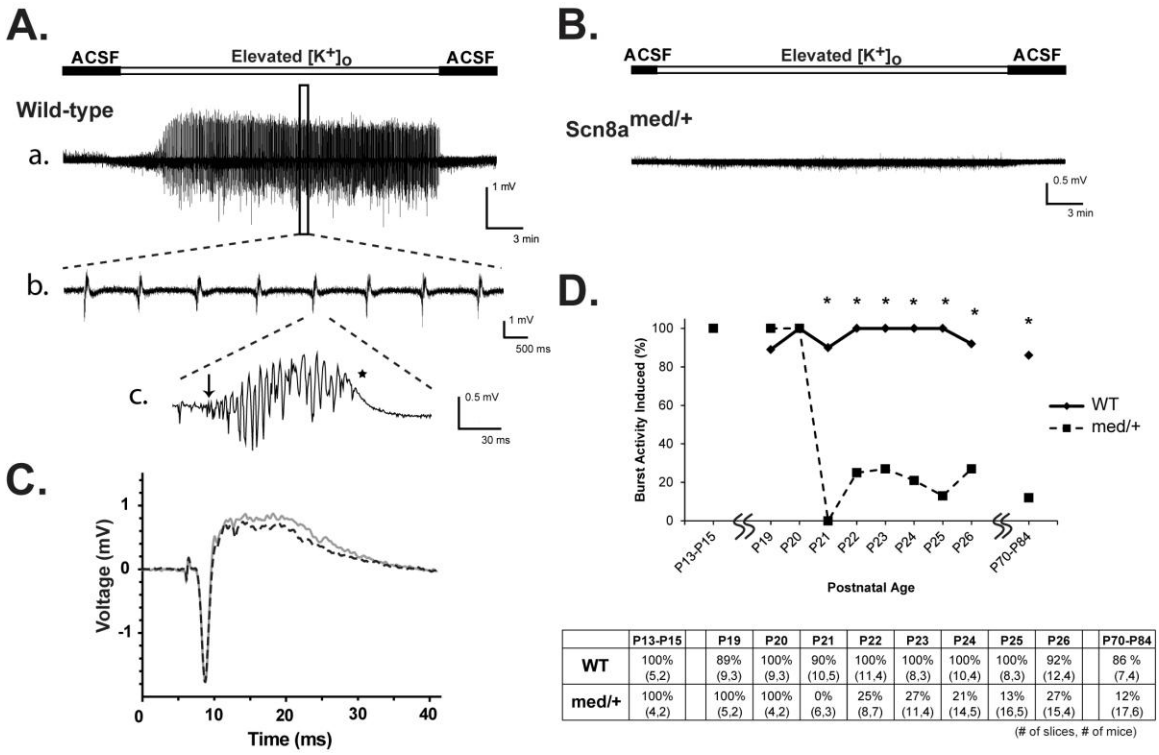

	P13-P15	P19	P20	P21	P22	P23	P24	P25	P26	P70-P84
WT	100% (5,2)	89% (9,3)	100% (9,3)	90% (10,5)	100% (11,4)	100% (8,3)	100% (10,4)	100% (8,3)	92% (12,4)	86 % (7,4)
med/+	100% (4,2)	100% (5,2)	100% (4,2)	0% (6,3)	25% (8,7)	27% (11,4)	21% (14,5)	13% (16,5)	27% (15,4)	12% (17,6)

(# of slices, # of mice)

Figure 2.1. Spontaneous seizure-like burst discharges in CA3 pyramidal cell layer induced by elevated potassium in hippocampal slices from *Scn8a*$^{med/+}$ mutant and WT mice

Aa, CA3 pyramidal cells did not show spontaneous burst activity in physiological 2.5 mM $[K^+]_o$; however, burst activity was induced when extracellular K^+ concentration was elevated to 8.5 mM $[K^+]_o$. ***Ab***, Expansion of a segment of spontaneous activity showed synchronous firing of burst activity. ***Ac***, Expansion of a single interictal-like burst discharge. Arrow indicates start of a burst discharge and star shows the end of a single burst. ***B***, Extracellular recording from CA3 pyramidal cell layer of a *Scn8a*$^{med/+}$ mutant mouse (P24). ***C***, Population spike amplitude before and after exposing hippocampal slice to 8.5 mM $[K^+]_o$. Solid gray – before perfusing 8.5 mM $[K^+]_o$ into the bath. Black dash – after exposing slice to 8.5 mM $[K^+]_o$ and washout with standard

2.5 mM $[K^+]_o$ ACSF. Population spikes were evoked with 50 μA stimulation for 100 μs. ***D***, Hippocampal slices from *Scn8a*$^{med/+}$ mutant and WT mice from P13-P20 demonstrated comparable levels of spontaneous burst discharge activity in elevated extracellular potassium. Beginning at P21, the propensity for burst activity dramatically decreased in hippocampal slices from *Scn8a*$^{med/+}$ mutant mice. Number of slices = 4-17, number of mice = 2-7. *$p < 0.001$ when compared to WT; Fisher's exact test with Bonferroni correction. These experiments were performed by Brian Tanaka in the laboratory of Alan Goldin at the University of California, Irvine.

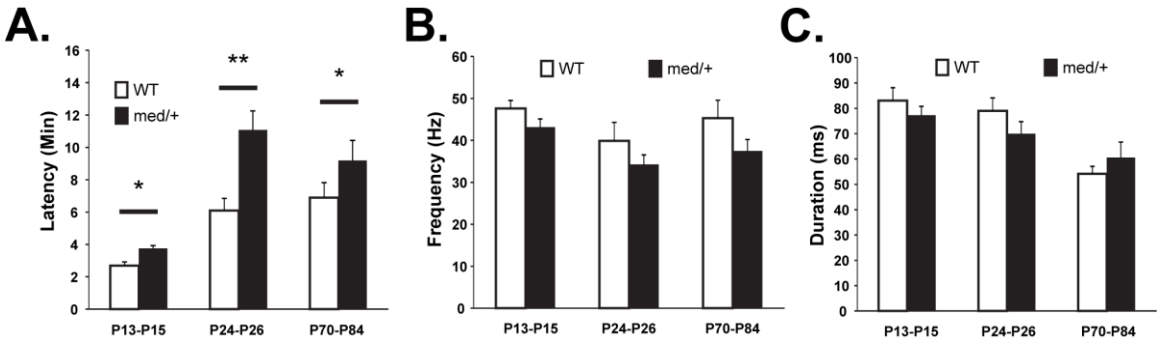

Figure 2.2. Analysis of burst characteristics between *Scn8a*$^{med/+}$ and WT mice

A, Hippocampal slices from *Scn8a*$^{med/+}$ mutants demonstrate longer latencies to the onset of burst activity compared to slices from WT mice for all age groups (WT *vs* mutant at P13-P15: 2.7 ± 0.2 min *vs* 3.8 ± 0.2 min, $p < 0.05$; WT *vs* mutant at P24-P26: 6.1 ± 0.8 min *vs* 11.1 ± 1.2 min, $p < 0.01$; WT *vs* mutant at P70-P84: 6.9 ± 0.9 min *vs* 9.2 ± 1.2 min, $p < 0.05$). Comparison of burst activity showed similar inter-burst frequency ***B***, and burst duration ***C***, between slices from *Scn8a*$^{med/+}$ mutants and WT mice. P13-P15, n = 4-5; P24-P26, n = 6-9; P70-P84, n = 3-5; Student's two-tailed t test, *$p < 0.05$; **$p < 0.001$; error bars indicate SEM. These experiments were performed by Brian Tanaka in the laboratory of Alan Goldin at the University of California, Irvine.

Genotype	Burst Occurrence	Burst Latency (min)	Inter-burst Frequency (Hz)
WT	9/9	7.3 ± 0.4 (9)	31.8 ± 2.9 (9)
Scn1a$^{RH/+}$	7/9	4.5 ± 0.3 (7)†	41.9 ± 6.2 (7)
Scn8a$^{med/+}$	2/14*	9.4, 12.7 (2)	20.2, 17.0 (2)
Scn1a$^{RH/+}$*; Scn8a*$^{med/+}$	1/13*$^{\#}$	6.3 (1)	14.3 (1)

Table 2.1. Decreased *Scn8a* expression reduced the occurrence of bursting in hippocampal slices from *Scn1a*$^{RH/+}$ mutant mice

Burst activity was recorded in slices exposed to elevated potassium from P24-P26 mice. The data are presented as means ± SEM, with the number of slices in the burst occurrence column and in parentheses. Values for burst latency and frequency are listed for *Scn8a*$^{med/+}$ mice. *$p < 0.006$ when compared to WT; Fisher's exact test with Bonferroni correction. $^{\#}p < 0.006$ when compared to *Scn1a*$^{RH/+}$ mice; Fisher's exact test with Bonferroni correction. $^{\dagger}p < 0.001$ when compared to WT; Student's t-test. These experiments were performed by Brian Tanaka in the laboratory of Alan Goldin at the University of California, Irvine.

Developmental expression profile of $Na_v1.6$ channels in the hippocampus

Because decreased burst activity was seen only in slices from *Scn8a*$^{med/+}$ mice older than P20, we investigated whether this decrease was correlated with changes in developmental expression of $Na_v1.6$ channels by performing Western blot analysis. $Na_v1.6$ was first detectable in the hippocampus at P10 and progressively increased until adult levels were reached between 3-4 weeks after birth (Fig. 3A). Expression levels of $Na_v1.6$ in *Scn8a*$^{med/+}$ mutant mice were qualitatively lower, as would be expected (Fig. 3A). To determine whether reduced *Scn8a* expression in *med* mutants is associated with altered levels of other VGSC alpha subunits, we compared *Scn1a* and *Scn2a* mRNA and protein levels from hippocampi of 3-month-old *Scn8a*$^{med/+}$ and WT littermates. Consistent with previous observations (Kearney et al., 2002), we found no significant differences in expression levels (Fig. 3 *B-C*).

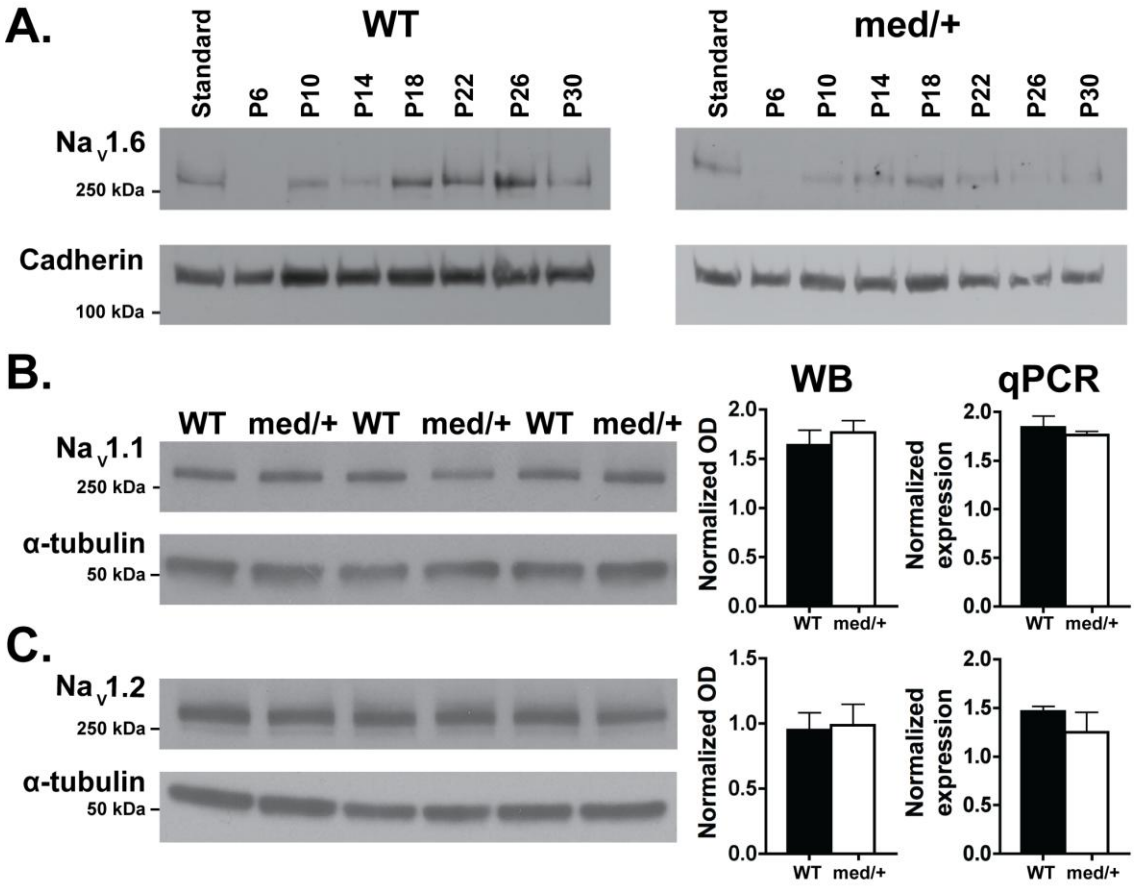

Figure 2.3. Developmental expression of VGSCs in the hippocampus of *Scn8a*$^{med/+}$ mutant and WT mice

A, Western blot analysis of hippocampal membrane fractions from WT and *Scn8a*$^{med/+}$ mutants (P6-P30) using rabbit anti-$Na_v1.6$ polyclonal antibody. Pan-cadherin (135 kDa) was used as a loading control. Hippocampal tissues from WT and *Scn8a*$^{med/+}$ mice were analyzed by Western blotting (WB) and qPCR for alterations in the expression of ***B***, *Scn1a* and ***C***, *Scn2a*. Alpha tubulin (50 kDa) was used a loading control. No significant differences in protein or RNA levels were observed. The standard sample consists of a mixture of WT P10, P22 and P30, as well as

Scn8a$^{med/+}$ mutant P10, P22 and P30 to achieve an average protein concentration to compare protein levels across different immunoblots. WB and qPCR data were analyzed by the Student's two-tailed t test, $p > 0.05$. WB, n = 7 per group; qPCR n = 4-5 per group. Error bars indicate SEM. Part ***A*** was performed by Brian Tanaka in the laboratory of Alan Goldin at the University of California, Irvine.

Cre recombinase induction leads to deletion of the floxed allele and reduced $Na_v1.6$ levels

To examine the effect of reducing *Scn8a* expression on seizure thresholds in adult mice, we crossed a tamoxifen (TAM)-inducible *Cre* line (*ER-Cre)* with *Scn8a* floxed mice to generate progeny in which inactivation of the *Scn8a* gene could be achieved by TAM injection. PCR analysis performed on hippocampal tissue from *flox/+,ER-Cre* mice 15 d after the last TAM injection detected a 300-bp PCR band, indicating deletion of exon 1 of the *Scn8a* gene (Fig. 4*A*). This PCR product was not observed in mice that were not administered TAM, or in mice that either lacked the floxed *Scn8a* allele or the *Cre* transgene (Fig. 4*A*). Reduced optical density (78% reduction) of the *Scn8a* band by Western blot analysis demonstrated reduced expression of the $Na_v1.6$ protein in *flox/flox,ER-Cre* mice that were administered TAM compared to *flox/flox,ER-Cre* mice that were administered vehicle (Fig. 4*B-C*).

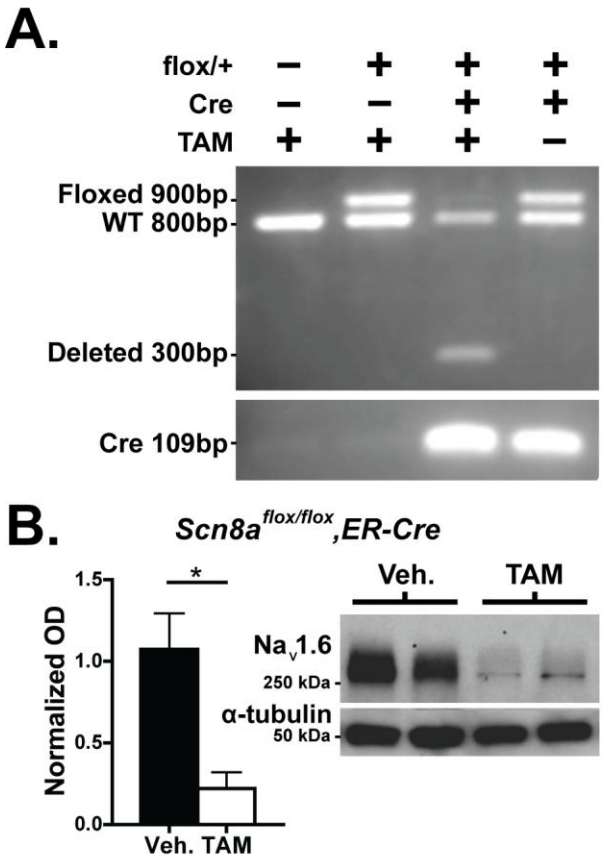

Figure 2.4. Tamoxifen-induced global deletion of the *Scn8a* gene

A, PCR product amplified from dissected neocortical tissue from *flox/+,ER-Cre,*TAM mice as well as control littermates (*flox/+,ER-Cre,*Veh) demonstrated that deletion is only detectable following TAM injection in mice that express the *ER-Cre* transgene and the floxed *Scn8a* allele (third lane). Additionally, the *Scn8a* floxed allele was only marginally detectable following TAM-initiated deletion, providing further evidence of efficient deletion. ***B***, Western blotting demonstrated significant (79%) knockdown of $Na_v1.6$ protein in homozygous floxed mice carrying the *ER-Cre* transgene following TAM injection (*flox/flox,ER-Cre,*TAM) compared to *flox/flox,ER-Cre* mice administered vehicle. n = 3 per group; Student's two-tailed t test, $*p < 0.05$; Error bars indicate SEM. ***C***. Representative Western blot from vehicle and TAM treated

flox/flox,ER-Cre mice demonstrates reduced band intensity in the TAM treated group. Error bars indicate SEM.

Inactivation of *Scn8a* leads to increased resistance to chemically and electrically induced seizures

Latencies to flurothyl-induced seizures following TAM-induced inactivation of the *Scn8a* allele were compared between *Scn8a*-deficiant animals (*flox/+*,*ER-Cre*,TAM) (white bar, Fig. 5*A*) and control littermates with normal levels of *Scn8a* (+/+,no *Cre*,TAM; +/+,ER-*Cre*,TAM; *flox/+*,no *Cre*,TAM; and *flox/+*,*ER-Cre*,Veh) (black bars, Fig. 5*A*). Myoclonic jerk latency was reduced in +/+,ER-*Cre*,TAM; *flox/+*,no *Cre*,TAM; and *flox/+*,*ER-Cre*,Veh animals but not +/+,no Cre,TAM mice compared to *flox/+*,*ER-Cre*,TAM animals. Significantly increased latencies to the GTCS were observed between *Scn8a*-deficient mice when compared to all control groups (Fig. 5*A*).

Latencies to KA-induced seizures were also compared between *Scn8a*-deficient (*flox/+*,*ER-Cre*,TAM) mice and control (*flox/+*,*ER-Cre*,Veh) mice. Latency to the first occurrence of each seizure stage on a modified Racine scale was recorded. Significantly increased latencies to stage 5 and stage 6 were observed in the *flox/+*,*ER-Cre*,TAM mice when compared to control littermates (Fig. 5*B*).

The 6-Hz model of psychomotor seizures was used to determine the effect of reducing *Scn8a* expression on electrically induced seizures. The severity of evoked seizures in $Scn8a^{flox/+}$,*ER-Cre* mice before and after TAM or vehicle administration was recorded using a modified Racine scale. A significant reduction in seizure severity was observed after TAM injection but not after vehicle injection (Fig. 5*C*). A trend toward a reduction in the percentage of mice exhibiting seizure activity was also observed following TAM administration, with 43% (3/7) of mice exhibiting seizures after TAM administration, compared to 89% (8/9) of mice exhibiting seizures after vehicle administration (Fig. 5*D*).

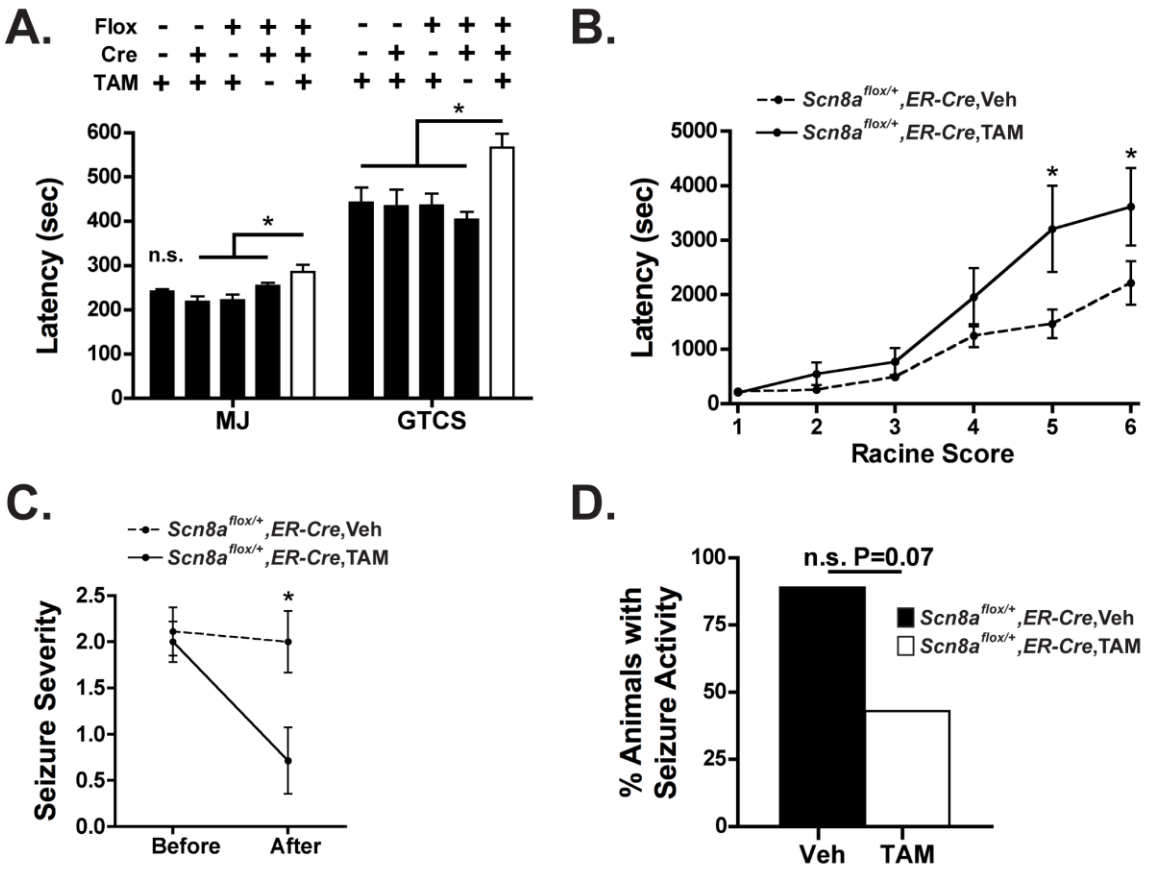

Figure 2.5. Inducible deletion of the *Scn8a* gene in the adult mouse is sufficient to increase the latency to flurothyl- and KA-induced seizures and to protect against electrically induced 6-Hz psychomotor seizures

A, Latencies to flurothyl-induced myoclonic jerk (MJ) and generalized tonic-clonic seizures (GTCS) were increased following TAM-induced inactivation of the *Scn8a* gene (*flox/+*,*ER-Cre*,TAM) (white bar) compared to control littermates (+/+,no *Cre*,TAM; +/+,ER-*Cre*,TAM; *flox/+*,no *Cre*,TAM; and *flox/+*,*ER-Cre*,Veh) (black bars). n = 10-12 per group. MJ and GTCS, one-way ANOVA, $p < 0.001$; Dunnett's post hoc, $p < 0.05$. ***B***, Latencies to KA-induced seizure events were increased following *Scn8a* deletion (*flox/+*,*ER-Cre*,TAM) (solid line) when

compared to vehicle-injected controls (*flox/+*,*ER-Cre*,Veh) (dashed line). Seizure activity was scored using a modified Racine scale: 1 = freezing, 2 = head nodding, 3 = tail clonus, 4 = forelimb clonus, 5 = rearing and falling, 6 = GTCS. n = 12-13 per group. Two-way ANOVA, $p < 0.01$; Bonferroni post hoc, $p < 0.05$. n = 12-13. ***C***, 6-Hz psychomotor seizure severity was decreased after TAM-initiated inactivation of *Scn8a* (*flox/+*,*ER-Cre*,TAM) (solid line) when compared to vehicle-injected controls (*flox/+*,*ER-Cre*,Veh) (dashed line). n = 7-9 per group. Mann-Whitney-U test, $p < 0.05$. Seizure activity was scored using the following modified Racine scale: 1 = freezing, 2 = head nodding 3 = rearing and falling. Average Racine scores: *flox/+*,*ER-Cre*,Veh. pre = 2.1, post = 2.0; *flox/+*,*ER-Cre*,TAM pre = 2.0, post = 0.4. ***D***, There was a trend toward reduced 6-Hz psychomotor seizure activity following inactivation of *Scn8a* (*flox/+*,*ER-Cre*,TAM) when compared to vehicle-injected controls (*flox/+*,*ER-Cre*,Veh). n = 7-9 per group; Fisher's exact test, n.s. $p = 0.07$. *$p < 0.05$; **$p < 0.01$; error bars indicate SEM

Lentiviral *Cre*-induced inactivation of the *Scn8a* gene in the hippocampus reduces seizure generation *in vivo*

To determine whether restricting *Scn8a* inactivation to the hippocampus would be sufficient to increase seizure resistance *in vivo*, LV-*Cre* or LV-*GFP* were injected into the hippocampus of *flox/flox* mice. *GFP*-positive cells were observed in the CA1, CA3, and DG layers of the hippocampus with highest expression in the DG and CA3 (Fig. 6*A*). Responses to picrotoxin (PT) were measured 15 days after injection of the lentiviral constructs. We observed a statistically significant reduction in the number of seizures in LV-*Cre*-injected mice compared to LV-*GFP*-injected controls (Fig. 6*B*); however, the average latency to the first seizure and the average seizure length were not significantly altered (Fig. 6*C-D*). Representative EEG recordings of baseline and seizure activity are shown for LV-*GFP*-injected controls and LV-*Cre*-injected mice (Fig. 6*E*).

Efficient shRNA-mediated knockdown of *Scn8a* in the hippocampus

An adeno-associated viral vector (AAV) expressing a small hairpin RNA (shRNA) against *Scn8a* **(**AAV-*Scn8a*-shRNA) or a control vector expressing a scrambled sequence (AAV-GFP) were injected into the hippocampus of WT and *Scn1a*$^{+/-}$ mice. Two weeks following injection, GFP positive cells were broadly observed in the CA1, CA3, and DG (Figure 2.7*A*). Hippocampi were dissected from WT and *Scn1a*$^{+/-}$ mice and $Na_v1.6$ (*Scn8a*), $Na_v1.1$ (*Scn1a*), and $Na_v1.2$ (*Scn2a*) protein levels were quantified by Western blot analysis. α-tubulin was detected on each blot and used to normalize protein loading (Figure 2.7*B*). Efficient knockdown (63.5%) of $Na_v1.6$ by the shRNA was observed in the hippocampus (Figure 2.7*C*). As expected, $Na_v1.1$ expression was reduced in *Scn1a*$^{+/-}$ animals. No significant change in $Na_v1.1$ or $Na_v1.2$ levels resulted from shRNA delivery.

Flurothyl thresholds are increased in WT and *Scn1a*$^{+/-}$ mice following shRNA-mediated knockdown of *Scn8a* expression in the hippocampus.

Latencies to flurothyl-induced seizures were measured in WT and *Scn1a*$^{+/-}$ mice two weeks following injection with either AAV-GFP or AAV-*Scn8a*-shRNA. The latency to the generalized tonic-clonic seizure was increased by 48% in WT animals injected with AAV-shRNA compared to WT animals injected with AAV-GFP (Mean GTCS latency, WT-shRNA = 461 ± 58 sec; WT-GFP = 238 ± 26 sec; one-way ANOVA, $p < 0.001$; Figure 2.8). Seizure latencies were increased by 46% in *Scn1a*$^{+/-}$ mice injected with AAV-shRNA compared to *Scn1a*$^{+/-}$ mice injected with AAV-GFP (Mean GTCS latency, *Scn1a*$^{+/-}$-shRNA = 255 ± 18 sec, *Scn1a*$^{+/-}$-GFP = 137 ± 23 sec; one-way ANOVA, $p < 0.05$; Figure 8). Seizure thresholds were not significantly different between WT mice injected with AAV-GFP and *Scn1a*$^{+/-}$ mice injected with AAV-shRNA (one-way ANOVA, $p > 0.05$; Figure 2.8), indicating that selective knockdown of *Scn8a* in *Scn1a* mutant mice was capable of restoring seizure latencies to WT levels.

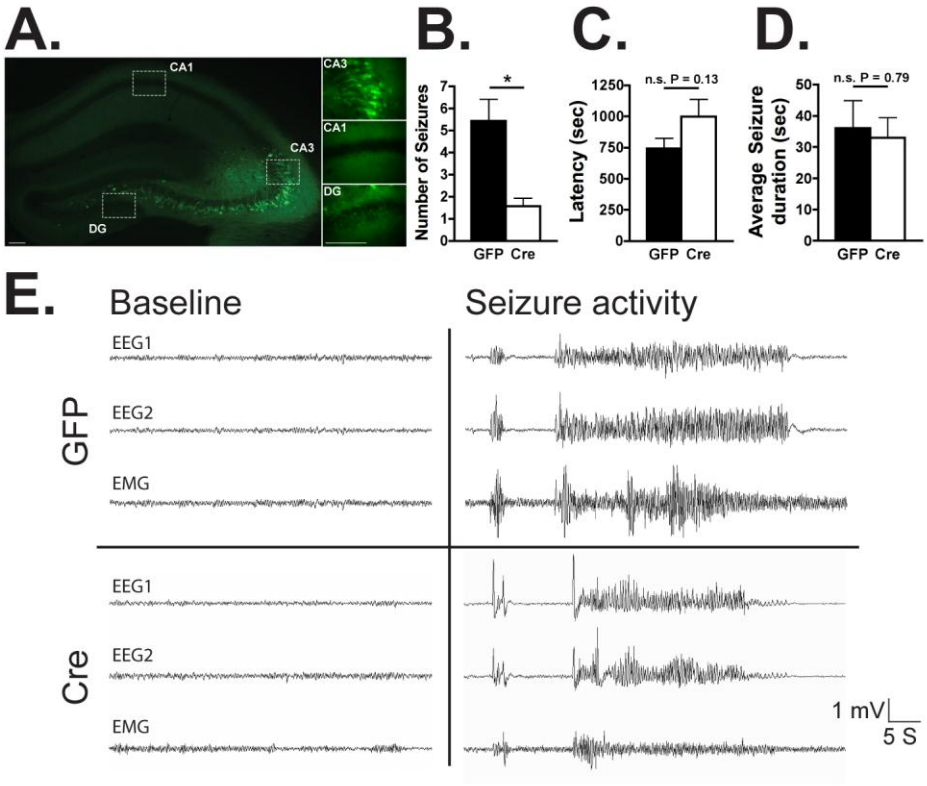

Figure 2.6. Lentiviral *Cre*-mediated knockdown of *Scn8a* in the hippocampus reduces seizure activity following PT administration

Scn8a$^{flox/flox}$ mice were injected with either LV-*GFP* or LV-*Cre* to achieve knockdown of *Scn8a* in the hippocampus. ***A***, *GFP*-positive cells were observed in the CA1, CA3, and DG layers of the hippocampus with highest expression in the DG and CA3. Images were captured at 4X and 40X magnification (inset), scale bar = 100 μm. ***B***, Fewer seizures were recorded in LV-*Cre*- compared to LV-*GFP*-treated mice following PT administration. No significant difference in the latency to the first seizure ***C***, or the average duration of each seizure event ***D***, was observed in LV-*Cre*-compared to LV-*GFP*-injected mice. ***E***, Representative examples of baseline EEG and seizure activity indicating normal baseline EEG activity in both *GFP* and *Cre* groups and seizure activity

in *Cre* and *GFP* groups following PT administration. n = 6-7 per group. Mann-Whitney-U test, *$p < 0.05$. Error bars indicate SEM.

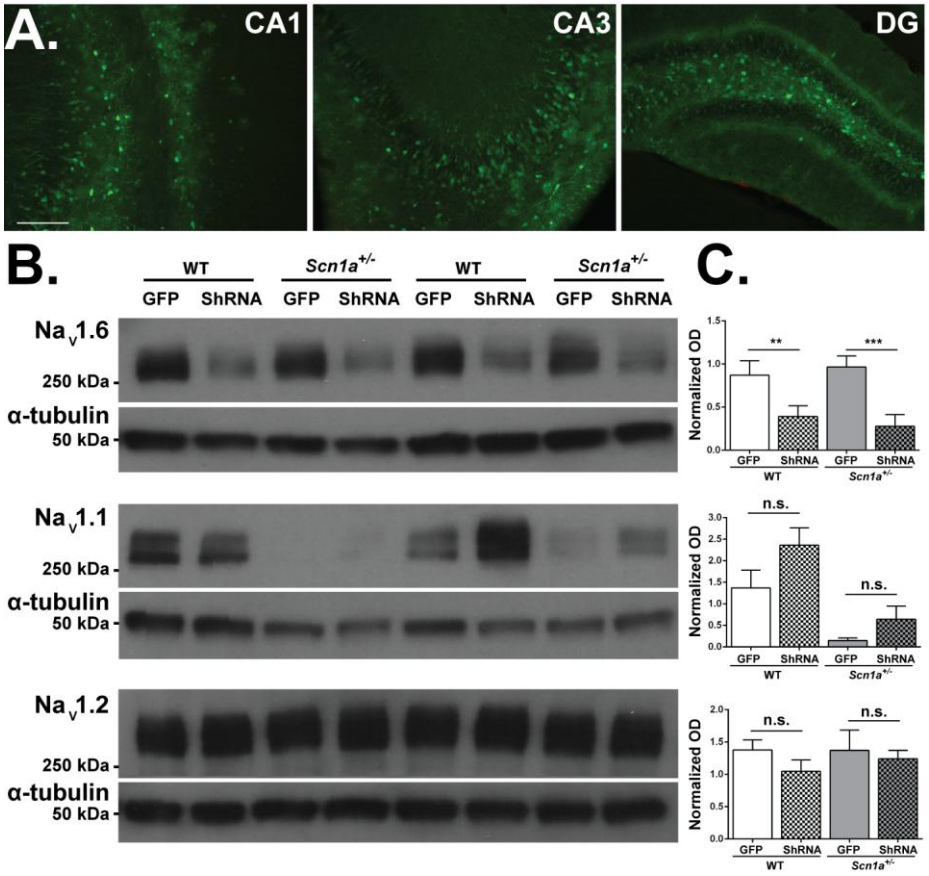

Figure 2.7. Efficient adeno-assoicated viral shRNA-mediated knockdown of the *Scn8a* gene in the hippocampus of *Scn1a*$^{+/-}$ and WT mice

A. GFP positive cells were observed in the CA1, CA3, and DG regions of the hippocampus following hippocampal injection of AAV-GFP and AAV-3 (*Scn8a*-shRNA) constructs. ***B.*** Representative immuno blots of dissected hippocampi taken from WT and *Scn8a*$^{+/-}$ mice two weeks following injection with either AAV-GFP (GFP) or AAV-shRNA (shRNA). Na$_v$1.6 (*Scn8a*), Na$_v$1.1 (*Scn1a*), and Na$_v$1.2 (*Scn2a*) were probed using the same hippocampal samples. α-tubulin was detected on each blot and used to normalize protein loading. **C.** Quantitative analysis of Western blots demonstrates efficient knockdown (63.5%) of Na$_v$1.6 by the shRNA in the hippocampus. As expected, Na$_v$1.1 expression is reduced in *Scn1a*$^{+/-}$ animals. The shRNA did not

significantly alter $Na_v1.1$ or $Na_v1.2$ levels. One-way ANOVA, Tukey *post-hoc*; $^{**}p < 0.01$, $^{***}p < 0.001$, n.s. $p > 0.05$; error bars represent SEM; n = 4 per group.

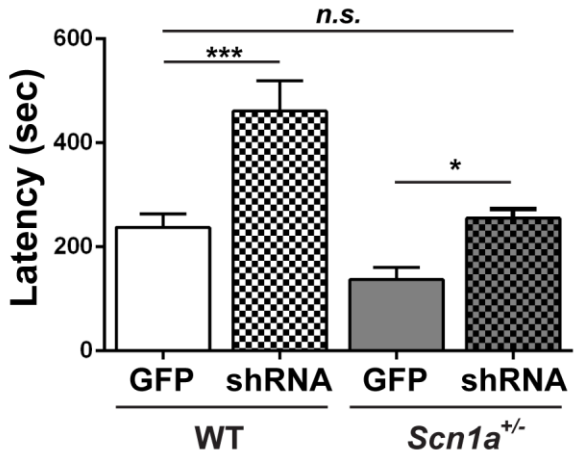

Figure 2.8. Adeno-associated viral shRNA-mediated knockdown of the *Scn8a* gene in the hippocampus increases flurothyl-induced seizure thresholds in *Scn1a*$^{+/-}$ and WT mice

GFP and shRNA AAV constructs were injected into the hippocampus of WT and *Scn1a*$^{+/-}$ mice. Seizure latencies in WT mice administered the shRNA were elevated when compared to GFP-injected WT littermates. Likewise, shRNA-knockdown increased seizure thresholds in *Scn1a*$^{+/-}$ mice when compared to GFP-injected *Scn1a*$^{+/-}$ littermates. No difference in seizure thresholds was detected between GFP-injected WT mice and shRNA-injected *Scn1a*$^{+/-}$ littermates. One-way ANOVA, Tukey *post-hoc*; *$p < 0.05$, ***$p < 0.001$, n.s. $p > 0.05$; n = 7-11 per group; error bars represent SEM.

2.4. Discussion

Previous studies examining the relationship between *Scn8a* and seizure resistance relied on the use of mice that expressed *Scn8a* mutations throughout development. To determine whether seizure protection would also be observed if *Scn8a* expression was reduced only in the adult brain, we used a TAM-inducible *Cre* transgenic line to initiate the inactivation of a floxed *Scn8a* allele in adult mice. We found that global reduction of *Scn8a* expression in the adult brain was capable of raising latencies to flurothyl- and KA-induced seizures. In addition, we found that reduced *Scn8a* expression in adult mice increased resistance to 6-Hz psychomotor seizures, a paradigm used to screen for novel anti-epileptic drugs (Brown, 1953; Barton et al., 2001). These results show that seizure protection can be achieved by reducing *Scn8a* expression in the adult brain, which is a critical requirement for an anticonvulsant therapy.

To test the hypothesis that reduced *Scn8a* expression leads to reduced hippocampal excitability and seizure suppression, we studied hippocampal slices from *Scn8a*$^{med/+}$ and WT littermates in a high-potassium model of epileptiform activity throughout postnatal development. We found that *Scn8a*$^{med/+}$ hippocampal slices were resistant to interictal-like burst discharges beginning at P20. There was an increase in the latency to epileptiform burst discharges in *Scn8a*$^{med/+}$ slices, suggesting that reduced *Scn8a* expression inhibits the initiation of bursting activity; however, there were no changes in inter-burst frequency or single burst duration relative to slices from WT mice. Our data indicate that there is a deficiency in epileptiform burst discharge initiation but not burst discharge propagation since epileptiform activity progresses comparably between WT and *Scn8a*-deficient slices following initiation.

$Na_v1.6$ channels have characteristic biophysical properties, including persistent current, resurgent current, and resistance to inactivation, which makes this isoform well suited for the sustained high-frequency firing that occurs at the axon initial segment and nodes of Ranvier, but

may also allow this channel to facilitate the propagation of high-frequency ictal activity (Raman et al., 1997; Zhou and Goldin, 2004). Despite these unique characteristics, *Scn8a*$^{med/+}$ mutant mice showed no significant changes in inter-burst frequency or single burst duration. It is possible that there are changes in action potential firing that we could not detect because they are below the sensitivity of our assay; or, it may be that the decreased seizure activity is a property of the overall network and therefore does not reflect simple changes in bursting in any one region. Prior studies have shown that mice with altered *Scn8a* expression have reduced persistent current and depolarized action potential spike thresholds in hippocampal pyramidal neurons that may impede the firing of repetitive action potentials (Royeck et al., 2008; Blumenfeld et al., 2009). These biophysical changes are consistent with the longer latency to the initial burst discharge and higher seizure threshold in *Scn8a*$^{med/+}$ mutants. These results suggest that reduced *Scn8a* expression leads to reduced hippocampal network excitability and consequently reduced susceptibility to epileptiform activity. We also demonstrated that reduced *Scn8a* expression suppresses the occurrence of burst discharges in the hippocampus of *Scn1a*$^{R1648H/+}$ mice thereby providing a mechanistic basis for our previous observations of ameliorated seizure phenotypes in *Scn1a* mutant mice that co-express *Scn8a* mutations (Martin et al., 2007; Hawkins et al., 2011). Parallel to our measurement of hippocampal bursting activity throughout early postnatal development, we also examined developmental changes in the expression levels of $Na_v1.6$ in the hippocampus. Consistent with previous observations, Western blot analysis revealed that $Na_v1.6$ is detectable by P10 and reaches adult levels by the third postnatal week (Plummer et al., 1997; Liao et al., 2010b). The emergence of reduced epileptiform burst discharges in *Scn8a*$^{med/+}$ mice coincided with the beginning of the developmental period in which *Scn8a* is highly expressed, and therefore likely to significantly influence neuronal excitability. This suggests that the reduced epileptiform bursting in *Scn8a*$^{med/+}$ mice is, in part, a consequence of lower *Scn8a* expression levels during this period. The expression levels of *Scn1a* ($Na_v1.1$) and *Scn2a* ($Na_v1.2$) were

unaltered in the hippocampi of adult *Scn8a*$^{med/+}$ mutants, which is consistent with previously reported observations on *Scn8a*$^{medJ/medJ}$ mice which have a 90% reduction in $Na_v1.6$ expression (Kearney et al., 2002).

Previous studies examining *Scn8a*-mediated seizure resistance raised the possibility of a self-reinforcing relationship between *Scn8a* expression and neuronal activity in which increases in neuronal activity lead to increased *Scn8a* expression, which in turn further increases neuronal excitability in the CA3 region of the hippocampus and contributes to epilepsy (Blumenfeld et al., 2009). Genetically reducing *Scn8a* expression might block this positive feedback cycle. An additional possibility is that *Scn8a* localization at the proximal axon initial segment of hippocampal DG neurons places these channels in a prime location to regulate the low-pass filtering capability of these neurons, which is thought to help protect the hippocampus from seizure activity (Hsu, 2007; Kress et al., 2010). Furthermore, DG neurons express comparatively lower levels of *Scn8a* when compared to CA3 (Kress et al., 2010), perhaps making their intrinsic excitability more sensitive to changes in *Scn8a* expression. These results, together with our findings, indicate that the hippocampus is a key region for *Scn8a*-mediated seizure resistance.

To directly test the hypothesis that targeting *Scn8a* in the hippocampus is sufficient to increase seizure resistance, we performed lentiviral-*Cre* and *GFP* injections into the hippocampus of conditional *Scn8a* mice (*flox/flox*) and measured response to PT administration. This approach resulted in a significant reduction in the number of electrographic seizures resulting from PT administration. However, the latency to the first electrographic seizure and the average duration of all seizure events were comparable between LV-*GFP* and LV-*Cre* groups.

Hippocampal hyperexcitability has previously been demonstrated in *Scn1a*$^{+/-}$ mice (Liautard et al., 2013). Moreover, hyperthermia-induced seizures were first detected in the hippocampus before spreading to the cortex (Liautard et al., 2013). These findings support the possibility that targeting the hippocampus may provide seizure protection in Dravet syndrome. To

test this hypothesis, we injected an AAV construct containing an shRNA that targets *Scn8a* into the hippocampus of WT and *Scn1a*$^{+/-}$ mice, which model Dravet syndrome. The shRNA produced efficient knockdown (63.5%) of the *Scn8a* protein ($Na_v1.6$) in the hippocampus. It is potentially interesting that a small but not statistically significant increase in *Scn1a* expression was observed in the hippocampus of WT mice injected with AAV-shRNA compared to AAV-GFP injected controls and also in *Scn1a*$^{+/-}$ mice injected with AAV-shRNA compared to *Scn1a*$^{+/-}$ mice injected with AAV-GFP (Figure 2.7). This may indicate that there is a compensatory increase in *Scn1a* expression in the hippocampus in response to loss of *Scn8a*. No change in *Scn2a* expression levels was observed in any group. Latencies to flurothyl-induced GTCS were found to be increased in both WT and *Scn1a*$^{+/-}$ mice compared to their genotype-matched AAV-GFP injected controls. Furthermore, no significant difference in average latency was observed between WT AAV-GFP and *Scn1a*$^{+/-}$ AAV-shRNA groups. Together, the LV-Cre and AAV-shRNA findings indicate that the hippocampus is an important regulator of *Scn8a*-dependent CNS excitability and supports the possibility that targeting of *Scn8a* may provide an efficacious treatment for some forms of epilepsy such as Dravet syndrome.

Although heterozygous *Scn8a* null mice (*Scn8a*$^{med/+}$) are visibly normal, they exhibit anxiety-like behavior and have spike-wave discharges that are characteristic of absence seizures (Burgess et al., 1995; McKinney et al., 2008; Papale et al., 2009). In one human family, *SCN8A* haploinsufficiency was associated with cognitive deficits (Trudeau et al., 2006). Additional studies will therefore be required to evaluate the effects on behavior and cognition of targeting *Scn8a* in epileptic animals. It is possible that normalizing the excitability of an epileptic region by targeting *Scn8a* will not result in the behavioral deficits that may occur when *Scn8a* is reduced in an otherwise normal animal. In addition, restricted targeting of *Scn8a* may reduce the likelihood of unwanted consequences. In support of this hypothesis, mice with hippocampal knockdown of *Scn8a* displayed normal visible behavior and no absence seizures during video/EEG recordings.

The *SCN8A* mutation N1786D was recently identified in a patient with severe epilepsy, cognitive deficits, and sudden unexpected death in epilepsy (SUDEP) (Veeramah et al., 2012). In addition, loss of the RNA-binding protein Celf4 has been shown to lead to an increase in *Scn8a* expression and to spontaneous seizure generation in mice (Sun et al., 2013). These findings seem to contradict observed improvements in seizure protection in *Scn8a* mutant mice. However, the available mouse models of *Scn8a* dysfunction have reduced sodium currents, whereas the N1786D is a gain-of-function mutation with increased persistent current (Veeramah et al., 2012), and Celf4 deficiency is believed to result in increased $Na_v1.6$ expression at the axon initial segment and increased persistent current (Sun et al., 2013). Thus, reduced $Na_v1.6$ currents likely lead to reduced neuronal excitability and seizure protection, whereas alterations that increase $Na_v1.6$ currents, in particular those that increase persistent current, lead to greater neuronal excitability and seizure susceptibility.

Conclusions

We have determined that hippocampal $Na_v1.6$ is an important regulator of neuronal excitability and seizure susceptibility. These results raise the possibility that targeting *Scn8a*, either genetically or with $Na_v1.6$ specific compounds, may be an efficacious treatment strategy for some forms of epilepsy.

2.5. Materials and Methods

Animals

C3HeB/FeJ-*Scn8a*^{med}/J mice (*Scn8a*$^{med/+}$, Jackson Laboratory, Bar Harbor, stock number 003798) were maintained on the C3HeB/FeJ background. The *med* mutation is the result of a spontaneous LINE element insertion in the second exon of the *Scn8a* gene leading to truncation and loss-of-

function of the channel (Kohrman et al., 1996a). *Scn8a*$^{med/+}$ male mice were crossed to C3HeB/FeJ females to generate *Scn8a*$^{med/+}$ and wild-type (WT) *Scn8a*$^{+/+}$ littermate controls. Mice expressing the UBC-Cre-ER^{T2} transgene (*ER-Cre*) were obtained from the Jackson Laboratory (stock number, 008085). *Scn8a*-floxed mice, in which exon 1 of the *Scn8a* gene is flanked by *loxP* sites (floxed allele), were a gift from Dr. Miriam Meisler at the University of Michigan, Ann Arbor (Levin and Meisler, 2004). The *ER-Cre* and *Scn8a*-floxed lines were maintained on the C57BL6/J background. Male *ER-Cre* mice were crossed to female *Scn8a*-floxed mice, producing progeny that express the floxed allele and the *ER-Cre* transgene (*flox/+*,*ER-Cre*). Controls consisted of offspring that express the floxed allele but lack the *ER-Cre* transgene (*flox/+*,no *Cre*), progeny that lack the floxed allele but carry the *Cre* transgene (+/+,*ER-Cre*), and progeny that lack the floxed allele and the *ER-Cre* transgene (+/+,no *Cre*). Vehicle-injected mice that carry both the floxed allele and the *ER-Cre* transgene were also used as controls (*flox/+*,*ER-Cre,* Veh.). Homozygous *Scn8a*-floxed mice that expressed the *ER-Cre* transgene *(flox/flox,ER-Cre*) were used to evaluate recombination efficiency. Homozygous floxed mice (*flox/flox*) were used for all experiments involving intrahippocampal viral *Cre* and *GFP* injections. AAV injections were performed on *Scn1a*$^{+/-}$ mice. These mice were a kind gift by William Catterall at the University of Washington. *Scn1a*$^{R1648H/+}$ mice were generated as previously described (Martin et al., 2010). Double heterozygous mutants (*Scn1a*$^{R1648H/+}$,*Scn8a*$^{med/+}$) were generated by crossing *Scn1a*$^{R1648H/+}$ with *Scn8a*$^{med/+}$ mutant mice. All crosses yielded genotypes in expected Mendelian ratios. Littermates were used for all experiments to minimize confounds associated with differences in rearing conditions and genetic background. Experimenters were blinded to subject groups during data collection and analysis. Mice were maintained on a 12 h light/dark cycle. Food and water were available *ad libitum*. All experimental procedures were performed in accordance with the guidelines of Emory University and the University of California, Irvine Institutional Animal Care and Use Committees.

Genotyping

The presence of the *Cre* transgene and the *Scn8a* floxed allele was determined by PCR analysis using the primer pairs CreF/CreR (TGA CCC GGC AAA ACA GGT AGT TA / TTC CCG CAG AAC CTG AAG ATG TT) and FloxF/FloxR (GTG TGT GAT TCT CAA CAG TGG GTT / GTC TGT AAG AAG GCC TGA AAG TGA), respectively (Levin and Meisler, 2004). The *Scn8a*-med mutation was identified as previously described (Martin et al., 2007) using the primer pair medF/medR (TCC AAT GCT TAT ACC AAA AGT CCC / GGA CGT GCA CAC TCA TTC CC). *Scn1a*$^{R1648H/+}$ mice were genotyped as previously described (Martin et al., 2010).

Tamoxifen-induced inactivation of Scn8a

Individually housed 2-month-old mice were intraperitoneally (i.p.) administered tamoxifen (TAM, 100 mg/kg, Sigma-Aldrich) or vehicle (corn oil, Sigma-Aldrich) for 5 consecutive days. TAM was prepared by dissolving in 100% ethanol and then mixing with 300 μl of corn oil. Excess ethanol was evaporated by vacuum centrifugation. Mice were left undisturbed for 15 days after the last injection.

Preparation and incubation of slices

Mice were anesthetized with halothane, decapitated, and their brains were placed in ice-cold sucrose artificial cerebrospinal fluid (ACSF) containing (in mM): 85 NaCl, 65 sucrose, 2.5 KCl, 25 glucose, 1.25 NaH_2PO_4, 4 $MgSO_4$, 0.5 $CaCl_2$, and 24 $NaHCO_3$. Transverse hippocampal slices (350 μm) were cut using a Leica VT1000S vibrating blade microtome (Leica, Germany). Slices were incubated at 33°C for at least 1 h before electrophysiological recordings in oxygenated

(95% O_2, 5% CO_2) standard ACSF containing (in mM): 126 NaCl, 2.5 KCl, 1.25 $NaHPO_4$, 1.2 $MgSO_4$, 10 glucose, 1.2 $CaCl_2$, and 24 $NaHCO_3$.

Electrophysiological recordings

Slices were submerged in a recording chamber and continuously perfused at 2 mL/min with oxygenated ACSF at 33°C during electrophysiological experiments. Cells were visualized with an upright microscope (Zeiss Axioskop Plus) equipped with infrared differential interference contrast optics. Recording pipettes (2-5 MΩ) were pulled from borosilicate glass (Sutter Instruments, Novato, CA) with a P-87 Flaming-Brown puller (Sutter Instruments). Electrophysiological recordings were obtained in current clamp mode using MultiClamp 700B amplifier at 100X AC (Molecular Devices, Union City, CA) and digitized with a Digidata 1322A digitizer (Molecular Devices). Continuous extracellular recordings were acquired at 10 kHz and population spikes were recorded at 50 kHz. All recordings were low-pass filtered at 1 kHz for offline analysis with pClamp 10.2 software (Molecular Devices).

For extracellular recordings, pipettes were filled with 150 mM NaCl and positioned in the CA3 stratum pyramidal layer. ACSF with elevated potassium was prepared by supplementing standard ACSF with 3 M KCl to raise the potassium concentration to 8.5 mM $[K^+]_O$. The experimental paradigm consisted of a control recording for 2-5 min in standard ACSF, followed by 20-25 min with 8.5 mM $[K^+]_O$, in which burst activity was recorded. To evoke population spikes, constant-current stimuli (100 msec) were applied via stimulus isolator (A365D; WPI, Sarasota, FL) using a bipolar tungsten electrode (50 μm in diameter; A-M Systems, Carlsborg, WA) positioned in the mossy fiber tract. Population spikes were evoked in physiological 2.5 mM $[K^+]_O$ before and after exposing the slice to 8.5 mM $[K^+]_O$. Slices in which population spike amplitudes did not change more than 20% after exposing the slice to 8.5 mM $[K^+]_O$ were used for analysis.

Protein extraction

Hippocampi were dissected and frozen at -80°C. To determine developmental changes in *Scn8a* expression, individual hippocampi were pooled from 10-15 mice at each age. Hippocampi from adult, 2-3-month-old, mice were not pooled. Hippocampi were homogenized on ice using a Dounce homogenizer in homogenization buffer (320 mM sucrose, 5 mM Na phosphate, pH 7.4, 100 mM Na fluoride and protease inhibitor (Pierce, Rockford, IL) or 50 mM Tris, pH = 7.5; 10 mM EGTA, and one complete EDTA-free protein inhibitor tablet (Roche, Germany) per 50 mL solution. Homogenates were centrifuged at 750 x g for 10 min at 4°C, and the supernatant was centrifuged at 39,000 x g for 30 or 60 min at 4°C. The pellet was suspended in protease inhibitor buffer and stored at -80°C. BCA (Thermo Fisher Scientific, Waltham, MA) or Bradford (Bio-Rad, Hercules, CA) protein assays were used to normalize protein concentrations across samples.

Western blot analysis

Membrane-enriched whole-brain or hippocampal tissue homogenates (15-30 ug) were subjected to SDS-PAGE electrophoresis. After blocking in 5% milk, blots were incubated overnight at 4°C in either polyclonal rabbit anti-$Na_v1.6$ primary antibody (1:200, Millipore, Billerica, MA), polyclonal rabbit anti-$Na_v1.6$ (1:225, Alomone, Israel), polyclonal rabbit anti-$Na_v1.1$ (1:200, Millipore), or monoclonal mouse anti-$Na_v1.2$ (1:1000, Neuromab, Davis, CA). Blots were then incubated in either HRP-conjugated donkey anti-rabbit secondary (1:10,000, GE Healthcare, United Kingdom), HRP-conjugated goat anti-mouse secondary (1:10,000, Jackson ImmunoResearch, West Grove, PA), or HRP-conjugated goat anti-rabbit secondary (Sigma, St. Louis, MO, 1:16,000) for 1 h followed by washing in SuperSignal West Pico Chemiluminescent substrate (Pierce) and imaging. Blots were also probed using a monoclonal mouse anti-α-tubulin

(1:10,000, Millipore) or monoclonal mouse anti-pan-cadherin (1:100,000, Sigma) antibody followed by HRP-conjugated goat anti-mouse secondary (1:10,000, Jackson ImmunoResearch) or HRP-conjugated goat anti-mouse secondary (Pierce, 1:26,000) for normalization of sample loading. Image quantification was performed using ImageJ software (NIH).

Quantitative real-time PCR

Total RNA was extracted from the hippocampus of WT and *Scn8a*$^{med/+}$ adult mice using the RNeasy Lipid Tissue Mini Kit (Qiagen, Germany). All RNA samples were quantified using a NanoDrop 1000 Spectrophotometer (Thermo Fisher Scientific), and RNA quality was determined by agarose gel electrophoresis. RNA was reverse-transcribed into cDNA using random hexamer primers and SuperScript III reverse transcriptase (Invitrogen, Carlsbad, CA). *Scn1a* (F: TCA GGA GGA AGG GGT TTC GCT TC, R: CCC CAC ATC CTT GGC TCG CCC TC) and *Scn2a* (F: CTG CAA CGG TGT GGT CTC CCT AG, R: ATG TAG GGT CTT CCA ACA AGT CC) primers were designed to span introns to avoid amplification of genomic DNA. Each primer pair generated standard curves with efficiencies of 90-100%. Real-time PCR (qPCR) data were generated from cDNA samples in technical triplicate using the BioRad CFX96 Real-Time PCR Detection System and SYBR Green fluorescent dye (BioRad). Expression levels were normalized to beta-actin (F: CAG CTT CTT TGC AGC TCC TT, R: ACG ATG GAG GGG AAT ACA GC). Expression analysis and statistics were performed using the GenEx 5 software (MultiD).

Lentiviral and adeno-associated viral constructs

Previously described viral vectors expressing green fluorescent protein (LV-*GFP*) or *Cre*-recombinase (LV-*Cre*) were obtained from the Emory University Viral Core (Heldt et al., 2007). Briefly, LV-*GFP* viral vectors were derived from the pLV-CMV-GFP-U3Nhe backbone. LV-*Cre* viral vectors were created by replacing the *GFP* coding sequence with *Cre*-recombinase coding

sequence using the BamH1/Sal1 restriction sites in the pLV-CMV-GFP-U3he backbone. Viral production procedures have been described previously (Miyoshi et al., 1998; Pfeifer et al., 2001). Viral titer of the LV-*GFP* and LV-*Cre* was assessed in HEK-293T cells and ranged from 1 x 10^8 to 1 x 10^9 infectious particles per ml.

Adeno-associated viral (AAV) constructs were produced by the University of Pennsylvania Vector Core. Scrambled sequence was placed downstream of the U6 promoter in addition to GFP. This virus is referred to as AAV-GFP. The shRNA construct was also placed downstream of the U6 promoter along with a GFP sequence. This construct is referred to as AAV-*Scn8a*-shRNA. Viral titer of the AAV-GFP and AAV-*Scn8a*-shRNA ranged from 1 x 10^8 to 1 x 10^9 infectious particles per ml.

Surgical procedures

Surgical implantation of EEG electrodes was performed as previously described (Martin et al., 2007; Dutton et al., 2012; Papale et al., 2013). Mice were anesthetized by isoflurane inhalation, and then fixed in a stereotaxic apparatus (Kopf, Tujunga, CA). Four holes were drilled in the skull above each injection site. Injections were performed using a Hamilton 0.5-μl microsyringe (model #75) and 30-gauge needle. Four injection sites were chosen to target the hippocampus at the following coordinates, from bregma: anteroposterior (AP), -1.9 mm; mediolateral (ML), ±1.1 mm, ±2.1 mm; dorsoventral (DV), -1.9 mm. The syringe was lowered to -2.0 mm, and then retracted to -1.9 mm and left in place for 4 min. Virus solution (1.0 μl) was injected into each site at a rate of 0.12 μl/min. After each injection, the syringe was left in place for 4 minutes before being retracted. Following viral injections, 4 sterile cortical screw electrodes (Vintage Machine Supplies, OH) were implanted subdurally in the skull for EEG recordings at the following

coordinates, from bregma: 1.5 mm (AP) and +2.1 mm ML; -1.9 mm AP and ±2.1 mm ML; 0.5 mm AP and -2.1 mm ML. Fine-wire electrodes were implanted into the neck muscle for EMG acquisition. Incisions were closed with tissue adhesive (Vetbond, 3M; St. Paul, NM), and the animal was allowed to recover on a heating pad. Postoperative analgesic (ibuprofen, 0.1 mg/kg) was provided for 3 days in the drinking water.

Histological procedures

Mice were anesthetized using isoflurane and transcardially perfused with 4% paraformaldehyde (PFA) 15-20 d following LV-*GFP* injection. Brains were post-fixed for 2 h in ice-cold 4% PFA, and then transferred to 30% sucrose for 3 d at 4°C. Coronal sections (45 μm) were sliced using a cryostat (Leica) between bregma -1.0 mm and -4.0 mm. Sections were washed in TBS/Triton-X and mounted. Images were collected using a Leica DM6000 B upright fluorescence microscope and Simple PCI software.

Seizure induction paradigms

Flurothyl seizure induction. Flurothyl seizure induction was performed as previously described (Martin et al., 2007; Martin et al., 2010). Briefly, 3-month-old mice were placed in a clear Plexiglas chamber. Flurothyl (2,2,2-trifluroethyl ether, Sigma-Aldrich) was introduced at a rate of 20 μl/min. The latencies to the first myoclonic jerk (MJ) and generalized tonic-clonic seizure (GTCS) were recorded. The MJ was defined as a jerking movement of the neck and shoulders sometimes associated with tail clonus. The GTCS was defined as complete loss of postural control associated with forelimb and hindlimb tonic-clonic movement lasting longer than 3 s.

Kainic acid (KA) seizure induction

Three-month-old mice were administered KA (i.p., 25 mg/kg, Sigma-Aldrich) and observed for 2 h. The latency to the first occurrence of each event on a modified Racine scale was recorded: 1 = freezing, 2 = head nodding, 3 = tail clonus, 4 = forelimb clonus, 5 = rearing and falling, 6 = GTCS. The GTCS was defined as complete loss of postural control associated with forelimb and hindlimb tonic-clonic movement lasting longer than 3 s.

6-Hz psychomotor seizure induction

A brief electric current (6-Hz, 26 mA, 3-ms pulse width, 3-s duration) was applied to the cornea of 3-month-old mice (Ugo Basile S.R.L, Germany). Seizure severity was recorded using the following modified Racine scale: 1 = staring, 2 = forelimb clonus, 3 = rearing and falling. Mice that did not exhibit seizure activity in response to the first exposure were excluded from the study and did not proceed to receive TAM or vehicle. Those mice that exhibited seizure activity were placed into two groups for TAM or vehicle administration. These groups were balanced based on seizure severity to ensure that seizure susceptibility was comparable between groups before administration of TAM or vehicle. TAM or vehicle injections were initiated one day after the first current exposure. Two weeks after the last TAM injection, the mice underwent 6-Hz seizure induction a second time.

Picrotoxin (PT) seizure induction

Fifteen days following either LV-*Cre* or LV-*GFP* hippocampal injection and surgical EEG implantation, PT seizure induction was performed as previously described (Distler et al., 2013). Video/EEG recordings were collected and amplified using the Stellate Harmony System and software (Natus Medical, Inc., San Carlos, CA). Signals were filtered (EEG 0.3-35 Hz bandpass, EMG 10-70 Hz bandpass) and digitized at a sampling rate of 200 Hz. Twenty min of baseline video/EEG recording was collected before administering PT. Following PT administration (i.p.,

10 mg/kg, Sigma-Aldrich), the latency to the first seizure, duration of each seizure, and number of seizures were recorded. Seizures were defined behaviorally by the presence of generalized convulsions and confirmed by the presence of highly synchronous EEG activity that reached at least twice the baseline amplitude in all cortical EEG channels and persisted for at least 3 s. Video/EEG monitoring was performed for at least 2 h following PT administration.

Statistics

All bar graphs indicate the mean and all error bars represent ± standard error of the mean (SEM). Statistical analyses were performed using SigmaPlot 11.0 software (Systat Software Inc., Chicago, IL), Prism 6 (GraphPad Software Inc, La Jolla, CA), and GenEx 5 software (Multi D). The Levene's test was used to assess for differences in the variance between groups, and the Shapiro-Wilk test was used to determine normality of continuous data sets. One-way analysis of variance (ANOVA) was used to evaluate seizure thresholds between ER-*Cre* groups treated with flurothyl. Two-way analysis of variance (ANOVA) was used to evaluate KA seizure thresholds. *Post-hoc* comparisons were performed using either the Dunnett's or Bonferroni test. The Student's two-tailed t test was used to analyze the percentage knockdown of *Scn8a* protein levels by the ER-*Cre* transgene and by LV-*Cre* injection, as well as to compare qPCR results between genotypes for each sodium channel. qPCR expression analysis and statistics were performed using the GenEx 5 software. Student's two-tailed t test was also used to determine the significance of burst discharge latency, duration, and frequency, and Fisher's exact test with Bonferroni correction was used to compare the occurrence of burst discharges. Fisher's exact test was used to assess categorical seizure outcomes following 6-Hz seizure induction. The Mann-Whitney-U test was used to assess PT seizure outcomes.

2.6. Acknowledgements

Research in this publication was supported by the National Institute of Neurological Disorders and Stroke (NINDS) of the National Institutes of Health (NIH) under award numbers R01NS072221 (A.E.), R01NS048336 (A.L.G.), R01NS065187 (A.E. and A.L.G.), and F31NS074717 (C.D.M). The content is solely the responsibility of the authors and does not necessarily represent the official views of the NIH. We would like to thank the Emory University Viral Core for assistance with reagents and Dr. Miriam Meisler for providing the *Scn8a* floxed line. We would also like to thank Karoni Dutt and Eric Velazquez for helpful discussions during the course of this work and Cheryl Strauss for editorial assistance.

CHAPTER 3

Effects of an Epilepsy Mutation in the Voltage Sensor of *Scn8a* on Seizure Susceptibility and Behavior

Chapter 3 contains material from the manuscript in preparation: Effects of an epilepsy mutation in the voltage sensor of *Scn8a* gene on seizure susceptibility and behavior, Makinson C.D., Dutt K., Papale A. L., Shankar A., Lin F., Liu R., Goldin A. L., Escayg A.

3.1. Summary

Voltage gated sodium channels are involved in the pathophysiology of epilepsy as they regulate neuronal excitability, facilitate synaptic integration, and contribute to the initiation and propagation of action potentials. Mutations in *SCN1A*, *SCN2A* and *SCN3A* have been identified in patients with various subtypes of epilepsy. In contrast, we demonstrated that *Scn8a*^{med} and *Scn8a*^{medjo} mice that carry mutations in the *Scn8a* gene display elevated thresholds to flurothyl and kainic acid-induced seizures. However, these mutants also display spontaneous absence epilepsy. To further investigate the relationship between altered *Scn8a* function and epilepsy, we introduced the R1648H-*SCN1A* mutation, identified in a family with generalized epilepsy with febrile seizures plus (GEFS+), into the corresponding position in *Scn8a* (R1627H). Mice homozygous for the *Scn8a* R1627H mutation (*Scn8a*$^{RH/RH}$) display a normal lifespan; however, they exhibit an unstable gait, impaired performance in the rotarod test and reduced locomotor activity. Heterozygous (*Scn8a*$^{RH/+}$) mice are more resistant to chemically and electrically-induced seizures when compared to wildtype littermates and the *Scn8a*-R1627H mutation was found to increase the lifespan and seizure thresholds of mice carrying the *Scn1a*-R1648H mutation. Interestingly, *Scn8a*$^{RH/RH}$ mice have comparable seizure thresholds to WT littermates and appear to be susceptible to audiogenic seizures. In addition, unlike previously reported *Scn8a* mutant mice, spontaneous absence seizures were not been observed in R1627H mutants. Together these results 1) support previous findings that altered *Scn8a* function provides resistance to seizures and leads to improvements in *Scn1a* epilepsy models; 2) demonstrate that some alterations of *Scn8a* function may provide resistance to generalized tonic clonic seizures without leading to absence epilepsy; 3) expands the known epilepsy phenotypes associated with altered *Scn8a*.

3.2. Introduction

Voltage-gated sodium channels (VGSCs) are important regulators of neuronal excitability and are responsible for the initiation and propagation of action potentials in neurons. Given their fundamental role in neuronal communication, disruptions in VGSC function can lead to a host of pathophysiological conditions (George, 2005; Mantegazza and Catterall, 2012). Most notably, mutations in the four VGSCs that are primarily localized to the CNS, *SCN1A*, *SCN2A*, *SCN3A*, and *SCN8A*, are responsible for several types of idiopathic epilepsy. Specifically, *SCN1A* mutations lead to genetic epilepsy with febrile seizures Plus (GEFS+) and Dravet syndrome (DS) (Escayg et al., 2000; Claes et al., 2001), *SCN2A* mutations cause benign familial neonatal-infantile seizures (Heron et al., 2002), mutations in *SCN3A* have been identified in patients with partial epilepsy (Holland et al., 2008; Estacion et al., 2010; Vanoye et al., 2013), and mutations in *SCN8A* were recently found in patients with epileptic encephalopathies (Veeramah et al., 2012; Carvill et al., 2013).

Based on the VGSC mutations that have been identified to date, it is clear that distinct seizure and behavioral outcomes can result from different mutations in the same VGSC gene, with the magnitude and direction of the observed phenotypes potentially reflecting specific biophysical changes caused by the mutation. For example, in the spectrum of *SCN1A* epilepsies, the most severe condition, DS, often results from null mutations in the *SCN1A* gene, while amino acid substitutions can give rise to less severe forms of epilepsy such as GEFS+ (reviewed in (Claes et al., 2009; Lossin, 2009; Escayg and Goldin, 2010). Furthermore, a gain-of-function substitution *SCN8A* mutation (N1768D), that was found to increase sodium currents, was identified in a patient with epileptic encephalopathy (Veeramah et al., 2012), whereas cognitive and motor deficits but not epilepsy has been described in a family with a loss-of-function truncation mutation in the *SCN8A* gene (Trudeau et al., 2006).

The introduction of clinically relevant VGSC mutations into mouse models have proven critical to our understanding of the functional consequences of distinct VGSC mutations on seizure and behavioral phenotypes. The expression of loss-of-function *Scn1a* mutations in mice recapitulates many of the clinical features of DS and GEFS+ (Yu et al., 2006; Martin et al., 2010). Similarly, mice with loss-of-function *Scn8a* mutations exhibit behavioral alterations that are consistent with psychiatric findings in patients (McKinney et al., 2008; Papale et al., 2010). Interestingly, we demonstrated that mutations that reduce the activity of *Scn8a* in the mouse confer resistance to induced seizures (Martin et al., 2007; Hawkins et al., 2011), and result in the generation of absence epilepsy (Papale et al., 2009).

To better understand the phenotypic consequences of altered *Scn8a* function, we generated a novel mouse mutant in which the well-characterized *SCN1A* mutation R1648H, first identified in a family with GEFS+ (Escayg et al. 2000), was knocked into the corresponding location in the mouse *Scn8a* gene. The mutant line (*Scn8a*-R1627H) was evaluated for seizure susceptibility, spontaneous seizure generation, behavioral deficits, and neuronal excitability.

3.3. Results

The R1627H mutation alters voltage dependent activation, recovery from inactivation and persistent current

In order to identify possible alterations in the biophysical properties of $Na_v1.6$ channels that result from the R1627H mutation, recordings of Xenopus oocytes expressing WT and mutant channels were first performed. We found that the R1627H mutation causes a depolarizing shift in the voltage dependence of activation (Figure 3.1*A*) and leads to accelerated recovery from inactivation (Figure 3.1*B*). Increased persistent current was observed in oocytes expressing R1627H channels (Figure 3.1*C*). No change in use dependence was observed (Figure 3.1*D*).

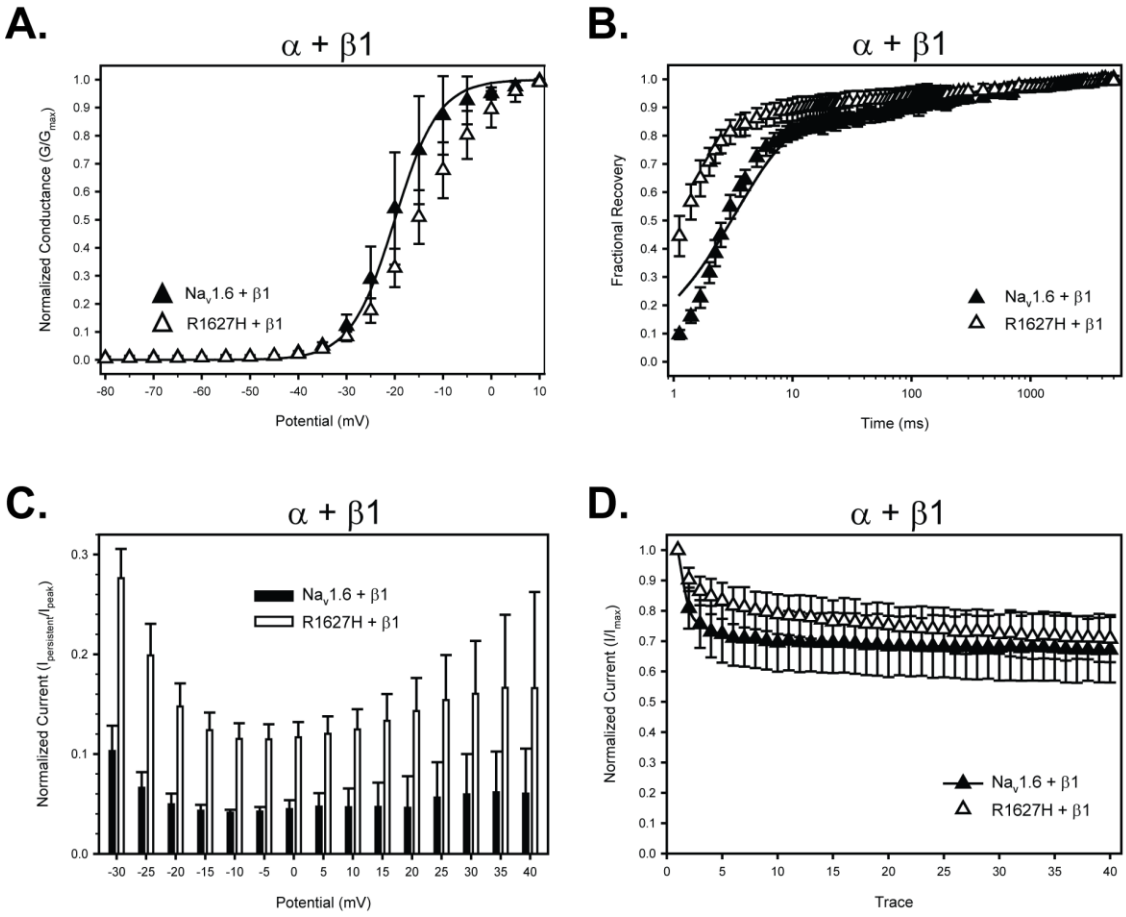

Figure 3.1. Characterization of the biophysical properties of *Scn8a*-R1627H channels

A. Xenopus oocyte recordings demonstrate that the R1627H mutation leads to a depolarizing shift in voltage-dependent activation. ***B.*** R1627H channels have accelerated recovery from inactivation. ***C.*** At holding potentials from -30 to +40 mV, R1627H channels exhibit increased persistent current. ***D.*** The R1627H mutation did not influence use dependence. These experiments were performed by A.J. Barela in the laboratory of Alan Goldin at the University of California, Irvine.

Targeted insertion of the R1627H into the mouse *Scn8a* gene

To further examine the effect of the R1627H mutation, we generated a mouse model of *Scn8a* dysfunction by knocking in the human *SCN1A* R1648H GEFS+ mutation into the corresponding position in the mouse *Scn8a* gene (R1627H) (Figure 3.2). Neomycin-resistant ES cell clones were screened for correct targeting by PCR amplification of the 3' and 5' arms of homology. Correct targeting was further verified by Southern blot analysis of the ES clones (Figure 3.2*A*). Selected ES cell clones were injected into blastocysts to generate chimeric mice. The targeted allele was confirmed in the knock-in mice by Southern blot analysis (Figure 3.2*B*). Western blotting was performed on whole brain membrane enriched tissue from three $Scn8a^{RH/RH}$, $Scn8a^{RH/+}$, and WT littermates. Protein levels of $Na_v1.1$, $Na_v1.2$, $Na_v1.3$, and $Na_v1.6$ were compared. No changes in VGSC expression was observed between WT, $Scn8a^{RH/+}$ or $Scn8a^{RH/RH}$ mice, indicating that knock-in of the R1627H mutation did not lead to altered protein levels (Figure 3.2*C*).

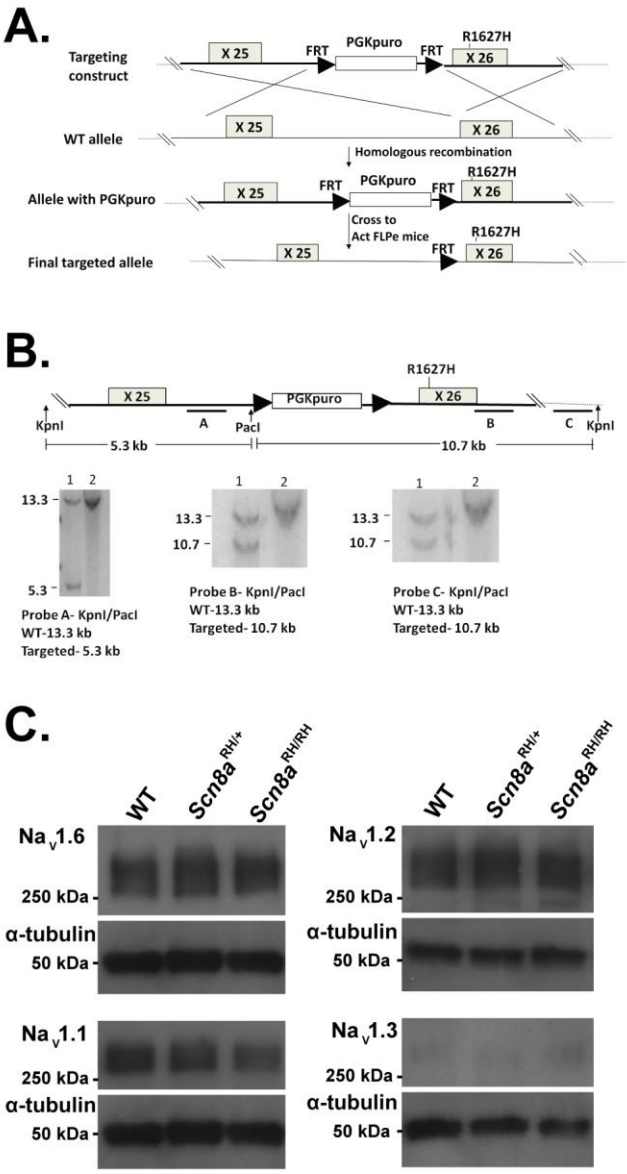

Figure 3.2. Generation of the R1627H mutant mouse line

A. Diagram of the strategy for introducing the R1627H mutation into the mouse *Scn8a* gene. The targeting construct was designed in introduce the R1627H mutation into exon 26 of the *Scn8a* gene and a PGKpuro transgene flanked by FRT sites for selecting embryonic stem cells that incorporated the construct. Targeted mice were crossed to FLP mice to remove the PGKpuro

transgene. ***B.*** Southern blotting was used to verify proper targeting of the construct. Arrows indicate expected fragment sizes on Southern blots following digestion with *Kpn*I and *Pac*I. *Kpn*I cuts upstream of the 5' arm and downstream of the 3' arm while PGKpuro contains the *Pac*I site. Three probes were used for hybridization, 2 internal probes (*A* and *B*) for the 5' and 3' arms of homology and an external probe *C* downstream of the 3' arm of homology. Each blot contains DNA from a targeted heterozygous ES cell (lane1) and a wild-type mouse (lane 2). Bands of the expected sizes corresponding to the targeted and wild-type alleles can be seen in lane 1 with all probe/enzyme combinations. A single band corresponding to the wild-type allele is seen in lane 2. ***C.*** Western blot analysis was used to confirm that R1627H knock-in mice have normal levels of expression of the major CNS VGSCs. No change in $Na_v1.6$. $Na_v1.1$, $Na_v1.2$, or $Na_v1.3$ was detected. α-tubulin was used to control for differences in loading (n = 3-4 per group). Experiments ***A-B*** were performed by Anupama Shankar in the laboratory of Andrew Escayg.

Survival, weight, and video monitoring of the R1627H line

Mice were monitored, weighed, and videotaped weekly from P10 to P120 in order to examine locomotor function and to make general assessments of health and survival. R1627H mice were born in the expected Mendelian ratio (1:2:1) (WT = 24, *Scn8a*$^{RH/+}$ = 36, *Scn8a*$^{RH/RH}$ = 28) and have a normal lifespan. However, *Scn8a*$^{RH/RH}$ mutants gain weight more slowly so that by 14 weeks of age the average weights of male and female *Scn8a*$^{RH/RH}$ mice were 5.6% (males) and 9.5% (females) less than WT and *Scn8a*$^{RH/+}$ sex-matched littermates, respectively (Figure 3.3). While WT and *Scn8a*$^{RH/+}$ mice appeared visibly normal, body tremors and uncoordinated gait were observed in *Scn8a*$^{RH/RH}$ mutants by the third postnatal week and persisted throughout the life of the animal. The hind legs of *Scn8a*$^{RH/RH}$ mice are rotated outward, possibly in order to provide a wide base for postural support. Repetitive "high stepping" movements often precede locomotion. These findings are consistent with recessive motor abnormalities that have been reported in other *Scn8a* mutant mouse lines (Kohrman et al., 1996b; Sprunger et al., 1999).

***Scn8a*$^{RH/RH}$ mutant mice have reduced motor function**

Because recessive motor dysfunction has been described in previous *Scn8a* mutant mice, we assessed motor function in the R1627H mice by measuring 24hr locomotor activity, rotating rod performance, and stride length. Significantly reduced locomotor activity was observed in *Scn8a*$^{RH/RH}$ mice compared to *Scn8a*$^{RH/+}$ and WT littermates in the first 5 hours of recording and at the beginning of the dark cycle, when mice are most active (two-way ANOVA, genotype X time, $p < 0.05$; Figure 3.4*A*). *Scn8a*$^{RH/RH}$ mice had significantly reduced latencies to fall from a rotating rod (one-way ANOVA, $p < 0.05$; Figure 3.4*B*). Average latency to fall was not significantly different between WT and *Scn8a*$^{RH/+}$ ($p > 0.05$; Figure 3.4*B*). Decreased stride lengths were observed in *Scn8a*$^{RH/RH}$, but not *Scn8a*$^{RH/+}$ mice compared to WT controls (one-way ANOVA, $p < 0.001$; Dunnett's *post hoc*, $p < 0.05$, Figure 3.4*C-D*).

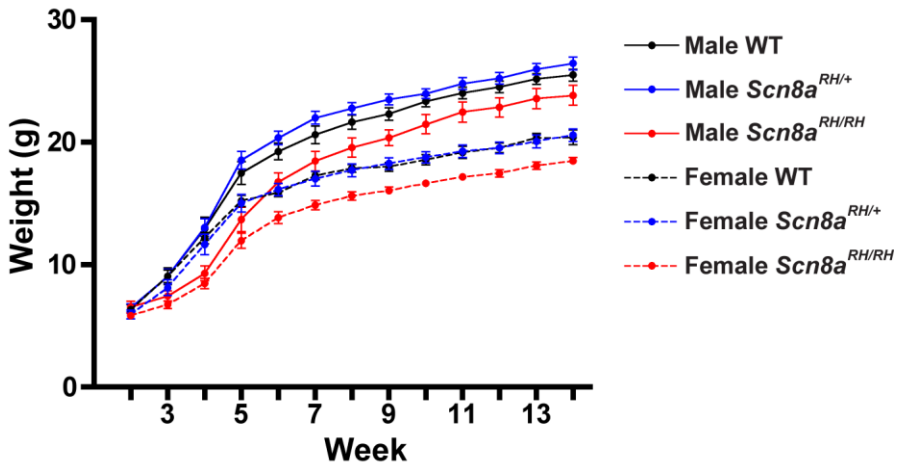

Figure 3.3. Homozygous *Scn8a*-R1627H mutants have reduced weight

Male and female WT, *Scn8a*$^{RH/+}$, and *Scn8a*$^{RH/RH}$ mice were weighed weekly from the 2nd to the 14th postnatal week. No differences were detected between WT and *Scn8a*$^{RH/+}$ mice at any time point. *Scn8a*$^{RH/RH}$ mice had significantly lower average weights compared to WT littermates (two-way ANOVA, genotype X week, $p < 0.05$). The maximum difference between WT and *Scn8a*$^{RH/RH}$ weights was 28 % (males) and 30 % (females) at 4 weeks after birth. At14 weeks after birth, the average weight of *Scn8a*$^{RH/RH}$ mice was lower by 5.6% (males) and 9.5% (females) when compared to WT littermates (Error bars represent SEM, n = 11-18).

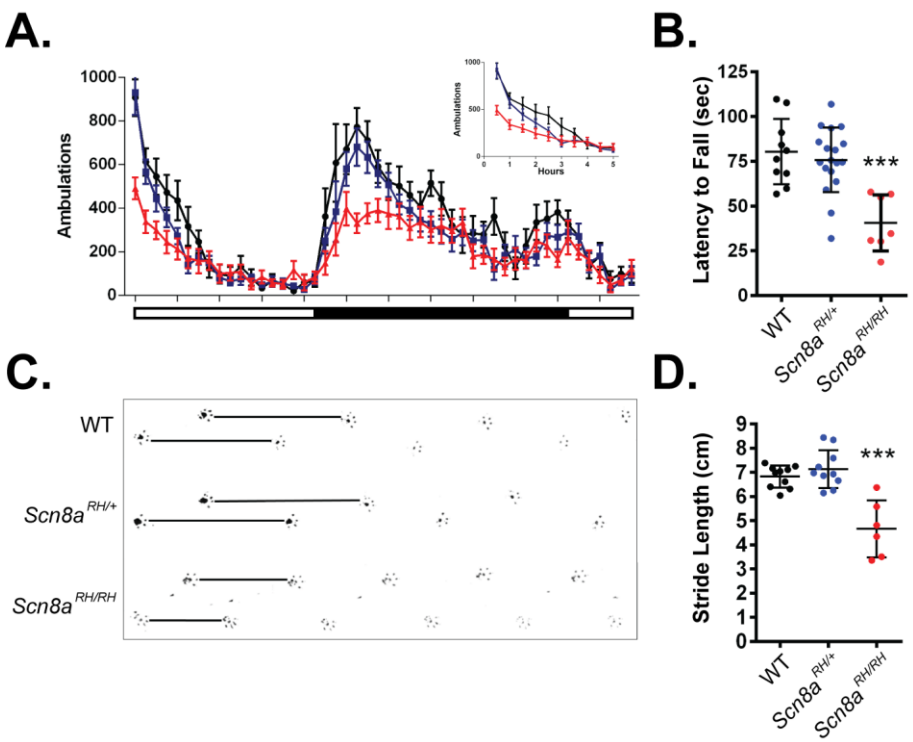

Figure 3.4. Recessive motor impairment in R1627H mice

A. Locomotor activity of *Scn8a*-R1627H mice in a new home cage was measured over a 24-hour period. A significant deficit in locomotor activity was detected between *Scn8a*$^{RH/RH}$ mice (red) and WT (black) littermates (two-way ANOVA, genotype X time, $p < 0.05$). No significant differences were detected between *Scn8a*$^{RH/+}$ (blue) and WT littermates ($p > 0.05$). Inset graph demonstrates that *Scn8a*$^{RH/RH}$ mice have reduced locomotor activity in a novel environment ($p < 0.05$). White and black bars under the X-axis represent the light-dark cycle. n = 9-12. ***B.*** Rotating rod performance was reduced in *Scn8a*$^{RH/RH}$ (red) but not WT (black) or *Scn8a*$^{RH/+}$ (blue) mice (one-way ANOVA, $p < 0.001$; Dunnett's *post hoc*, $p < 0.05$; n = 7-18). ***C.*** Representative example of stride length paw prints reveals reduced stride length in *Scn8a*$^{RH/RH}$ mice. Black lines show relative stride length. ***D.*** Stride lengths were found to be significantly reduced in *Scn8a*$^{RH/RH}$ but not *Scn8a*$^{RH/+}$ mice compared to WT littermates (one-way ANOVA, $p < 0.001$; Dunnett's *post hoc*, $p < 0.05$, Error bars represent SEM, n = 6-10).

The R1627H mutation is not associated with deficits in performance on anxiety, depression-like, or learning and memory tasks

Scn8a mutations have been reported to cause altered performance on anxiety and learning behavioral tasks in mice (McKinney et al., 2008; Sawyer et al., 2013) and psychiatric and cognitive deficits in humans (Wasserman et al., 2005; Trudeau et al., 2006; Wang et al., 2008). However, R1627H mutants did not show significant differences in the percentage of time spent in the open arm or the number of entries into the open arm of an elevated plus maze (Table 3.1). Likewise, no significant changes were observed in the time spent in the center zone or the number of entries into the center of the open field (Table 3.1). Significantly increased struggling time and decreased immobile time was observed in the tail suspension task in $Scn8a^{RH/RH}$ mice compared to $Scn8a^{RH/+}$ and WT littermates (one-way ANOVA, $p < 0.05$) (Table 3.1). However, no alterations in time struggling or time floating were observed in the forced swim task (Table 3.1). Likewise, preference for sucrose was comparable between $Scn8a^{RH/RH}$ mice and $Scn8a^{RH/+}$ and WT littermates (Table 3.1).

We previously reported modest increases in spatial memory in mice with the $Scn8a^{medjo}$ mutation (Papale et al., 2010). In contrast, comparable performance was observed between WT, $Scn8a^{RH/+}$, and $Scn8a^{RH/RH}$ littermates in the novel object recognition task. However, $Scn8a^{RH/RH}$ mice had modestly increased performance in spatial learning as measured by the Y-maze (one-way ANOVA, $p < 0.05$) (Table 3.1). However, this increase failed to reach statistical significance by Dunnett's *post hoc* test.

Category	Test	# of Animals	Measurement	Genotype	Average	s.e.m.	*p*	*Post hoc Test*	Comparison	Significance
Survival	Survival	WT = 24 RH/+ = 36 RH/RH = 28	4 mo % mortality	WT	0.0%	-	-	-	-	-
				RH/+	0.0%	-			-	-
				RH/RH	0.0%	-			-	-
Anxiety	Elevated Plus Maze	WT = 10 RH/+ = 12 RH/RH = 10	% time in open arm	WT	25.14	3.78	0.84	-	-	-
				RH/+	26.85	2.61			-	-
				RH/RH	28.62	5.46			-	-
			Open arm entries	WT	13.30	2.50	0.73	-	-	-
				RH/+	12.08	1.57			-	-
				RH/RH	10.80	2.38			-	-
			Distance traveled (cm)	WT	106.22	8.14	0.64	-	-	-
				RH/+	115.90	7.30			-	-
				RH/RH	104.56	12.59			-	-
	Open Field	WT = 8 RH/+ = 12 RH/RH = 10	Time in center (sec)	WT	5.34	5.47	0.05	-	-	-
				RH/+	7.91	8.46			-	-
				RH/RH	1.08	1.99			-	-
			Number of entries into the center	WT	2.75	2.05	$p < 0.01$	Dunnett's Test	-	-
				RH/+	3.58	2.54			WT vs. RH/+	$p > 0.05$
				RH/RH	0.6	0.70			WT vs. RH/RH	$p > 0.05$
			Latency to first center entry (sec)	WT	67.3	86.42	0.23	-	-	-
				RH/+	131.99	93.92			-	-
				RH/RH	65.6	108.64			-	-
Depression-like	Forced Swim	WT = 10 RH/+ = 10 RH/RH = 10	Time swimming (sec)	WT	90.12	10.30	0.57	-	-	-
				RH/+	83.58	11.21			-	-
				RH/RH	99.47	8.61			-	-
			Time floating (sec)	WT	122.21	22.29	0.2	-	-	-
				RH/+	121.46	24.50			-	-
				RH/RH	71.18	15.78			-	-
	Tail Suspension	WT = 10 RH/+ = 15 RH/RH = 10	Time struggling (sec)	WT	170.73	8.41	$p < 0.01$	Dunnett's Test	-	-
				RH/+	171.84	10.61			WT vs. RH/+	$p > 0.05$
				RH/RH	247.66	7.22			WT vs. RH/RH	$p < 0.05$
			Time immobile (sec)	WT	229.48	4.96	$p < 0.05$	Dunnett's Test	-	-
				RH/+	220.69	12.90			WT vs. RH/+	$p > 0.05$
				RH/RH	164.12	8.48			WT vs. RH/RH	$p < 0.05$
	Sucrose Preference	WT = 11 RH/+ = 10 RH/RH = 11	Sucrose preference (sucrose g / total g) *100	WT	96.91	2.94	0.64	-	-	-
				RH/+	96.97	1.88			-	-
				RH/RH	89.46	10.74			-	-
Learning/Memory	Novel Object Recognition (20 min exposure)	WT = 8 RH/+ = 10 RH/RH = 12	Novel object preference	WT	59.68	4.86	0.77	-	-	-
				RH/+	62.09	6.75			-	-
				RH/RH	55.11	10.91			-	-
			Novel position preference	WT	56.24	4.86	0.41	-	-	-
				RH/+	62.58	6.77			-	-
				RH/RH	64.78	10.91			-	-
	Novel Object Recognition (5 min exposure)	WT = 8 RH/+ = 10 RH/RH = 12	Novel object preference	WT	69.63	10.32	0.923	-	-	-
				RH/+	58.51	8.81			-	-
				RH/RH	66.41	7.78			-	-
			Novel position preference	WT	61.92	10.80	0.136	-	-	-
				RH/+	60.59	5.88			-	-
				RH/RH	70.93	12.95			-	-
	Y-Maze	WT = 10 RH/+ = 12 RH/RH = 10	% correct rotations	WT	59.28	2.19	0.031	Dunnett's Test	-	-
				RH/+	56.82	1.40			WT vs. RH/+	$p > 0.05$
				RH/RH	64.22	6.42			WT vs. RH/RH	$p > 0.05$
			Distance traveled (cm)	WT	331.39	19.32	0.021	Dunnett's Test	-	-
				RH/+	352.29	18.74			WT vs. RH/+	$p > 0.05$
				RH/RH	264.32	27.11			WT vs. RH/RH	$p > 0.05$

Table 3.1. Summary of behavioral tasks performed on the R1627H line

$Scn8a^{RH/RH}$ mice do not exhibit spontaneous absence seizures

We previously reported that *Scn8a* mutants exhibit spontaneous absence seizures (Papale et al., 2009). To determine if the R1627H mutation also leads to absence seizure generation, ten days of continuous video-EEG recordings were collected from WT, $Scn8a^{RH/+}$, and $Scn8a^{RH/RH}$ mice. No seizures were detected in any mice (n = 4-6). To exclude the possibility that the observed lack of absence seizures was due to differences in genetic background, $Scn8a^{RH/+}$ mice were back-crossed for five generations to C3H/HeJ mice, which are susceptible to absence seizures. No absence seizures were observed over five days of continuous video-EEG recordings collected from $Scn8a^{RH/+}$ mutants and WT littermates at this generation.

$Scn8a^{RH/+}$ but not $Scn8a^{RH/RH}$ mice are resistant to 6Hz- and flurothyl-induced seizures and have reduced hippocampal bursting activity in the presence of high extracellular potassium

Latencies to flurothyl-induced seizures were determined for WT, $Scn8a^{RH/+}$, and $Scn8a^{RH/RH}$ mice. The average latencies to the myoclonic jerk (MJ) and the generalized tonic-clonic seizure (GTCS) were significantly increased in $Scn8a^{RH/+}$ mice when compared to $Scn8a^{RH/RH}$ and WT littermates (one-way ANOVA, $p < 0.05$; Figure 3.5*A*). The severity of flurothyl-induced seizures, as assessed by the presence of hindlimb extension and mortality following the GTCS, was reduced in both $Scn8a^{RH/+}$ and $Scn8a^{RH/RH}$ mice when compared to WT littermates (X^2, $p < 0.05$; Figure 3.5*B*). $Scn8a^{RH/+}$ but not $Scn8a^{RH/RH}$ mice were found to be resistant to 6hz-induced psychomotor seizures when compared to WT littermates (Figure 3.5*C*). However, reduced 6 Hz-induced seizure severity was observed in both $Scn8a^{RH/+}$ and $Scn8a^{RH/RH}$ mice at current intensities of 20, 22, and 24 mA (one-way ANOVA, $p < 0.0001$; Dunnett's *post hoc*, $p < 0.001$; Figure 3.5*D*).

Extracellular recordings were performed in hippocampal slices in the presence of high extracellular potassium to compare susceptibility to epileptiform burst discharges between WT,

Scn8a$^{RH/+}$ and *Scn8a*$^{RH/RH}$ mice. The average latency to the onset of bursting was higher in *Scn8a*$^{RH/+}$ slices (20.0 min) compared to WT (6.1 min) and *Scn8a*$^{RH/RH}$ mice (6.3 min) (Figure 3.5*E.a.*). The intra-burst spiking frequency was reduced in *Scn8a*$^{RH/+}$ mice (32.0 Hz) compared to WT (61.5 Hz), and *Scn8a*$^{RH/RH}$ mice (49.3 Hz) (Figure 3.5*E.b*). The percentage of slices exhibiting bursting was lower in *Scn8a*$^{RH/+}$ mice (1/8, 12.5%) when compared to WT (5/5, 100%) and *Scn8a*$^{RH/RH}$ 57.1% (4/7, 57.1%) mice (Figure 3.5*F*).

The *Scn8a*-R1627H mutation increases the lifespan and seizure thresholds of *Scn1a*-R1648H GEFS+ mice

We previously demonstrated that the *Scn8a*^{medjo} mutation was capable of increasing the lifespan and seizure thresholds of mice with GEFS+ and DS *Scn1a* mutations (Martin et al., 2007; Hawkins et al., 2011). To determine the effect on survival and seizure thresholds of the R1627H mutation in a GEFS+ model, we generated mice that carry both the GEFS+ *Scn1a*-R1648H and the *Scn8a*-R1627H mutations. *Scn1a*$^{RH/+}$ and *Scn1a*$^{RH/RH}$ mice experienced 18% (2/11) and 100% (11/11) mortality, respectively, by 3 months of age. In contrast, the survival of WT, *Scn8a*$^{RH/+}$, and *Scn1a*$^{RH/+}$/*Scn8a*$^{RH/+}$ mice were comparable, and 40% of *Scn1a*$^{RH/RH}$/*Scn8a*$^{RH/+}$ mutants survived to at least three months of age (Figure 3.6*A*). Latencies to flurothyl-induced seizures were also measured in these mice (Figure 3.6*B*). Consistent with our previous findings in *Scn8a* mutant mice, average latencies to the MJ and GTCS were increased in mice carrying the *Scn8a*$^{RH/+}$ mutation, while mice carrying the *Scn1a*$^{RH/+}$ mutation had reduced latencies to the GTCS. Latencies to the GTCS were comparable between *Scn1a*$^{RH/+}$/*Scn8a*$^{RH/+}$ mutants and WT littermates, indicating that the *Scn8a* mutation was capable of elevating seizure latencies in *Scn1a* mice to normal levels. However, significantly lower latencies to the MJ and GTCS were still observed in *Scn1a*$^{RH/RH}$/*Scn8a*$^{RH/+}$ mutants (one-way ANOVA, Dunnett's *post hoc*, $*p < 0.05$, $***p < 0.001$, Figure 3.6*B*).

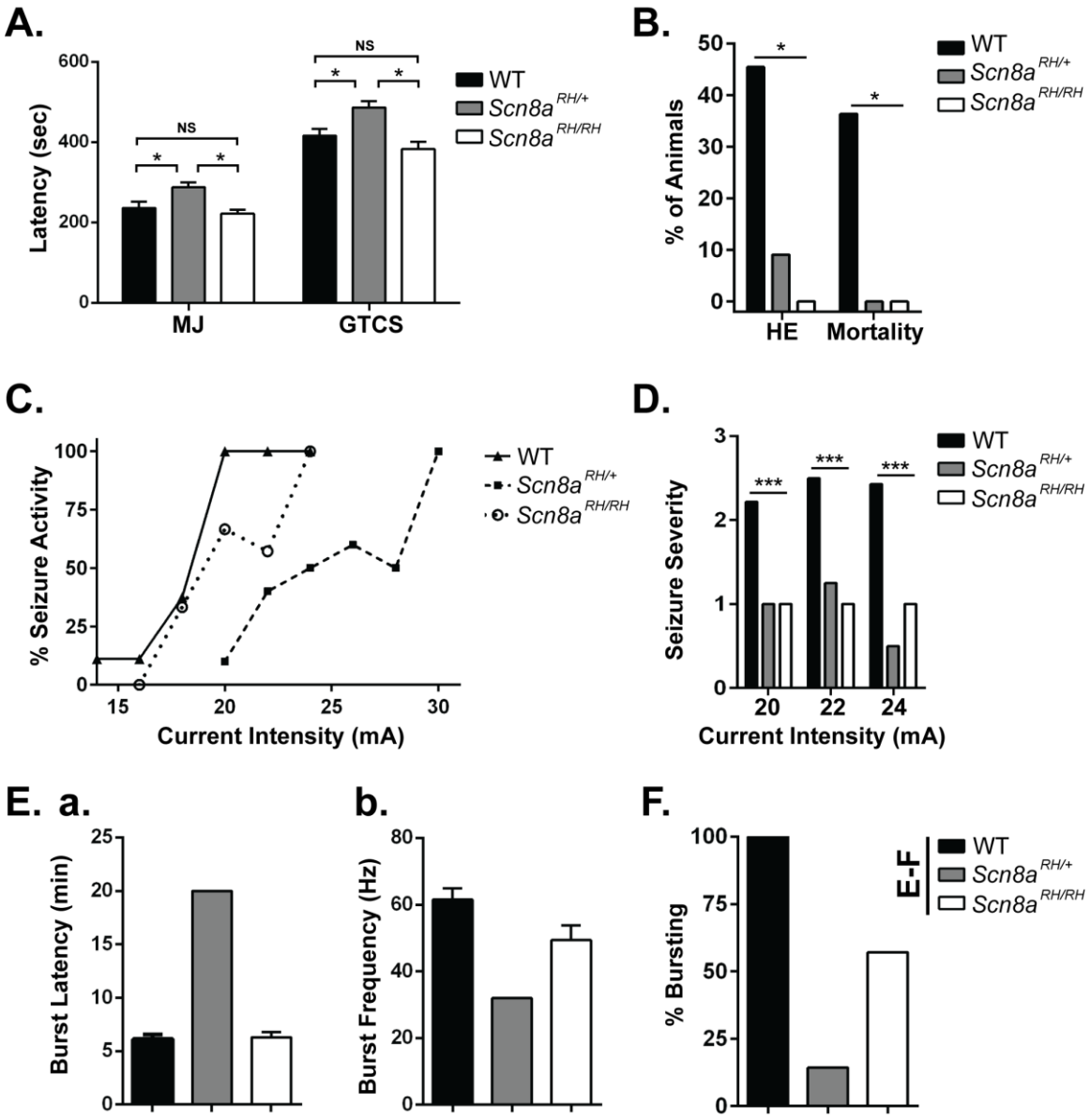

Figure 3.5. Effects of the R1627H mutation on flurothyl- and 6 Hz-induced seizure susceptibility and hippocampal bursting

A. *Scn8a*$^{RH/+}$ but not *Scn8a*$^{RH/+}$ mice have longer latencies to flurothyl-induced seizures (one-way ANOVA, MJ and GTCS, Tukey *post hoc*, * $p < 0.05$; n = 11-12). ***B.*** Seizure severity, as measured

by hindlimb extension (HE) and death, were reduced in *Scn8a*$^{RH/+}$ and *Scn8a*$^{RH/RH}$ mice (X^2, *$p <$ 0.05). ***C-D.*** *Scn8a*$^{RH/+}$ mice have increased thresholds to 6 Hz seizures compared to *Scn8a*$^{RH/RH}$ and WT littermates. ***D.*** Both *Scn8a*$^{RH/+}$ and *Scn8a*$^{RH/RH}$ mice experience less severe seizures in response to stimulus intensities of 20, 22, and 24 mA compared to WT littermates (one-way ANOVA, $p < 0.0001$; Dunnett's *post hoc*, $p < 0.001$; n = 8-10). ***E.a.*** The latency to the occurrence of bursting activity in the presence of high potassium (K^+) in hippocampal slices was increased in slices from *Scn8a*$^{RH/+}$ but not WT or *Scn8a*$^{RH/RH}$ littermates (n = 1-5). ***E.b.*** The frequency of intra-burst high amplitude spiking activity was reduced in *Scn8a*$^{RH/+}$ compared to WT and *Scn8a*$^{RH/RH}$ littermates. ***F.*** The percentage of slices that exhibited bursting in the presence of high K^+ was WT (5/5, 100%), *Scn8a*$^{RH/+}$ (1/8, 12.5%), and *Scn8a*$^{RH/RH}$ (4/7, 57.1%). Experiments ***E-F*** were performed by Karoni Dutt in the laboratory of Alan Goldin at the University of California, Irvine.

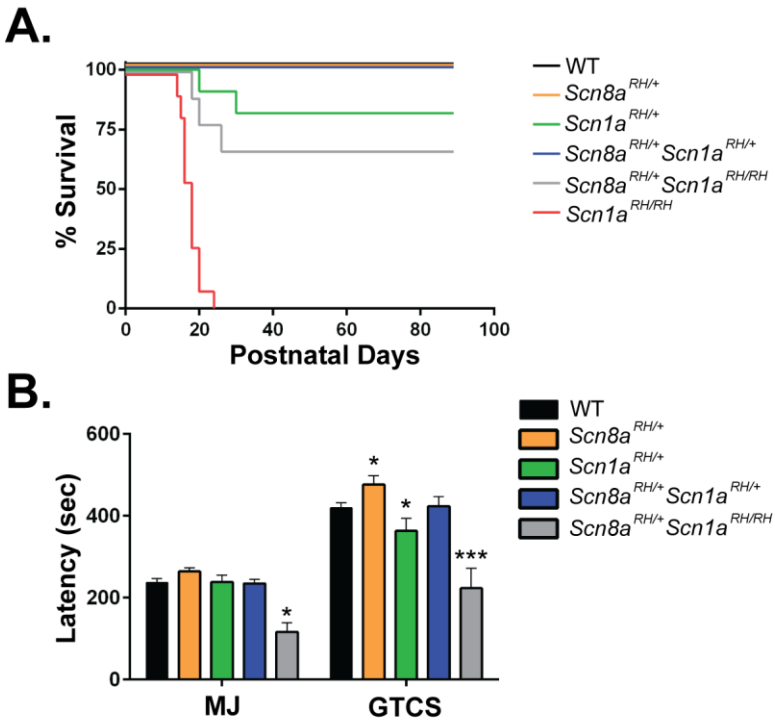

Figure 3.6. The *Scn8a*-R1627H mutation increases lifespan and seizure resistance in a mouse model of GEFS+ (*Scn1a*-R1648H)

A. Normal survival was observed over the first three months of postnatal development in WT, *Scn8a*$^{RH/+}$, and *Scn1a*$^{RH/+}$*Scn8a*$^{RH/+}$ mice. In contrast, *Scn1a*$^{RH/+}$ and *Scn1a*$^{RH/RH}$ mice experienced 18% (2/11) and 100% (11/11) mortality respectively. *Scn1a*$^{RH/RH}$/*Scn8a*$^{RH/+}$ mice experienced 60% (6/10) mortality. ***B.*** The R1627H mutation is capable of increasing seizure thresholds and restoring seizure thresholds in *Scn1a*$^{RH/+}$ mice. *Scn1a*$^{RH/+}$ mutants (green) have lower latencies to flurothyl-induced GTCS latency, while *Scn8a*$^{RH/+}$ mutants (orange) exhibit elevated latencies when compared to WT littermates. Normal latencies were restored in *Scn1a*$^{RH/+}$/*Scn8a*$^{RH/+}$ mice (blue). *Scn1a*$^{RH/RH}$/*Scn8a*$^{RH/+}$ mice (grey) have reduced latencies to the MJ and GTCS. One-way ANOVA, Dunnett's *post hoc*, *p < 0.05, ***p <0.001; Error bars represent SEM; n = 5-17).

Scn8a$^{RH/RH}$ mice exhibit sound-induced wild running behavior

To evaluate responses to high intensity auditory stimuli, WT, *Scn8a*$^{RH/+}$, and *Scn8a*$^{RH/RH}$ mice were exposed to tones (12 kHz, 80 dB) or broad-spectrum (13-85 kHz, 50-80 dB) acoustic stimulus (Figure 3.7). Approximately 36% (11/31) of *Scn8a*$^{RH/RH}$ mice exhibited wild running behavior followed by loss of postural control and forelimb and hindlimb clonus in response to broad-spectrum stimuli (X^2, $*p < 0.05$; Figure 3.8*A*). In contrast, only one WT littermate (1/15) exhibited wild running behavior in response to sound stimuli. The WT mouse progressed to tonic hindlimb extension, which was not a feature of the response observed in the *Scn8a*$^{RH/RH}$ mutants. No *Scn8a*$^{RH/+}$ (0/10) mice exhibited audiogenic responses. High amplitude EEG signals were recorded in the inferior colliculus, a major audiogenic seizure region, during acoustic stimulus in *Scn8a*$^{RH/RH}$ mice (Figure 3.7*B*). C-Fos epression in the cortex, hippocampus, superior colliculus (SC) and IC was qualitatively evaluated (Figure 3.7*C-D*). Low levels of c-Fos expression was observed in the cortex and hippocampus of all animals (Figure 3.7*D*). High levels of c-Fos were observed in the SC and IC of responding *Scn8a*$^{RH/RH}$ mice but not, non-responding *Scn8a*$^{RH/RH}$, WT, or *Scn8a*$^{RH/+}$ mice (Figure 3.7*D*).

Scn8a$^{RH/RH}$ mice have reduced auditory brainstem nuclei responses (ABRs)

In order to test the possiblity that the auditory-induced wild running behavior in *Scn8a*$^{RH/RH}$ mice is a result of increased sensitivity to acoustic stimulus, auditory brainstem nuclei responses (ABR) to sound stimuli were recorded (Figure 3.8). 5-24 kHz tones from 110-20 dB were played to WT, *Scn8a*$^{RH/+}$ and *Scn8a*$^{RH/RH}$ mice while measuring ABR responses. *Scn8a*$^{RH/RH}$ mice were found to have reduced auditory responses between 12-15 kHz (two-way ANOVA, genotype X frequency, Dunnett's *post hoc*, $*p < 0.05$; Figure 3.8*A,C*). No differences in ABR thresholds at 12 kHz was observed between *Scn8a*$^{RH/RH}$ mice that are not suceptible to audiogenic wild-running

behavior (non-responders) compared to *Scn8a*$^{RH/RH}$ mice that were found to be suceptible (responders) (Student's t-test, $p > 0.05$; Figure 3.8*B*).

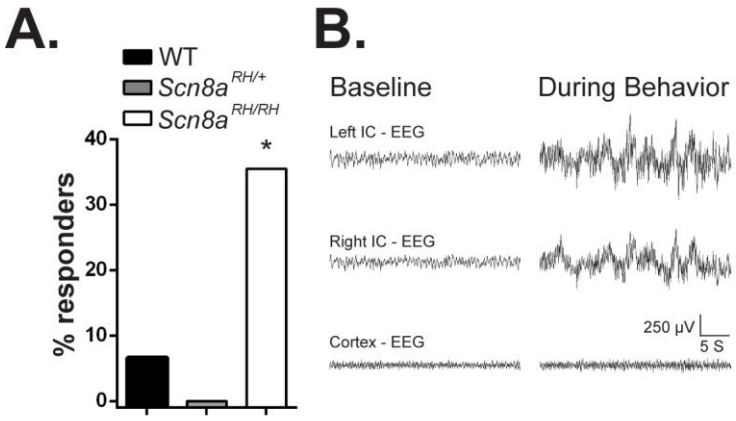

D.

c-Fos Immunoreactivity

Anatomical Region	RH/RH Responder	RH/RH Non-Responder	RH/+	+/+
Cortex	+	+	+	+
Hippocampus	++	+	+	+
Superior Colliculus	++++	+	+	+
Inferior Colliculus	++++	+	+	+

Figure 3.7. *Scn8a*$^{RH/RH}$ mice are susceptiable to audiogenic seizures

A. *Scn8a*$^{RH/RH}$, *Scn8a*$^{RH/+}$, and WT mice were exposed to 5 minute duration tones (12 kHz, 80 dB) or broad-spectrum (13-85 kHz, 50-80 dB) acoustic stimulus to induce audiogenic seizures. Aproximately 6.7% (1/15) of WT, 0% (0/10) of *Scn8a*$^{RH/+}$, and 35.5% (11/31) of *Scn8a*$^{RH/RH}$ mice responded to broad-spectrum stimuli (X^2, $*p < 0.05$). ***B.*** Representative example of inferior colliculus (IC) and cortical EEG activity before (baseline) and during (during behavior) audiogenic seizure in a *Scn8a*$^{RH/RH}$ mouse. ***C.*** Representative image of c-Fos expression in the IC of a responding and non-responding *Scn8a*$^{RH/RH}$ mouse 2 h following exposure to sound stimulus.

E. Regional expression of c-Fos 2 h following exposure to sound stimulus. The relative c-Fos expression was qualtiatively evaluated: (+) low; (++) light; (+++) moderate; (++++) high. High levels of c-fos expression were observed in the SC and IC of *Scn8a*$^{RH/RH}$ responding animals but not non-responding *Scn8a*$^{RH/RH}$, *Scn8a*$^{RH/+}$ or WT littermates. Low to light levels of c-Fos was observed in the hippocampus and cortex of all animals.

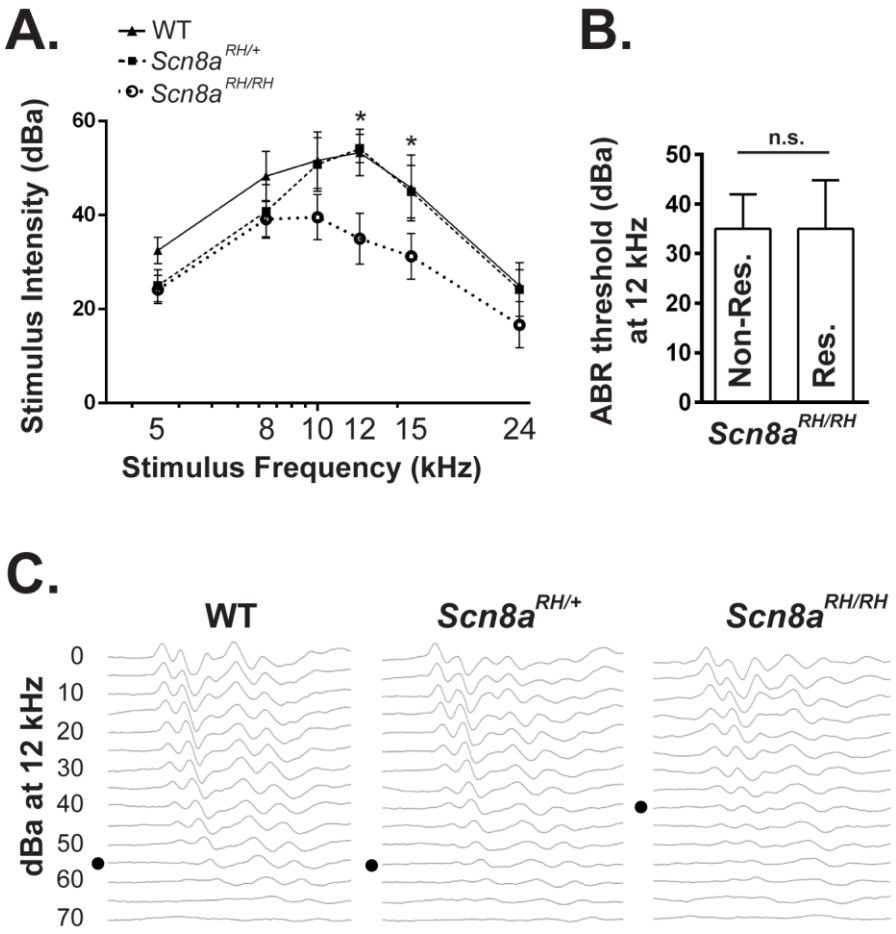

Figure 3.8. *Scn8a*$^{RH/RH}$ mice have reduced auditory brainstem nuclei responses (ABRs)

A. Auditory brainstem nuclei responses (ABR) were measured in response to 5-24 kHz tones in WT, *Scn8a*$^{RH/+}$ and *Scn8a*$^{RH/RH}$ mice. *Scn8a*$^{RH/RH}$ mice were found to have reduced auditory responses between 12-15 kHz (two-way ANOVA, Dunnett's *post hoc*, *$p < 0.05$; n = 8-10). ***B.*** No differences in ABR thresholds at 12 kHz were observed between *Scn8a*$^{RH/RH}$ mice that are not susceptible to audiogenic seizure (non-responders) compared to *Scn8a*$^{RH/RH}$ mice that were found to be susceptible to audiogenic seizure (responders) (Student's t test, $p > 0.05$; n = 4-8). ***C.*** Representative examples of ABR responses in WT and R1627H mutant mice. Black dot indicates threshold at which response is no longer detectable. Error bars represent SEM.

Reduced latencies to flurothyl-induced seizures and susceptibility to audiogenic wild-running behavior in mice carrying the *Scn8a*-medjo mutation

To determine if unaltered seizure thresholds and suceptability to auditory-induced wild running behavior, observed in $Scn8a^{RH/RH}$ animals, are also features of a different *Scn8a* mutation, we measured latencies to flurothyl-induced seizures and responses to high intensity sound stimuli in *Scn8a*-medjo mice. We measured latencies to flurothyl-induced seizures and responses to high intensity sound stimuli in *Scn8a*-medjo mice. $Scn8a^{medjo/+}$ mice were found to have increased resistance to flurothyl-induced MJ and GTCS when compared to WT littermates (one-way ANOVA, $p < 0.001$;Tukey post hoc, MJ $*p < 0.05$, GTCS $***p < 0.001$; Figure 3.9*A*). Homozygous $Scn8a^{medjo/medjo}$ mice however, were found to have reduced latencies to the MJ and equivalent latencies to the GTCS when compared to WT littermates (one-way ANOVA, $p < 0.001$; Tukey post hoc , MJ $***p < 0.001$, GTCS $*p < 0.05$; Figure 3.9*A*). Seizure severity, as measured by hindlimb extension (HE) and death, were reduced in $Scn8a^{medjo/+}$ and $Scn8a^{medjo/medjo}$ mutants (X^2, $*p < 0.05$; Figure 3.10*B*). Wild-running responses during 5-minute exposures to an 80 dB, 12 kHz tone were observed in 22% of $Scn8a^{medjo/medjo}$ (2/9). No WT (0/10) or $Scn8a^{medjo/+}$ (0/10) mice exhibited wild-running behavior in response to acoustic stimulus (Figure 3.9*C*).

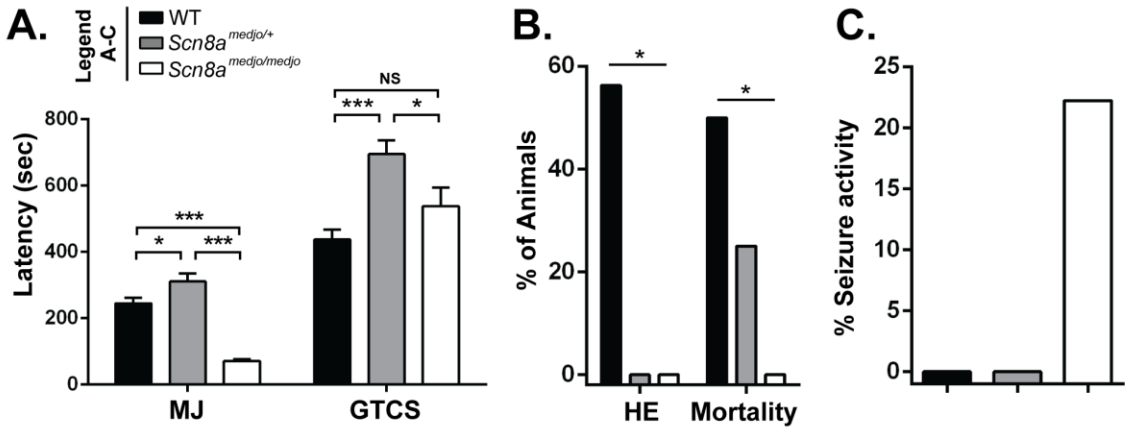

Figure 3.9. Flurothyl seizure thresholds and response to acoustic stimuli in mice carrying the *Scn8a*-medjo mutation

A-B. Flurothyl seizure induction was performed on *Scn8a*-medjo mutant mice. ***A.*** *Scn8a*$^{medjo/+}$ mice were found to have increased latencies to flurothyl-induced seizures compared to WT littermates (one-way ANOVA, $p < 0.001$;Tukey post hoc, MJ $*p < 0.05$, GTCS $***p < 0.001$). *Scn8a*$^{medjo/medjo}$ mice were found to have reduced latency to the MJ and equivalent latency to the GTCS when compared to WT littermates (one-way ANOVA, $p < 0.001$; Tukey post hoc , MJ $***p < 0.001$, GTCS $*p < 0.05$; n = 12-16). ***B.*** Seizure severity, measured by the presence of hindlimb extension (HE) and death, was reduced in *Scn8a*$^{medjo/+}$ and *Scn8a*$^{medjo/medjo}$ mice (X^2, $*p < 0.05$; n = 12-16). ***C.*** Responses to high intensity acoustic stimuli were assessed in WT, *Scn8a*$^{medjo/+}$, and *Scn8a*$^{medjo/medjo}$ mice. Wild-running behavior was observed in 22% of *Scn8a*$^{medjo/medjo}$ mice (2/9). No WT (0/10) or *Scn8a*$^{medjo/+}$ (0/10) mice exhibited wild-running behavior.

3.4. Discussion

We have introduced a GEFS+ epilepsy mutation, *Scn1a*-R1648H, into the corresponding position in the voltage sensor of the *Scn8a* gene, *Scn8a*-R1627H. In *Xenopus* oocytes this mutation was found to reduce voltage-dependent activation, increase recovery from inactivation, and increase persistent sodium current in *Xenopus* oocytes (Fig. 3.1). These alterations are predicted to increase channel activity which is particularly interesting given that a gain-of-function mutation in the *SCN8A* gene was recently identified in a patient with epilepsy (Veeramah et al., 2012). In further support of a role for *Scn8a* in epilepsy, a mutation in the *Celf4* gene was reported to cause increased *Scn8a* expression, increased neuronal persistent sodium current, and seizures in mice (Sun et al., 2013).

We have found that the *Scn8a*-R1627H mutation leads to recessive motor impairment and reduced locomotor activity, similar to previously described *Scn8a* rodent models (Dickie, 1965; Kearney et al., 2002; Hamann et al., 2003). Interestingly, the *Scn8a*-R1627H mutation confers both seizure protection and seizure susceptibility in a gene-dose dependent manner. In the heterozygous state, the *Scn8a* R1627H mutation reduces susceptibility to chemically and electrically-induced seizures and increases the lifespan of mice with the *Scn1a*-GEFS+ mutation (R1648H), which is consistent with findings in other *Scn8a* rodent mutations (Martin et al., 2007; Hawkins et al., 2011). However, surprisingly, homozygous *Scn8a*-R1627H mice (*Scn8a*$^{RH/RH}$) are not resistant to chemically- and electrically-induced seizures and likely experience seizures in response to auditory stimuli. We propose that the auditory-induced wild running and forelimb-hindlimb clonic behaviors observed in 36% of homozygous R1627H mice are audiogenic seizures (AGSs) based on three observations. First, the behavioral responses of *Scn8a*$^{RH/RH}$ mutants to high-intensity auditory stimuli are similar to flurothyl-induced brainstem seizure behaviors (Samoriski et al., 1998), consisting of loss of posture and forelimb and hindlimb clonus. Secondly, high levels of c-Fos expression were observed in the brainstem, including inferior

colliculus (IC), following exposure to auditory stimuli in *Scn8a*$^{RH/RH}$ mice that exhibited seizure-like behavior. c-Fos expression was not increased in the midbrain and brainstem of non-responding *Scn8a*$^{RH/RH}$, *Scn8a*$^{RH/+}$, or WT littermates and comparatively little c-Fos expression was observed outside of AGS brainstem regions in *Scn8a*$^{RH/RH}$ responders following auditory stimulus. The IC is considered to be the site of initiation of AGS (Kesner, 1966; Willott and Lu, 1980; Browning, 1986) and c-Fos expression in brainstem nuclei following exposure to sound stimuli is a hallmark of AGS (Le Gal La Salle and Naquet, 1990; Snyder-Keller and Pierson, 1992; Kwon and Pierson, 1997; Klein et al., 2004). Thirdly, we observed high amplitude EEG activity in the IC during seizure-like behaviors in *Scn8a*$^{RH/RH}$ mice.

We sought to determine if auditory responses in R1627H mice are a consequence of increased sensory response to sound stimulus by recording auditory brainstem nuclei responses (ABR). We observed reduced ABRs in *Scn8a*$^{RH/RH}$ mice, while responses in *Scn8a*$^{RH/+}$ mice were comparable to WT (Fig. 3.8). Reduced ABRs were similarly observed in the *Scn8a* mutant 'Cloth-ears', leading to the hypothesis that *Scn8a* dysfunction may contribute to neural hearing loss (Mackenzie et al., 2009). This finding reduces the possibility that the audiogenic seizures in *Scn8a*$^{RH/RH}$ mice were due to an increased sensitivity to sound.

In contrast to previously described *Scn8a* mutants, the R1627H mutation was not associated with alterations in measures of anxiety, depression, or learning and memory (McKinney et al., 2008; Papale et al., 2010). Furthermore the R1627H mutation did not result in the generation of absence seizures, which were observed in mice expressing *Scn8a*-8J, *Scn8a*-med, and *Scn8a*-medjo alleles (Papale et al., 2009). This raises the possibility that it may be possible, in a therapeutic setting, to decouple the seizure protection conferred by altered *Scn8a* function from the generation of absence epilepsy or negative behavioral outcomes. Furthermore, it is possible that rodent *Scn8a*-behavioral abnormalities are, in part, a consequence of disruptions caused by absence seizures, which were not observed in R1627H mice.

In order to determine if the major seizure findings observed over the course of investigating the R1627H mutation extend to other *Scn8a* mutations, we evaluated responses to auditory stimuli and proconvulsants in mice with the *Scn8a*-medjo mutation. We found that *Scn8a*$^{medjo/medjo}$ mice respond similarly to flurothyl and audiogenic stimuli as *Scn8a*$^{RH/RH}$ mice, indicating that recessive seizure susceptibility may be a common feature of *Scn8a* dysfunction.

3.5. Methods

Generation of construct for expression in Xenopus oocytes

We introduced the *Scn1a*-R1648H mutation plus two additional silent substitutions into exon 26 of the *Scn8a* cDNA plasmid (R1627H), which contains the entire coding region of mouse $Na_v1.6$. A targeting construct was produced using the following primers (R1627H arm LF: TAG ATT CCC GAA AGC CGG ACG AGC AGC CTG, R1648H arm LmutR: TGG CGC CCT TGA TGA GGT GCA AGA TGC GCC, 636bp product; R1627H arm RmutF: GGC GCA TCT TGC ACC TCA TCA AGG GCG CCA, R1648H arm RR: CCA GCG GCA TCA GCA CCT TGT CGC CTT GCG, 1862bp product).

To clone the mutation into the plasmid, the targeting construct and the plasmid were digested with *Bst*EII, which cuts just 5' to exon 26, and *Not*I, which cuts just 3' to exon 26. The targeting construct and plasmid were then ligated and transfected into chemically competent HB101 cells.

Expression and Electrophysiology

The R1627H mutation was cloned into the rat cDNA clone encoding $mNa_v1.6$. Electrophysiological properties of the channels were determined in the absence and presence of the β1 subunit by expression in *Xenopus* oocytes.

Wild-type or mutant sodium channel α subunit RNA was transcribed *in vitro* from *Not*I linearized DNA templates using the T7 mMESSAGE mMACHINE kit (Ambion, Austin, TX). Stage V oocytes that were removed from adult female *Xenopus laevis* frogs were injected with between 1 and 200 pg of RNA to obtain current amplitudes between 1 μA and 5 μA, as described previously (Goldin, 1991).

Sodium currents were recorded using an OC-725B two-electrode voltage-clamp (Warner Instruments, Hamden, CT) at room temperature with a DigiData 1322A interface (Molecular Devices, Foster City, CA) and pCLAMP 8.0 software (Molecular Devices), as described previously (Patton and Goldin, 1991) and the OpusXpress 6000A workstation consisting of eight parallel two-electrode voltage-clamps (Axon Instruments, Union City, CA) at room temperature with a DigiData 1322A interface (Molecular Devices) and OpusXpress Clampex 1.1 software (Molecular Devices). Recordings were performed in ND96 solution (in mM: 96 NaCl, 2 KCl, 1.8 $CaCl_2$, 1 $MgCl_2$, and 5 HEPES, pH 7.5). Capacitive transients were eliminated by subtraction of currents recorded in the presence of 500 nM tetrodotoxin (TTX) for voltage dependence of activation protocols.

Generation of mice expressing the Scn8a R1627H mutation

A targeting construct consisting of a 4.5-kb 5' arm of homology, the R1627H stubstitution, a neomycin cassette flanked by *FLP1* recombinase (Fft) sites, and a 4-kb 3' arm of homology, was electroporated into 129X1/SvJ-derived PAT-5 embryonic stem (ES) cells at the University of Michigan Transgenic Core. PCR analysis and Southern blotting were performed to identify correctly targeted ES cells.

Animal breeding and maintenance

All mice were housed in a temperature and humidity controlled vivarium and provided drinking water and food *ad libitum*. R1627H targeted mice were crossed to mice carrying FLP recombinase to remove a neomycin cassette included in the targeting vector. Mice were then crossed to C57BL6/J wildtype (WT) for three generations. Heterozygous males and females from this generation (N3) were crossed together to generate WT, heterozygous (*Scn8a*$^{RH/+}$), and homozygous (*Scn8a*$^{RH/RH}$) mice (N3F1) for experiments. The following strategy was used to generate mice carrying both the *Scn8a*-R1627H and the *Scn1a*-R1648H mutations. *Scn8a*$^{RH/+}$ (N3) females were crossed to *Scn1a*$^{RH/+}$ (N10) males to produce *Scn8a*$^{RH/+}$/*Scn1a*$^{RH/+}$ offspring. *Scn8a*$^{RH/+}$/*Scn1a*$^{RH/+}$ males were then crossed to N10 *Scn1a*$^{RH/+}$ females to produce WT, *Scn8a*$^{RH/+}$, *Scn1a*$^{RH/+}$, *Scn8a*$^{RH/+}$/*Scn1a*$^{RH/+}$, *Scn1a*$^{RH/RH}$, and *Scn8a*$^{RH/+}$/*Scn1a*$^{RH/RH}$ offspring. *Scn8a*$^{RH/+}$ mice (N3 generation) were also crossed to C3/HeJ for three generations and used for EEG analysis. A cohort of N3F1 mice were monitored, weighed, and videotaped weekly from P10 to P120 in order to assess locomotor function and to make general assessments of health and survival.

Genotyping of mutants

Genotyping of R1627H mutant mice was performed by PCR analysis of DNA extracted from tail biopsies. A 400 bp PCR product spanning the R1627H mutation was amplified using the following primers: (R1627H F, 5’-AAG ACA GGT TAT CTG TGT AAA CTG-3’; R1627H R, 5’-AAT CGG TTT TGT CTG CAA GAC TGG-3’) to produce 600bp (R1627H) and 500bp (WT) products. Genotyping of *Scn1a* R1648H mutant mice was performed as we previously reported (Martin et al., 2010). The *Scn8a* medjo mutation was identified by PCR amplification using the primer pair (medjo F 5'-ATG CCA CAG AAG TGT CAT TCC-3'; medjo R 5'-GGT ATT TCC

CAG CAA ACA GGT-3') followed by enzymatic digestion by MsII to yield bands of 129, 102, and 75 bp (Kohrman et al., 1996b).

Protein extraction

Protein extraction was performed as described in chapter 2. Briefly, three month-old mice were anesthetized with isoflurane. Whole brains were removed and homogenized in protease inhibitor buffer (50mM Tris (pH 7.5), 10mM EGTA, and 1 protease inhibitor tablet (Roche) per 50 ml PI buffer). Homogenates were centrifuged for 10 min at 3500 rpm to remove debris, and the supernatant was further centrifuged at 38,000 rpm for 30 min. The resulting pellet was re-suspended in 400 µl PI buffer. Protein concentration was determined by BCA assay (Thermo). Protein was diluted to a final concentration of 1µg/µl in 1X protein loading dye (Fisher). Isolated protein was stored at -80°C.

Western blot analysis

Western blotting was performed as described in Chapter 2. Briefly, protein (10 µg) was subjected to SDS-PAGE electrophoresis and transferred to a PVDF membrane. The following primary antibodies were used: rabbit anti-*Scn8a* (1:75, Millipore), mouse anti-*Scn1a* (1:75, Neuromab), rabbit anti-*Scn2a* (1:75, Millipore), and mouse anti-alpha tubulin (1:10,000, Abcam). The following secondary antibodies were used: peroxidase-conjugated secondary antibody donkey anti-rabbit IgG, (1:10,000; GE Healthcare) and peroxidase-conjugated goat anti-mouse secondary (1:10,000, Jackson Immuno Research)

Animal behavior

Video analysis of open field, forced swim, tail suspension, and novel object recognition tasks were performed using Any-Maze video tracking software (Stoelting Co. IL). All behavioral

procedures were conducted between the hours of 10:00AM and 3:00PM to minimize possible circadian rhythm effects.

Locomotor activity was measured by photobeam breaks of individually housed mice (San Diego Instruments, La Jolla, CA, USA) over a 24-hour period. Ambulations were counted as consecutive beam breaks.

Rotating rod performance was assessed by measuring the latency to fall from an accelerating rotating rod (Columbus Instruments, Rotamex-5 1.3). Each mouse was trained to walk on the rod three times per day for three days. Training trials were 5 minute duration at 5 r.p.m., with each training trial separated by 60 minutes. Mice that fell from the rod during the training trial were placed back on the rod a maximum of three times. Following training, rod acceleration was increased in 0.2 r.p.m. increments every second starting at 0 r.p.m. and reaching a maximum of 50 r.p.m. Falls were detected by photobeam break.

Stride length was determined by measuring the distance between paw prints as mice walked across a 5 cm wide 60 cm long corridor. Mice were trained daily for 5 consecutive days to walk down the corridor. On training days, each mouse was placed at the beginning of the corridor and the home cage was placed on its side at the other end of the corridor. Once mice traversed the lengh of the corridor to their home cage they were allowed to remain for at least 5 minutes before the next training trial. No more than three training trials were conducted on each day. Mouse forepaws were dipped in black ink so that a print would be left on white paper as the mouse traversed the corridor. Strides were measured from the tip of one paw print to the base of the next paw print on the same side. Stride length was measured in instances in which at least 5 consecutive uninterrupted strides occurred. A minimum of 15 strides were collected for each mouse to determine average stride length.

The elevated-plus maze consisted of four 12-inch arms (two open and two enclosed), suspended 30 inches above the floor. Each test began with the mouse oriented toward an open

arm. Each mouse was given 5 minutes to freely explore the apparatus during which time beam breaks were recorded to track movement and location. The percentage of time spent in the open arm was recorded and used as a measure of anxiety as mice naturally prefer the enclosed arms and anxiolytics have been shown to increase the time rodents spend in the open arm (Pellow et al., 1985). The percentage of time spent exploring the open arms was calculated by dividing the time spent in the open arms by the combined time spent in the open and closed arms. Total distance traveled in the apparatus was also recorded.

Open field performance was measured by individually placing each mouse in an opaque Plexiglas box (61 cm X 61 cm) for 5 minutes. The center of the open field was set 15 cm from the each side of the box. The time each mouse was in the center, the number of entries into the center, and the latency to entry into the center of the open field were measured.

Forced swim performance was measured by placing each mouse in a beaker (diameter 30 cm) filled with water 27°C ±1°C. Swimming behavior was scored for the first 6 minutes and defined as forelimb movement in which forelimbs broke the surface of the water. Floating was defined as a lack of active movement except to remain afloat (treading).

Tail suspension performance was assessed by suspending each mouse from its tail at a height of 15 cm above a surface. Struggling was defined as forelimb and hindlimb movement or twisting movements. Mice were considered to be immobile if their forelimb and hindlimbs were not moving. Swinging was not scored as movement. Behavior was scored for the first 6 minutes.

Sucrose preference was assessed by providing two food cups to individually housed mice. One cup contained between 1-2 g of standard rodent diet (Purina, Lab Diet 5001) the second cup contained high sucrose diet (AIN-76A Rodent Tablets, TestDiet). The amounts of the sucrose and standard diets consumed over the course of 1 h was determined by subtracting the post-feeding weight of the food from the pre-feeding weight of the food. This procedure was

repeated on 3 consecutive days. The reported sucrose preference values were collected on the third day.

The novel object recognition task was performed as we previously described (Papale et al., 2010). Briefly, mice were acclimated to an open-field box for five consecutive days for 10 minutes each day. On the sixth day each animal was placed in the open-field box for 5 minutes and then returned to the home cage for 2 minutes. Mice were then returned to the open field box where they were given 5 minutes to explore three objects arranged in three of the four corners of the box, at least 10 inches from the edge. Mice were returned to their home cage for either 5 (short exposure) or 20 (long exposure) minutes. Mice were returned to the open-field box for 5 minutes where one object had changed position (novel position), one object had been exchanged for a different object (novel object), and one object was the same (familiar object). The time each mouse spent exploring each object at the second exposure was recorded.

Y-maze performance was determined by placing each mouse at the end of one arm of the Y-maze and allowing free exploration of the apparatus for 8 minutes. The Y-maze consists of three identical arms and a center zone. Spontaneous alternations were recorded by video camera.

Continuous video-electrocorticogram monitoring

Video-EEG recordings to detect cortical seizure activity were collected and analyzed as we previously described (Martin et al., 2007; Papale et al., 2009; Dutton et al., 2012). EEG recordings from the inferior colliculus were collected as follows. Mice were anesthetized by isoflurane (2-chloro-2-(difluromethoxy)-1,1,1-trifluoro-thane) inhalation. Two sterile 0-80x3/32 sterile screw electrodes (Vintage Machine Supplies, Medina, OH) were implanted in the skull at the following coordinates from Bregma (anteroposterior (AP) 1.5 mm and mediolateral (ML) 1.2 mm; AP 1.0 mm and ML 1.2 mm). Stainless steel electrodes (diameter 0.25 mm, length 1.5 mm; Plastics one, Roanoke, VA) were implanted at the following coordinates (AP -3.5 mm, ML ±1.5

mm, depth 1.2 mm from the surface of the skull). Two fine-wire electrodes were implanted in the neck muscle for electromyography (EMG) acquisition. Electrodes were covered with dental acrylic following implantation. After a minimum of five days for recovery from surgery, mice were moved to a recording chamber were they were allowed to freely move and were provided food and water *ad libitum* during EEG acquisition. EEG recordings were sampled at 200 Hz. Signals were digitized, amplified and processed by Stellate Harmonie EEG system (Natus Medical, Inc.). EEG traces were manually scored.

Seizure induction

Flurothyl seizure induction was performed as we previously described (Martin et al., 2007). Latencies to the first occurrence of the myoclonic jerk (MJ) and generalized tonic-clonic seizure (GTCS) were recorded. MJ presents as a jerk of the upper body sometimes accompanied by tail-limb clonus. The GTCS was defined by complete loss of postural control and clonus of all limbs. Mice were also observed for the presence of hind-limb extension immediately following the GTCS.

Partial psychomotor seizures were evoked as described in Chapter 2. Briefly, mice were administered a corneal analgesic 30 minutes prior to stimulation. Corneal electrical stimulation (6-Hz, 3 sec, 14 mA to 30 mA) was applied. Resulting seizures were scored according to the following modified Racine scale. 1 = staring, 2 = forelimb clonus, 3 = rearing and falling.

Audiogenic seizures were induced using a key ringing method and by the use of a high-intensity tone. For the key ringing method, each mouse was placed in a clear Plexiglas box and keys were shaken for 5 minutes approximately 25 cm above the mouse. Shaking a key bundle was found to produce a broad-spectrum acoustic stimulus (13-85 kHz) at an intensity ranging from 50-80 dB, as determined by a 1/4" Brüel & Kjaer microphone (Brüel & Kjaer, Denmark). For the high-intensity tone method, a wide range speaker (Model RT1.3, HiVi inc., Arcadia, CA)

was used to produce a 12 kHz, 80 dB tone. Each mouse was exposed to this tone for 5 min and audiogenic seizures were defined by wild-running behavior progressing to loss of posture and forelimb and hindlimb clonus, sometimes followed by tonic hindlimb extension.

Preparation and incubation of slices

Mice (p26-p28) were anesthetized with halothane before removing their brains. Transverse hippocampal slices (350 μm) were cut using a Leica VT1200S microtome in oxygenated (95% O_2, 5% CO_2) ice cold sucrose ACSF (sACSF) containing (in mM): 85 NaCl, 65 sucrose, 2.5 KCl, 25 glucose, 1.25 NaH_2PO_4, 4 $MgSO_4$, 0.5 $CaCl_2$, and 24 $NaHCO_3$. Slices were incubated at 33°C for at least 1 h before electrophysiological recordings in oxygenated standard ACSF containing (in mM): 126 NaCl, 2.5 KCl, 1.25 $NaHPO_4$, 1.2 $MgSO_4$, 10 glucose, 1.2 $CaCl_2$, and 24 $NaHCO_3$.

Electrophysiological slice recordings

Slices were held at 33°C and perused with oxygenated standard ACSF at 2 mL/min during electrophysiological experiments. Cells were visualized with an upright microscope (Zeiss) equipped with infrared differential interference contrast optics. Recording pipettes (2-3 MΩ) were pulled from borosilicate glass with a P-87 Flaming-Brown puller (Sutter Instruments, Novato, CA). Electrophysiological experiments were obtained using MultiClamp 700B amplifier (Molecular Devices, Union City, CA) and digitized with a Digidata 1322A digitizer (Molecular Devices). Data were acquired and analyzed with pClamp 10.2 software (Molecular Devices). Pipettes were filled with 150 mM NaCl and positioned in the CA3 stratum pyramidal layer. ACSF with elevated potassium was prepared by supplementing standard ACSF with 3 M KCl to raise the potassium concentration to 8.5 mM $[K^+]_O$. The experimental paradigm consisted of a control recording for 2 min in standard ACSF, followed by 15-25 min with 8.5 mM K+ ACSF perfusion,

in which burst activity was recorded. This was followed by a 7 minute washout with standard ACSF. Population spikes were elicited in the CA3 pyramidal layer by stimulation of the mossy fiber tract with a tungsten wire. Population spikes were evoked in physiological 2.5 mM $[K^+]_O$ before and after exposing the slice to 8.5 mM $[K^+]_O$. Slices in which population spike amplitudes did not change more than 20% after exposing the slice to 8.5 mM $[K^+]_O$ were used for analysis.

Auditory Brainstem Nuclei Response

Mice were anesthetized with ketamine and xylazine (i.p., 100 and 10 mg/kg respectively) and placed in a heated (25°C) sound attenuating booth (Industrial Acoustics Company, Bronx, NY). ABRs were recorded using Tucker Davis Technologies BioSigRP© software running on a System 3 platform equipped with an RX5 Pentusa Base Station connected to subdermal electrodes via an RA4LI low impedance headstage (TDT, Alachua, FL, USA). Sets of tone pips at different frequencies were presented in a random order to each animal to avoid possible ordering effects.

A subdermal needle electrode was placed over the skull vertex as the active lead. The ground was placed ventral lateral to the left external pinna and the reference was placed ventral lateral to the right external pinna. The bioelectric signals were sampled at 25 kS/s, bandpass filtered between 100 Hz - 3000 Hz, amplified 200,000 times and averaged over 500 consecutive responses, following a previously established ABR screening protocol in mice (Zheng et al., 1999). To determine the ABR threshold, we reduced the stimulus intensity in 10 dB steps and then 5 dB steps until the lowest intensity at which the dominant ABR wave was visible. Thresholds were then finally determined offline with the observer blinded to an animal's group identity.

Auditory stimuli

Calibrated stimuli were generated using TDT SigGenRP© software and presented through BioSigRP© software via a TDT RX6 digital signal processor at a sample rate of 195 kS/s. Sounds were attenuated by a TDT PA5 programmable attenuator and played from an Infinity EMIT tweeter placed 90° to the right side of the animal. Absolute sound pressure levels (SPL) of sound stimuli were measured prior to ABR recording experiments using a calibrated ¼" Brüel and Kjaer (B&K, Denmark) Type 4139 microphone with a Type 2669 preamplifier. Pure tone pips of 3 ms duration with 1.5 ms cos2 rise/fall times were presented for 5, 8, 10, 12, 15, and 24 kHz at a rate of 21 per second.

Immunohistochemistry

Following auditory stimuli exposure, mice were transcardially perfused with ice-cold 4% paraformaldehide (PFA). Brains were extracted and stored in 30% sucrose for 5 days before slicing. Coronal slices (45 μm) were cut using a cryostat (Leica, Germany). Every fifth slice was washed in phosphate buffered saline (PBS) and incubated overnight in primary rabbit anti-c-Fos antibody (Abcam, 1:5,000). Slices were washed in PBS and incubated in secondary antibody horseradish peroxidase conjugated goat anti-rabbit (GE, 1:5,000) for 30 minutes. Staining was performed using the Vectastain Elite ABC System (Vector). Images were collected using the Microbrightfield stereology system (MBF Bioscience, Williston, VT).

Statistics

All behavioral tests and flurothyl latencies were analyzed using a one-way analysis of variance (ANOVA) followed by Dunnett's or Tukey's *post hoc* tests. Binary seizure outcomes were analyzed using the X^2 test. Weight data was analyzed using a two-way analysis of variance, genotype X time. ABRs were analyzed by two-way ANOVA or by the Student's t-test.

3.6. Acknowledgments

We would like to thank the Emory University Rodent Behavioral Core for assistance with assessing locomotor activity. In particular we would like to thank David Weinshenker and Jason Schroeder of the Rodent Behavior Core for their assistance.

CHAPTER 4

Contrasting Effects on Seizure Susceptibility of Conditional Cell-Type Specific Inactivation of the *Scn8a* Gene

Chapter 4 contains material from the manuscript in preparation: Contrasting effects on seizure susceptibility of conditional cell-type specific inactivation of the *Scn8a* gene, Makinson C.D., Tanaka, B., Papale A. L., Christian C., Huguenard, J.R., Goldin A. L., Escayg A.

4.1. Summary

Voltage gated sodium channels (VGSCs) are critical regulators of neuronal excitability and synchrony and play important roles in the pathophysiology of many disorders including epilepsy. Mutations in the VGSC gene *Scn8a* lead paradoxically to protection against induced seizures and the generation of spontaneous absence seizures in mice. To determine the relative contribution of excitatory and inhibitory cells to these seizure phenotypes, we generated mice in which *Scn8a* was selectively deleted from these cell types and evaluated seizure susceptibility and spontaneous seizure activity. Reduced *Scn8a* expression in excitatory cells of the hippocampus and cortex was found to elevate seizure thresholds, reduce hippocampal epileptiform bursting in the presence of high extracellular potassium, and normalize the survival of mice carrying a human *Scn1a* epilepsy mutation. In contrast, broad, inhibitory cell-specific deletion of the *Scn8a* gene had no effect on seizure thresholds or hippocampal bursting, but resulted in the generation of spontaneous spike-wave discharges (SWD). *Scn8a* immunoreactivity was assessed in major inhibitory neuronal populations of the thalamocortical circuit which is important for generating SWDs. Inhibitory thalamic reticular neurons but not inhibitory cortical neurons were found to express high levels of *Scn8a*. Intracellular recordings from thalamic reticular neurons revealed robust deficits in tonic but not bursting outputs. These findings demonstrate that the two major seizure phenotypes associated with loss of *Scn8a*, resistance to tonic-clonic seizures and susceptibility to absence epilepsy, can be decoupled and attributed to loss of channel activity in forebrain excitatory cells and inhibitory interneurons, respectively. Loss of *Scn8a* leads to profound deficits in nRT output, which likely contributes to the generation of SWD.

4.2. Introduction

High levels of *Scn8a* expression have been observed at the axon initial segments of excitatory neurons of the hippocampus and cortex (Boiko et al., 2003; Van Wart et al., 2007; Lorincz and Nusser, 2008; Kress et al., 2010; Liao et al., 2010b) where it sets the thresholds for action potential generation (Hu et al., 2009) and contributes to subthreshold sodium currents (Cooper et al., 2005; Hargus et al., 2013). As revealed by electrophysiological examination of *Scn8a* deficient mice, loss of this channel reduces the excitability of hippocampal and cortical excitatory neurons (Royeck et al., 2008). Additionally, in Chapter 2 we demonstrated that hippocampal slice preparations from *Scn8a*-med mice exhibit less bursting activity, and that selective *in vivo* reduction of *Scn8a* in the hippocampus increases resistance to picrotoxin- and flurothyl-induced seizures and ameliorates the seizure phenotype of *Scn1a* mutants.

Paradoxically, we also identified spike-and-wave discharges (SWD), a hallmark of absence epilepsy, in three separate mouse models of *Scn8a* dysfunction, indicating that *Scn8a* mutations can also cause absence epilepsy in mice (Papale et al., 2009). This finding was unexpected given that loss of VGSC function is expected to reduce neuronal excitability but absence seizures are thought to be a consequence of hyperexcitability of thalamocortical circuitry.

A better understanding of the mechanistic basis underlying the relationship between *Scn8a*-associated seizure protective and absence seizure generation is necessary in order to accurately access the feasibility of selectively targeting *SCN8A* as a treatment for refractory seizure disorders such as Dravet Syndrome.

Here we propose a mechanism to describe each of the major seizure phenotypes that result from loss of *Scn8a* activity. We demonstrate that loss of *Scn8a* expression in forebrain excitatory circuits leads to resistance to induced tonic-clonic seizures, and increased survival and seizure resistance in an *Scn1a*-GEFS+ epilepsy model. Additionally, we demonstrate that loss of *Scn8a* from CNS interneurons does not influence seizure thresholds but is sufficient to generate

spontaneous SWDs. We further propose that loss of *Scn8a* expression leads to deficits in nRT output that may contribute to SWDs.

4.3. Results

The floxed *Scn8a* allele does not alter $Na_v1.6$ (*Scn8a*) protein levels or flurothyl-induced seizure thresholds.

To determine if the floxed *Scn8a* allele alters $Na_v1.6$ (*Scn8a*) expression levels in the absence of *Cre* recombinase, we quantified and compared $Na_v1.6$ levels by Western blot analysis of whole brain homogenates between WT and homozygous *Scn8a*-floxed (*Scn8a*$^{f/f}$) littermates. Normalized optical densities (OD) were not statistically different (mean normalized OD, WT = 5.7 ± 0.9, *Scn8a*$^{f/f}$ = 5.0 ± 0.6; Student's t test $p > 0.05$; Fig. 4.1, *A*). To determine if the floxed *Scn8a* allele alters seizure susceptibility in the absence of *Cre*, we measured latencies to flurothyl-induced seizures in WT and *Scn8a*$^{f/f}$ littermates. No significant differences in the average latencies to the myoclonic jerk (MJ) or the generalized tonic clonic seizure (GTCS) were observed (Mann-Whitney U test MJ $p > 0.05$, GTCS $p > 0.05$; Fig. 4.1*B*).

The floxed *Scn8a* allele is efficiently recombined by the Emx1- and Dlx5/6-*Cre* transgenes.

To determine if the Emx1- (Gorski et al., 2002) and Dlx5/6-*Cre* (Monory et al., 2006) lines are capable of driving recombination of the *Scn8a* floxed allele in the expected brain regions, PCR detection of DNA isolated from the cortex, hippocampus, and thalamus of Emx1-*Cre*/*Scn8a*$^{f/+}$, Dlx5/6-*Cre*/*Scn8a*$^{f/+}$, and *Cre* negative littermates (no-*Cre*/*Scn8a*$^{f/+}$) was performed. A 325 bp PCR band indicating deletion of the floxed allele was detected in samples from the cortex, hippocampus, and thalamus of Dlx5/6-*Cre*/*Scn8a*$^{f/+}$ mice but not from tail-derived DNA or in samples from no-*Cre*/*Scn8a*$^{flox/+}$ littermates (Fig. 4.1*C*). A 325 bp PCR product indicating deletion of the floxed allele was detected in samples from the cortex and hippocampus of Emx1-

Cre/*Scn8a*$^{f/+}$ mice but not in the thalamus, tail-derived DNA or samples from no-*Cre*/*Scn8a*$^{flox/+}$ littermates (Fig. 4.1*C*). The intensity of the deleted bands isolated from the cortex and hippocampus of Emx1-*Cre*/*Scn8a*$^{f/+}$ mice were qualitatively more intense than the bands from the same regions of Dlx5/6-*Cre*/*Scn8a*$^{f/+}$ mice.

Verification of cell-type and region specificity of *Cre* lines

To verify the brain region and cell-type specificity of Emx1- and Dlx5/6-*Cre*-driven recombination, these lines were crossed to a *ROSA* reporter. Anti-GluR2 immunoreactivity was used to detect excitatory neurons and GAD67 was used as a marker of inhibitory neurons. The percentage of reporter positive cells that colocalized with each cell type marker was recorded. High levels of reporter expression were observed in the majority of hippocampal and cortical regions in Emx1-*ROSA* mice: dentate gyrus (DG) 98% (333/340), CA1 99% (92/93); layer 2-3 85% (55/65), layer 4 91% (50/55), layer 5-6 59% (36/63) (Table 4.1). Emx1-*Cre* positive neurons were not observed in the CA3 region of the hippocampus. Very few Emx1-*Cre* positive cells were detected outside of the forebrain including the caudate putamen 50% (2/4) and thalamic reticular nucleus (nRT) 0%. High levels of co-localization was observed between Dlx5/6-reporter and GAD67 expression in most brain regions that were evaluated including: hippocampal subfields, DG 83% (10/12), CA3 100% (3/3), CA1 90% (9/10); cortex, layer 2-3 93% (14/15), layer 4 100% (3/3), layer 5-6 100% (7/7) (Table 4.1). GAD67 colocalization with reporter expression was also observed in other regions including the caudate putamen 8% (16/198), amygdala 54% (14/26), and the thalamic reticular nucleus 100% (64/64) (Table 4.1).

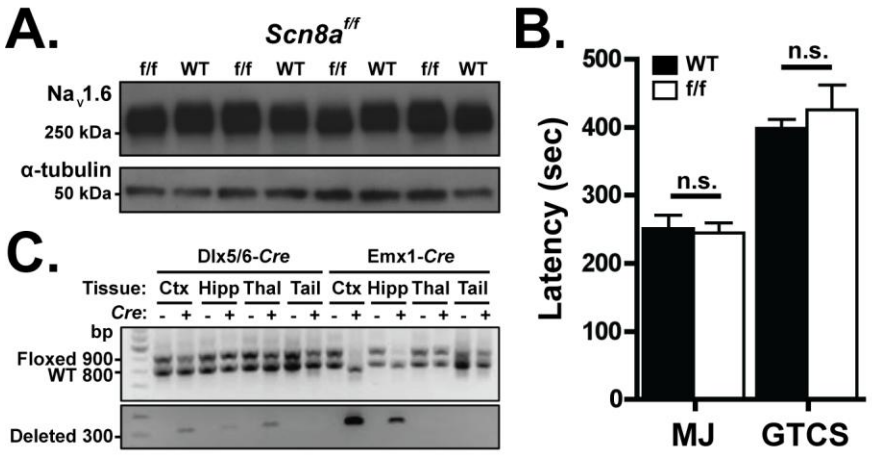

Figure 4.1. The floxed *Scn8a* allele does not alter $Na_v1.6$ (*Scn8a*) protein levels or flurothyl-induced seizure thresholds in the absence of *Cre* but is efficiently recombined in expected brain regions by the Emx1- and Dlx5/6-*Cre* drivers

A. No change in $Na_v1.6$ levels was detected by Western blot analysis of membrane-enriched whole brain samples isolated from WT and *Scn8a*$^{f/f}$ mice (Student's t test, $p > 0.05$; n = 4 per group). ***B.*** Likewise, the latency to the myoclonic jerk (MJ) and the generalized tonic-clonic seizure were not significantly different between WT and *Scn8a*$^{f/f}$ mice (Mann-Whitney U test, MJ n.s. $p > 0.05$, GTCS n.s. $p > 0.05$; n = 9 per group). ***C.*** PCR detection of DNA isolated from the cortex, hippocampus, and thalamus and tail of *Scn8a*$^{f/+}$/Emx1-*Cre*, *Scn8a*$^{f/+}$/Dlx5/6-*Cre*, and *Cre* negative littermates (*Scn8a*$^{f/+}$/no-*Cre*) was performed. Deleted product was detected in samples from the cortex, hippocampus, and thalamus of *Scn8a*$^{f/+}$/Dlx5/6-*Cre* mice but not from the tail or in samples from *Scn8a*$^{f/+}$/no-*Cre* littermates. Deleted product (325 bp) was detected in samples from the cortex and hippocampus of *Scn8a*$^{f/+}$/Emx1-*Cre* mice but not in the thalamus or tail or in samples from *Scn8a*$^{f/+}$/no-*Cre* littermates.

	Emx1		Dlx5/6	
Brain Region	***% GluR2 & Cre+***	***Cells Counted***	***% GAD67 & Cre+***	***Cells Counted***
Hippocampus				
Dentate Gyrus	98%	340	83%	12
CA 3	-	-	100%	3
CA 1	99%	93	90%	10
Cerebral Cortex				
Layer 1	0%	0	97%	16
Layer 2-3	85%	65	93%	15
Layer 4	91%	55	100%	3
Layer 5-6	59%	63	100%	7
Other				
Caudate Putamen	50%	4	8%	198
Amygdala	0%	15	54%	26
Reticular Nucleus	-	-	100%	64

Table 4.1. Summary of colocalization of Dlx5/6-*Cre* and Emx1-*Cre* expression in the CNS

Immunofluorescence detection of cell-type markers was performed in brain slices of Dlx5/6-*Cre-ROSA* and Emx1-*Cre-ROSA* animals. The percentage of reporter positive cells that also express the cell-type marker are indicated. High levels of colocalization between Emx1-*Cre* and Glur2 immunoreactivity was detected in most regions of the forebrain. High levels of colocalization were observed between Dlx5/6-*Cre* and GAD67 immunoreactivity in the forebrain and nRT. These experiments were performed by Brian Tanaka in the laboratory of Alan Goldin at the University of California, Irvine.

Conditional inactivation of *Scn8a* in excitatory neurons confers resistance to flurothyl-induced seizures.

Cell-type specific *Cre*-mediated deletion of the floxed *Scn8a* allele was used to determine the contribution of relevant cell types to *Scn8a*-associated seizure resistance. Four *Cre* transgenic lines were chosen based on cell-type and region specificity. The Emx1- and Camk2a-*Cre* lines were used to achieve selective reduction of *Scn8a* expression in excitatory neurons. The Dlx5/6-*Cre* line was used to achieve broad interneuron deletion of the floxed *Scn8a* allele and the Ppp1r2-*Cre* line was used to primarily reduce *Scn8a* expression in parvalbumin interneurons of the forebrain. Latencies to flurothyl-induced seizures were increased following *Scn8a* deletion by both *Cre* lines that target excitatory neurons (Mann-Whitney U test, Emx1, MJ n.s. $p = 0.055$, GTCS $p < 0.01$; Camk2a; $p < 0.05$; Fig. 4.2*A*-*B*). Susceptibility to flurothyl-induced seizures was not altered in mice expressing the floxed allele and *Cre* transgenes from either the Dlx5/6 or the Ppp1r2-*Cre* lines (Mann-Whitney U test $p > 0.05$, Fig. 4.2*C*-*D*).

Conditional inactivation of *Scn8a* in excitatory neurons confers resistance to hippocampal epileptiform burst discharges in slice preparations.

To establish that excitatory cell-specific deletion of *Scn8a* is protective in a separate seizure model, we measured epileptiform burst discharges, elicited by high extracellular potassium, in hippocampal slices of *Scn8a*$^{f/+}$/Emx1-*Cre* and *Scn8a*$^{f/+}$/Dlx5/6-*Cre* mice (Fig. 4.3). Consistent with our seizure susceptibility data, we observed reductions in the latency and frequency of burst discharges in Emx1-*Cre* but not in Dlx5/6-*Cre* animals when compared to *Cre* negative controls (Student's t-test, Emx1-*Cre* $p < 0.05$; Dlx5/6-*Cre* $p > 0.05$; Fig. 4.3).

Resistance to flurothyl-induced seizures increase with increasing levels of *Scn8a* inactivation in excitatory forebrain neurons

In Chapter 2 we showed that the *Scn8a* mutations, R1627H and medjo, increase resistance to flurothyl-induced seizures in heterozygous mutants but not in homozygous mutants. To determine if a similar gene-dosage relationship exists following excitatory cell-specific deletion of *Scn8a*, we crossed *Scn8a*$^{f/+}$/Emx1-*Cre* mice to *Scn8a*$^{f/f}$ mice and compared susceptibility to flurothyl-induced seizures between homozygous (*Scn8a*$^{f/f}$/Emx1-*Cre*) and heterozygous (*Scn8a*$^{f/+}$/Emx1-*Cre*) deletion of *Scn8a*. Littermates in which *Scn8a* was not deleted (*Scn8a*$^{f/+}$/no-*Cre*) served as controls (Fig. 4.4). In contrast to mice globally expressing *Scn8a* mutations, we found that the order of seizure resistance was; *Scn8a*$^{f/f}$/Emx1-*Cre* > *Scn8a*$^{f/+}$/Emx1-*Cre* > *Scn8a*$^{f/+}$/no-*Cre* (one-way ANOVA $p < 0.05$; Tukey *post hoc* MJ, *Scn8a*$^{f/+}$/no-*Cre* vs. *Scn8a*$^{f/f}$/Emx1-*Cre* $p < 0.01$; GTCS, *Scn8a*$^{f/+}$/no-*Cre* vs. *Scn8a*$^{f/+}$/Emx1-*Cre* $p < 0.01$, *Scn8a*$^{f/+}$/no-*Cre* vs. *Scn8a*$^{f/f}$/Emx1-*Cre* $p < 0.0001$, *Scn8a*$^{f/+}$/Emx1-*Cre* vs. *Scn8a*$^{f/f}$/Emx1-*Cre* $p < 0.05$; Fig. 4.4).

Forebrain excitatory cell-specific deletion of *Scn8a* increases seizure resistance and survival of *Scn1a*-R1648H GEFS+ mutants

Increased survival and seizure thresholds have been observed in *Scn1a* GEFS+ (Hawkins et al., 2011) and DS (Martin et al., 2007) mutants that also express *Scn8a* mutations. Also, we showed that reduced *Scn8a* activity can reduce induced epileptiform bursting in hippocampal slices from *Scn1a*-R1648H mutants (Chapter 2). To determine if selectively reducing *Scn8a* expression in forebrain excitatory neurons would similarly lead to increased seizure resistance and prolong survival, we crossed mice carrying the *Scn8a*-floxed allele to mice carrying the *Scn1a*-R1648H GEFS+ mutation and the Emx1-*Cre* gene and evaluated survival and susceptibility to flurothyl-induced seizures in the offspring (Fig. 4.5). Survival was reduced by 20% in *Scn8a*$^{f/+}$/no-

Cre/*Scn1a*$^{RH/+}$ mice, but normal in *Scn8a*$^{f/+}$/Emx1-*Cre*/*Scn1a*$^{+/+}$ and *Scn8a*$^{f/+}$/Emx1-*Cre*/*Scn1a*$^{RH/+}$ mice (Fig. 4.5*A*). No significant changes in average latencies to the MJ were observed between any of the genotypes (Fig 4.5*B*). However, average latencies to GTCS were increased in *Scn8a*$^{f/+}$/Emx1-*Cre*/*Scn1a*$^{+/+}$ and *Scn8a*$^{f/+}$/Emx1-*Cre*/*Scn1a*$^{RH/+}$mice, and reduced in *Scn8a*$^{f/+}$/no-*Cre*/*Scn1a*$^{RH?+}$ mice when compared to WT littermates (Fig. 4.5.*B*).

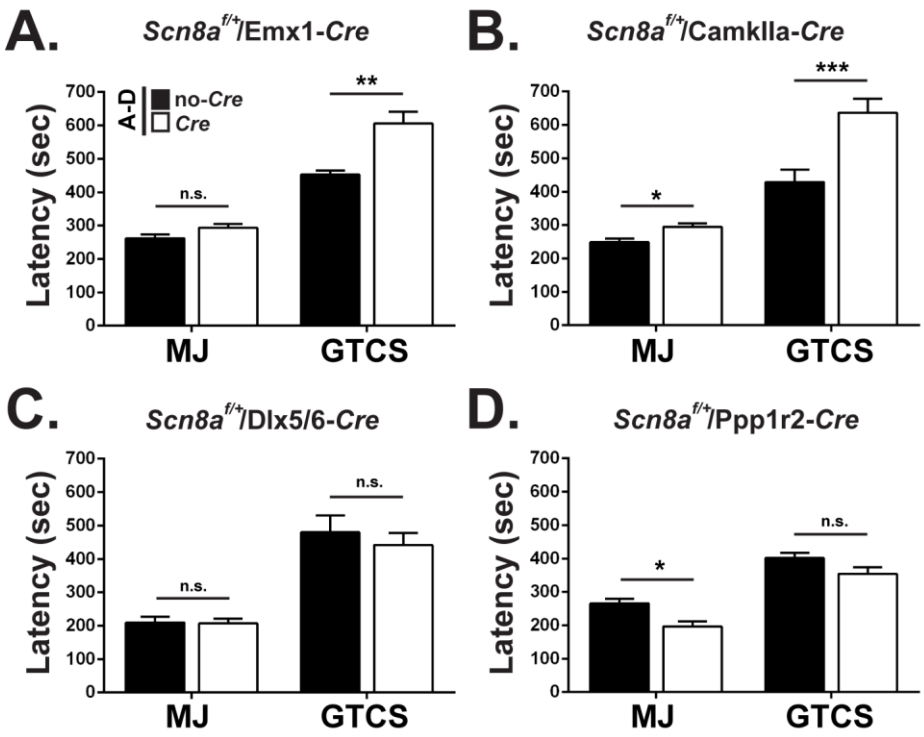

Figure 4.2. Seizure thresholds are increased by loss of *Scn8a* from excitatory but not inhibitory neurons

A. Inactivation of the *Scn8a* gene in excitatory forebrain neurons by the Emx1-*Cre* line increased seizure thresholds to the GTCS but not MJ (Mann-Whitney U test, MJ n.s. $p > 0.05$, GTCS $^{**}p < 0.01$; n = 13-17 per group). ***B.*** Inactivation of the *Scn8a* gene in excitatory neurons by the Camk2a-*Cre* line increased thresholds to flurothyl-induced MJ and GTCS (Mann-Whitney U test, MJ $^{*}p < 0.05$, GTCS $^{***}p < 0.001$; n = 15-16 per group). ***C.*** Flurothyl thresholds were not significantly altered by inactivation of *Scn8a* in inhibitory neurons (Mann-Whitney U test, MJ n.s. $p > 0.05$, GTCS n.s. $p > 0.05$; n = 6-8 per group). ***D.*** Latencies to the MJ but not the GTCS were decreased in mice with preferential inactivation of *Scn8a* in forebrain parvalbumin interneurons (Mann-Whitney U test, MJ $^{*}p < 0.05$, GTCS n.s. $p > 0.05$; n = 11-15 per group).

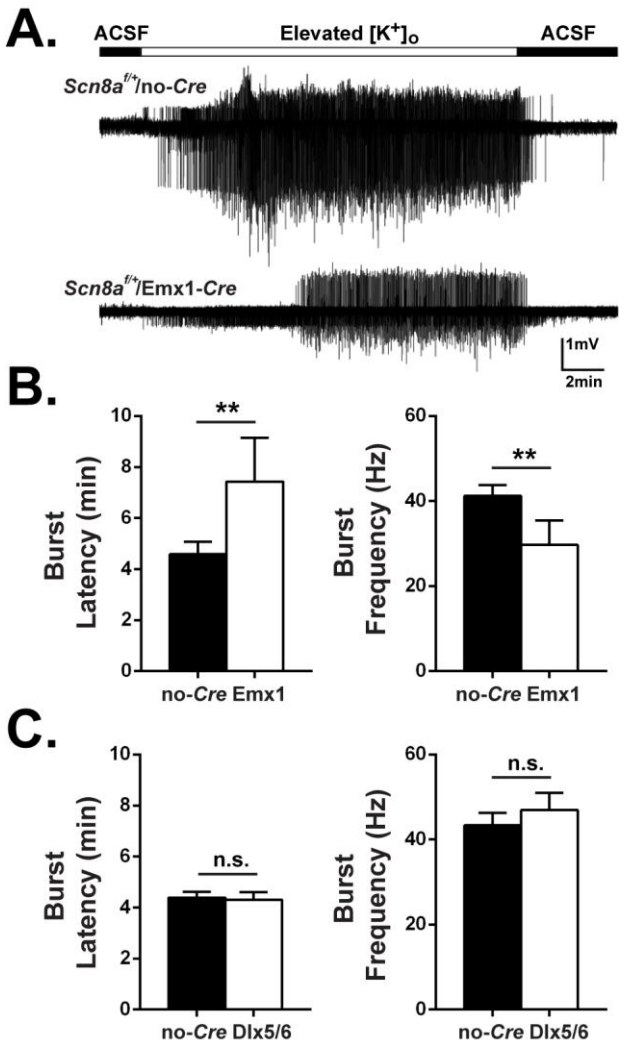

Figure 4.3. Inactivation of *Scn8a* in excitatory forebrain neurons increases resistance to induced epileptiform hippocampal bursting activity

A. Representative example of hippocampal bursting activity in an animal without *Cre* (top trace) and an animal with Emx1-*Cre*-mediated inactivation of *Scn8a* (bottom trace). ***B.*** The latency to the initiation of bursting was reduced in animals carrying the Emx1-*Cre* gene compared to littermates without *Cre* (Student's t test $^{**}p < 0.01$; n = 7-8 per group). Intra-burst frequency was also reduced in animal carrying Emx1-*Cre* compared to controls without *Cre* (Student's t test $^{**}p < 0.01$; n = 7-8 per group). ***C.*** No significant changes to the burst latency or to the burst frequency

were observed between animals carrying Dlx5/6-*Cre* and animals without *Cre* (Student's t test, burst latency $p > 0.05$, burst frequency $p > 0.05$; n = 9 per group). Error bars represent SEM. These experiments were performed by Brian Tanaka in the laboratory of Alan Goldin at the University of California, Irvine.

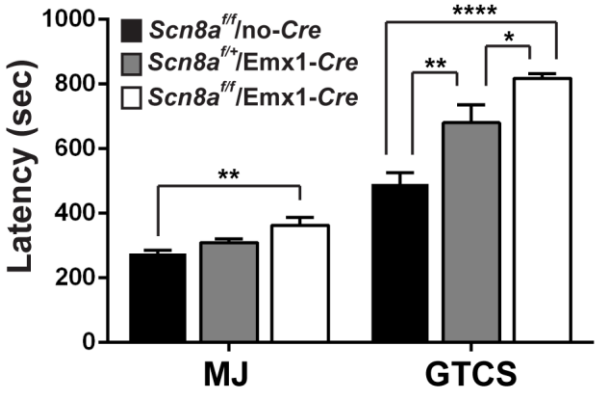

Figure 4.4. Resistance to flurothyl-induced seizures is influenced by the level of inactivation of *Scn8a* in excitatory forebrain neurons

Latencies to the MJ were not altered in *Scn8a*$^{f/+}$/Emx1-*Cre* mice but were increased in *Scn8a*$^{f/f}$/Emx1-*Cre* mice compared to no-*Cre* littermates (one-way ANOVA, MJ $p < 0.01$; Tukey *post-hoc*, *Scn8a*$^{f/f}$/no-*Cre* vs. *Scn8a*$^{f/+}$/Emx1-*Cre* n.s. $p > 0.05$, *Scn8a*$^{f/f}$/no-*Cre* vs. *Scn8a*$^{f/f}$/Emx1-*Cre* $^{**}p < 0.01$, *Scn8a*$^{f/+}$/Emx1-*Cre* vs. *Scn8a*$^{f/f}$/Emx1-*Cre* n.s. $p > 0.05$). Mice with heterozygous inactivation of *Scn8a* in forebrain excitatory neurons (*Scn8a*$^{f/+}$/Emx1-*Cre*) experienced higher latencies to the GTCS that no-*Cre* controls, and mice with homozygous inactivation of *Scn8a* (*Scn8a*$^{f/f}$/Emx1-*Cre*) experienced increased latencies to over mice with heterozygous inactivation (*Scn8a*$^{f/+}$/Emx1-*Cre*) (one-way ANOVA, GTCS $p < 0.0001$; Tukey *post-hoc*, GTCS, *Scn8a*$^{f/f}$/no-*Cre* vs. *Scn8a*$^{f/+}$/Emx1-*Cre* $^{**}p < 0.05$, *Scn8a*$^{f/f}$/no-*Cre* vs. *Scn8a*$^{f/f}$/Emx1-*Cre* $^{****}p < 0.0001$, *Scn8a*$^{f/+}$/Emx1-*Cre* vs. *Scn8a*$^{f/f}$/Emx1-*Cre* $^{*}p < 0.05$; n = 8-16). Error bars represent SEM.

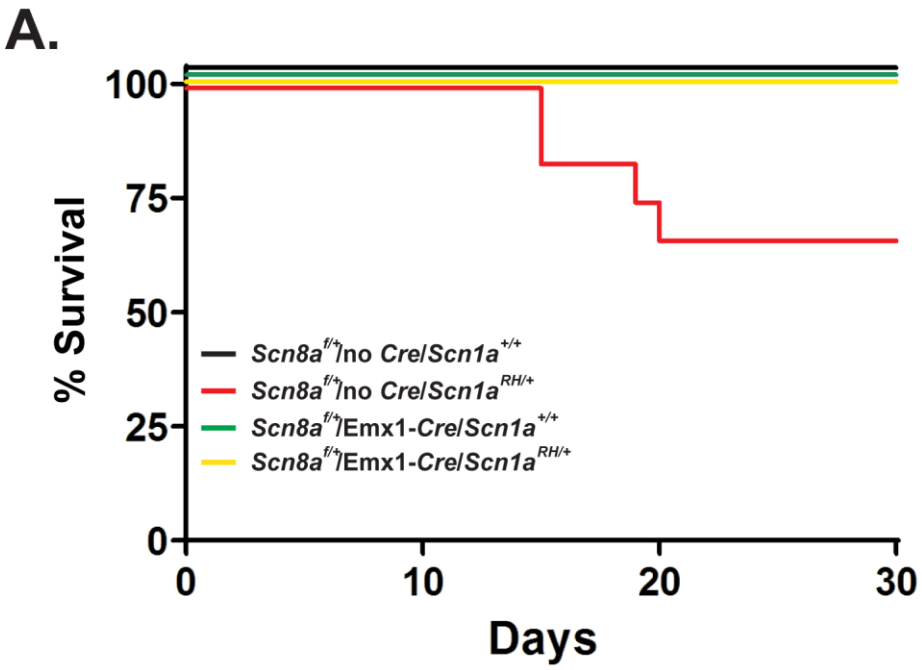
A.
100
75
50
25
0
% Survival
0
10
20
30
Days
Scn8a f/+ /no Cre/Scn1a +/+
Scn8a f/+ /no Cre/Scn1a RH/+
Scn8a f/+ /Emx1-Cre/Scn1a +/+
Scn8a f/+ /Emx1-Cre/Scn1a RH/+

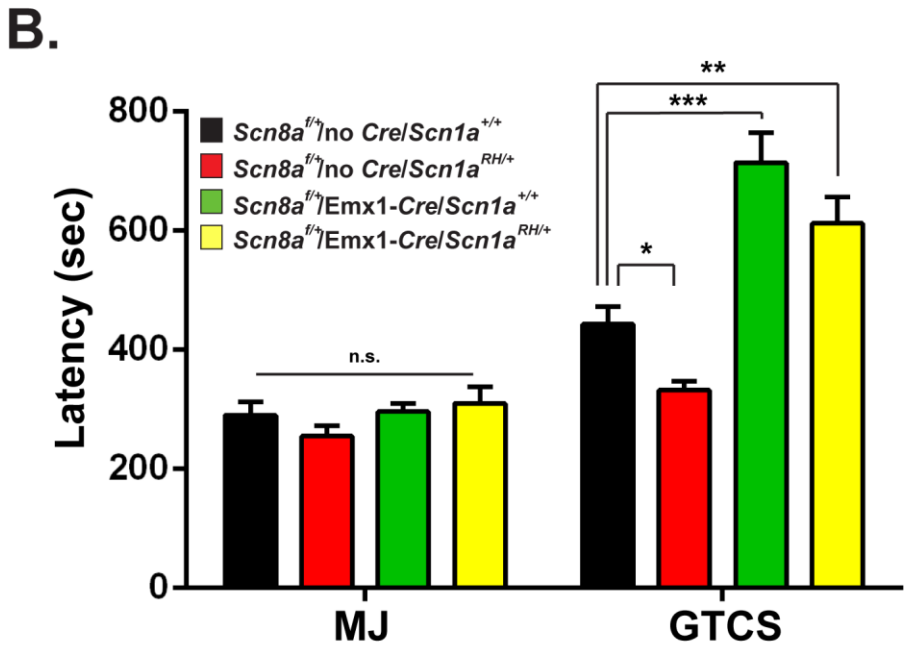
B.
800
600
400
200
0
Latency (sec)
Scn8a f/+ /no Cre/Scn1a +/+
Scn8a f/+ /no Cre/Scn1a RH/+
Scn8a f/+ /Emx1-Cre/Scn1a +/+
Scn8a f/+ /Emx1-Cre/Scn1a RH/+
n.s.
*
***
**
MJ
GTCS

Figure 4.5. Selective inactivation of *Scn8a* in excitatory forebrain neurons in *Scn1a* mutant mice improves survival and increases resistance to flurothyl-induced seizures

Survival (***A***) and flurothyl-induced seizure latencies (***B***) were examined in mice carrying the *Scn1a* R1648H mutation (*Scn1a*$^{RH/+}$) the Emx1-*Cre* transgene and the *Scn8a*-floxed allele (*Scn8a*$^{f/+}$). ***A.*** Survival was reduced by 33% (4/12) in *Scn8a*$^{f/+}$/no-*Cre*/ *Scn1a*$^{RH/+}$ mice. No premature mortality was observed in GEFS+ mice with the Emx1-*Cre* (*Scn8a*$^{f/+}$/Emx1-*Cre*/ *Scn1a*$^{RH/+}$, n=8), Emx1-*Cre*/ *Scn1a*$^{+/+}$ (n= 7), and *Scn8a*$^{f/f}$/no-*Cre*/*Scn1a*$^{+/+}$ (n=9). ***B.*** No significant alterations in MJ latencies were observed (one-way ANOVA, MJ, n.s. $p > 0.01$). As expected, latencies to the GTCS were decreased in *Scn1a* mutant mice (*Scn8a*$^{f/+}$/no-*Cre*/ *Scn1a*$^{RH/+}$), but were increased in *Scn8a*$^{f/+}$/Emx1-*Cre*/ *Scn1a*$^{+/+}$ mice as well as *Scn8a*$^{f/+}$/Emx1-*Cre*/ *Scn1a*$^{RH/+}$ mice when compared to control littermates without *Cre* (*Scn8a*$^{f/f}$/no-*Cre*/*Scn1a*$^{+/+}$). **(**one-way ANOVA, GTCS, $p < 0.0001$; Dunnett's *post-hoc*, GTCS, *Scn8a*$^{f/f}$/no-*Cre*/*Scn1a*$^{+/+}$ vs. *Scn8a*$^{f/+}$/no-*Cre*/ *Scn1a*$^{RH/+}$ $*p < 0.05$, *Scn8a*$^{f/f}$/no-*Cre*/*Scn1a*$^{+/+}$ vs. *Scn8a*$^{f/+}$/Emx1-*Cre*/ *Scn1a*$^{+/+}$ $***p < 0.001$, *Scn8a*$^{f/f}$/no-*Cre*/*Scn1a*$^{+/+}$ vs. *Scn8a*$^{f/+}$/Emx1-*Cre*/ *Scn1a*$^{RH/+}$ $**p < 0.01$; n = 8-14; error bars represent SEM).

Inhibitory inactivation of the *Scn8a* gene leads to spontaneous SWD generation

Spontaneous absence seizures are observed in mice with mutations in the *Scn8a* gene (Papale et al., 2009). To evaluate the relative contribution of excitatory forebrain neurons and inhibitory neurons to SWD generation in *Scn8a* mutants, we performed continuous video/EEG recordings of mice with cell-type specific deletion of *Scn8a*. At least five continuous days of recordings were obtained from *Scn8a*$^{f/+}$/Emx1-*Cre* and *Scn8a*$^{f/+}$/Dlx-*Cre* mice and *Cre* negative littermates. No tonic-clonic seizure activity was observed in any mouse over the recording period. No SWDs were observed in *Scn8a*$^{f/+}$/Emx1-*Cre* animals. However, spontaneous SWDs were observed in mice in which *Scn8a* expression was selectively reduced in interneurons (*Scn8a*$^{f/+}$/Dlx5/6-*Cre*, average SWD per hr = 4.63, n = 5, Fig 4.6*A*). Because SWD frequency in *Scn8a* mutant mice is known to be influenced by genetic background (Papale et al., 2009), the Dlx5/6-*Cre* and Emx1-*Cre* lines were crossed together so that comparisons could diretly be made between littermates (Fig. 4.6*C*). SWDs were observed in *Scn8a* floxed mice with the Dlx5/6-*Cre* transgene (*Scn8a*$^{f/+}$/Dlx5/6-*Cre*) and in *Scn8a* floxed mice expressing both *Cre* transgenes (*Scn8a*$^{f/+}$/Emx1-*Cre*/Dlx5/6-*Cre*), but not in *Scn8a*$^{f/+}$/Emx1-*Cre* or no-*Cre* littermates. Fewer SWDs were observed in mice with both *Cre* genes, *Scn8a*$^{f/+}$/Emx1-*Cre*/Dlx5/6-*Cre* when compared to *Scn8a* floxed mice with only the Dlx-*Cre* transgene (Fig. 4.6*C*).

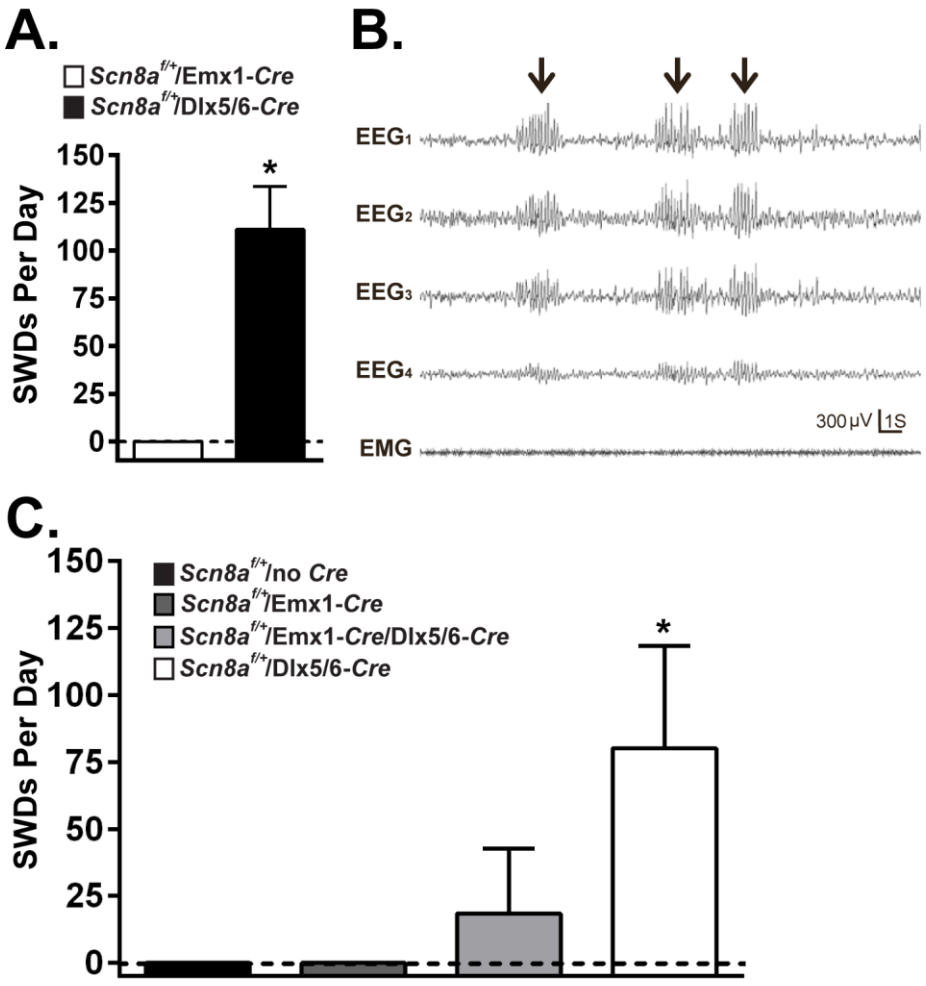

Figure 4.6. Inhibitory neuron-specific but not forebrain excitatory neuron-specific inactivation of the *Scn8a* gene is sufficient to produce SWDs

A. Continuous EEG recordings were performed of mice carrying the floxed *Scn8a* allele and either the Emx1- or Dlx5/6-*Cre* transgenes to assess for the presence of SWDs. No SWDs were observed in mice lacking *Cre* expression (*Scn8a*$^{f/f}$/no-*Cre*; not shown) or in mice with forebrain excitatory neuron-specific *Scn8a* inactivation (*Scn8a*$^{f/+}$/Emx1-*Cre*). Frequent SWDs were observed in mice with inhibitory neuron-specific inactivation of *Scn8a* (*Scn8a*$^{f/+}$/Dlx5/6-*Cre*) (Mann-Whitney U test *$p < 0.05$, n = 4-5 per group). ***B.*** Representative image of SWDs in

Scn8a$^{f/+}$/Dlx5/6-*Cre* mice. ***C.*** SWDs were not observed in *Scn8a* floxed mice without *Cre* (black bar) or *Scn8a* floxed mice with the Emx1-*Cre* transgene (light grey bar). A low frequency of SWDs was observed in mice with both excitatory and inhibitory neuron-specific inactivation of *Scn8a* (dark grey bar). Highest levels of SWDs were observed in mice with only inhibitory neuron-specific inactivation of *Scn8a* (white bar) (one-way ANOVA $p < 0.05$, Tukey post-hoc $*p < 0.05$; n = 5 per group). Error bars represent SEM.

Scn8a immunoreactivity in forebrain and thalamic interneurons

Scn8a immunoreactivity was evaluated in brain slices from WT mice to establish channel expression in cell types and regions that are known to play an important role in the generation of SWDs. *Scn8a* expression was not observed in neurites or soma of inhibitory interneurons in the forebrain (Fig. 4.7*A*). However, *Scn8a* expression was observed in inhibitory neurons of the thalamic reticular nucleus (nRT) (Fig. 4.7*B*-*C*). Brain sections from homozygous *Scn8a* null mutants ($Scn8a^{med/med}$) were used to verify the specificity of the *Scn8a* antibody. Only a low level of background fluorescence was detected in $Scn8a^{med/med}$ tissue probed for *Scn8a* immunoreactivity (Fig. 4.7*D*).

Scn8a deficiency leads to reduced tonic firing in nRT neurons

Current-clamp recordings were performed to determine the firing properties of nRT neurons in WT and $Scn8a^{med/+}$ mice. Reduced ability to maintain repetitive firing in response to prolonged depolarizing current injections was observed in $Scn8a^{med/+}$ nRT neurons (Fig. 4.9*B*) when compared to WT (Fig. 4.9*A*). However, no deficit in calcium-dependent rebound burst firing was observed (Fig. 4.9*A*-*B*).

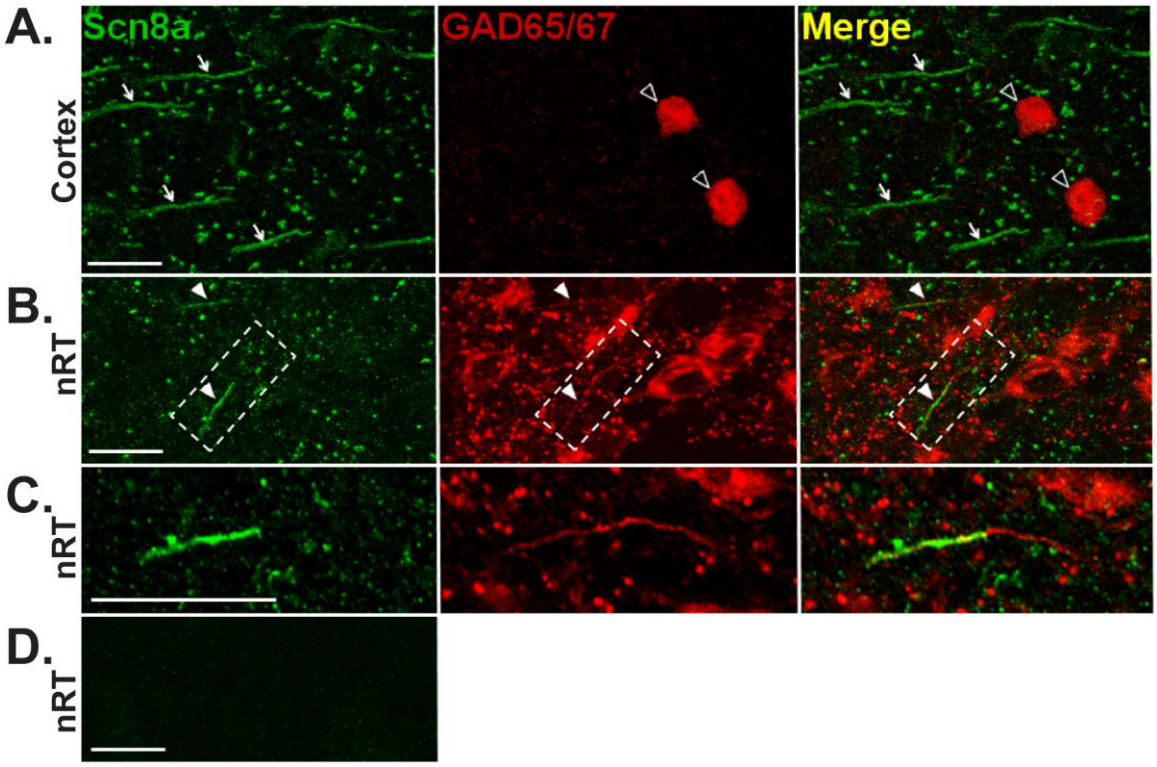

Figure 4.7. Evaluation of *Scn8a* expression in interneuronal populations of thalamocortical circuitry

Scn8a immunoreactivity with the inhibitory neuron marker GAD65/67 is shown in the cortex and nRT. ***A.*** Colocalization of *Scn8a* immunoreactivity and GAD65/67 immunoreactivity was not observed in neuronal soma or neurites in the cortex. ***B.*** Colocalization between *Scn8a* and GAD65/67 was observed in the nRT. ***C.*** Inset of area designated by dashed lines in B to show colocalization. ***D.*** Lack of immunoreactivity in $Scn8a^{med/med}$ (null) negative control tissue. Arrows indicate selected *Scn8a* positive processes that are negative for cell type markers. Open arrowheads indicate cells that are negative for *Scn8a*. Closed arrowheads indicate colocalization. Images were captured at 100X magnification. Scale bars, 10 μm.

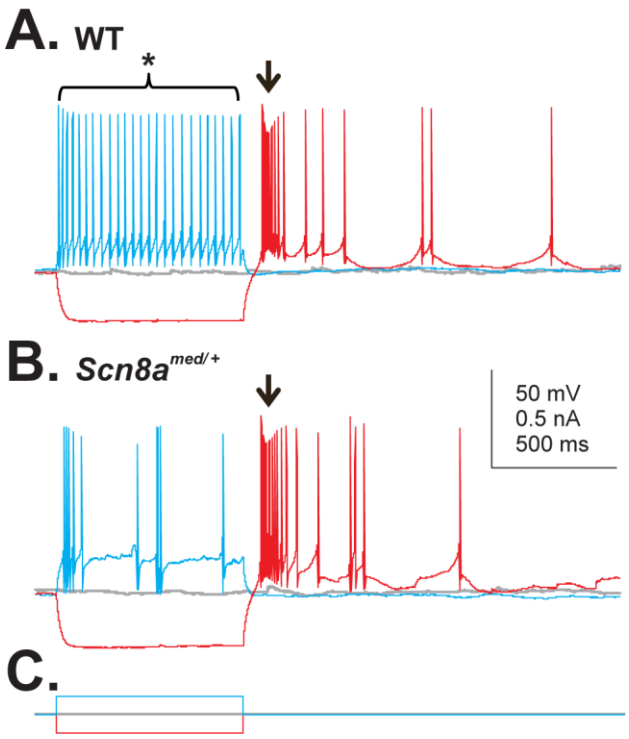

Figure 4.8. nRT neurons of *Scn8a*-deficient mice have impaired tonic firing

Representative electrophysiological recordings in the nRT reveal a robust decrease in AP generation in response to prolonged depolarizing currents (blue traces) in WT (***A***) vs. *Scn8a*$^{med/+}$ (***B***) mice. Ca^{++}-mediated rebound bursts (arrows) following hyperpolarization (red traces) were not perturbed in *Scn8a*$^{med/+}$ nRT neurons. ***C.*** Indicates current injection protocol. Grey trace indicates baseline (no current injection). * indicates tonic firing modes. Arrows indicate burst firing modes. n = 10-11 cells. Recordings were performed by Catherine Christian in the Huguenard lab at Stanford.

Developmental progression of absence seizures in *Scn8a*-deficient mice

EEG recordings were collected of *Scn8a*$^{med/+}$ and WT mice from P15 to P52 to establish the onset and progression of absence seizures. Two hours of EEG recordings were obtained daily from each mouse from P15-P32 and on P42 and P52. Seizures were first detected at P17 and reached adult levels by P28. No SWDs were detected in WT littermates (not shown) (Fig. 4.9).

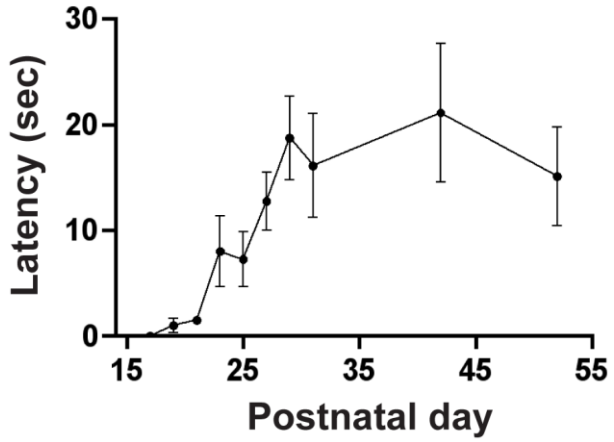

Figure 4.9. Developmental increases in SWDs in *Scn8a*$^{med/+}$ mice

EEG recordings were collected from P15-P52 of mice with global *Scn8a* deficiency (*Scn8a*$^{med/+}$) and WT littermates (not shown) to determine the age of onset and the developmental progression of SWDs. SWDs were first observed on P17 and increased in frequency until reaching adult levels in the fifth postnatal week. SWDs were not observed in WT animals.

4.4. Discussion

Using a combination of genetic, immunohistochemical, and electrophysiological approaches, we investigated the mechanism underlying our previous paradoxical findings that mutations in the *Scn8a* gene lead both to seizure protection and absence seizure generation.

We found that selective *Cre*-mediated deletion of *Scn8a* from excitatory neurons in the forebrain was sufficient to confer resistance to induced seizures. In contrast, deletion of *Scn8a* from inhibitory interneurons had no effect on latencies to flurothyl-induced seizures or bursting activity in hippocampal slice preparations, indicating that the observed seizure resistance (Martin et al., 2007; Hawkins et al., 2011) is forebrain excitatory neuron dependent. Increased *Scn8a* expression/activity, in contrast, has been hypothesized to promote seizure generation. *Scn8a* expression and neuronal excitability were found to be increased in layer V neurons of epileptic mice that are deficient for *Celf4* (Sun et al., 2013). Furthermore, increased *Scn8a* expression was observed in the hippocampus of amygdala-kindled rats (Blumenfeld et al., 2009), and in the entorhinal cortex in an electrical simulation model of TLE (Hargus et al., 2011). In humans, a gain-of-function *SCN8A* mutation was identified in a patient with infantile epileptic encephalopathy and sudden unexplained death in epilepsy (SUDEP) (Veeramah et al., 2012). Our results, together with previous reports support a model of *Scn8a* in epilepsy in which increased *Scn8a* expression leads to increased neuronal excitability and seizure susceptibility while loss of *Scn8a* from excitatory forebrain neurons leads to reduced network excitability and seizure resistance.

In Chapter 3 we demonstrated that mice that are homozygous for the *Scn8a* amino acid substitutions R1627H and medjo do not exhibit increased resistance to flurothyl- or 6Hz-induced seizures or hippocampal burst discharges evoked by high potassium. Interestingly, this gene-dose relationship was not observed in animals with homozygous Emx1-*Cre*-mediated deletion of *Scn8a* (Fig. 4.4). Substitution mutations alter channel activity but not channel expression, while

null mutations or conditional inactivation leads to reduced channel levels at the plasma membrane. This critical difference might underlie the different effect of these mutations on seizure phenotypes. The effect of homozygous recessive null *Scn8a* mutations on seizure phenotypes have not previously been explored because these mutations lead to progressive paralysis and premature death in the first weeks of life. However, homozygous Emx-*Cre* animals were visibly normal and did not display tremor or gate abnormalities.

We have previously reported that mutations in *Scn8a* lead to spontaneous absence seizure generation (Papale et al., 2009). Interestingly, we found that broadly inactivating *Scn8a* in inhibitory neuronal populations using the Dlx5/6-*Cre* line results in the generation of SWDs, consistent with mouse models of absence epilepsy. Inactivation of *Scn8a* in excitatory projection neurons, including corticothalamic neurons, did not produce SWDs.

SWDs are the result of oscillatory activity between the cortex and thalamus, specifically involving interplay between reciprocally connected corticothalamic neurons and thalamocortical neurons as well as GABAergic neurons of the thalamic reticular nucleus (nRT) which send inhibitory projections to thalamocortical cells (TC) and also back onto the nRT itself. Thus, loss of VGSC expression in inhibitory neurons could directly lead to absence seizure generation by affecting the activity of inhibitory nRT neurons or indirectly through inhibitory connections onto layer VI corticothalamic neurons. To distinguish between these possibilities, we performed immunohistochemistry for *Scn8a* and GAD65/67 in the cortex and nRT of mouse brain slices. We were unable to detect colocalization between *Scn8a* and GAD65/67 in the cortex; however, we did observe colocalization of *Scn8a* and GAD65/67 in the nRT.

To determine if *Scn8a* expression in the nRT is important for the activity of these neurons, current clamp recordings were performed on mice that were heterozygous for a null *Scn8a* mutation (*Scn8a*$^{med/+}$) and WT littermates. We found that *Scn8a*$^{med/+}$ mice have a profound reduction in their ability to maintain tonic firing, but have normal burst firing.

During SWDs nRT neurons produce high frequency bursts of activity that are capable of strongly inhibiting TC neurons. The strength of this input is highly related to the generation of thalamocortical oscillations as strong nRT-TC hyperpolarization is capable of deinactivating T-type Ca^{2+} channels, leading to rebound bursts of TC activity once self-limiting nRT bursts terminate (von Krosigk et al., 1993; Warren et al., 1994; Huguenard, 1996; von Krosigk et al., 1999; Beenhakker and Huguenard, 2009). Reinforcement of nRT bursting either through increased excitatory input or reduced inhibitory input has been shown to promote SWDs (Bal et al., 1995; Paz et al., 2011). Since tonic but not bursting nRT outputs are perturbed in *Scn8a*$^{med/+}$ mice, we speculate that the nRT in these animals receive less recurrent tonic inhibition which leads to hyperexcitability of the nRT and increased production of rhythmogenic bursting outputs. In support of this hypothesis, we have found that mice carrying both the Emx1- and the Dlx5/6-*Cre* transgenes experience fewer SWDs than mice only carrying the Dlx5/6-*Cre* transgene. The nRT in these mice is likely less excitable due to a loss of excitatory input from corticothalamic neurons, which have reduced *Scn8a* expression due to Emx1-*Cre* mediated inactivation.

We have demonstrated that seizure resistance and absence seizure susceptibility phenotypes in *Scn8a*-mutant animals involve perturbations to separate neuronal populations. This finding indicates that specifically targeting *SCN8A* activity in glutamatergic forebrain neurons might be beneficial in patients with epilepsy. These results also demonstrate a previously unrealized role for *Scn8a* in thalamocortical circuitry which implicates this channel in the regulation of critical thalamic processes including sleep, sensation, perception, and consciousness.

4.5. Experimental Procedures

Animals

Mice carrying each *Cre* transgene were crossed to the fluorescent ROSA reporter line B6;129-Gt(ROSA)26Sor$_{tm1Joe}$/J. *Cre* expression induces recombination of an upstream floxed stop sequence leading to induction of fluorescent reporter expression in cells which express *Cre* recombinase. *Scn8a*-floxed mice were a kind gift from Miriam Meisler at the University of Michigan, Ann Arbor (Levin and Meisler, 2004). Homozygous female *Scn8a*-floxed mice (*Scn8a*$^{f/f}$) were crossed to 4 different *Cre* transgenic lines: Emx-1 B6.129-$^{Emx1tm1(cre)Krj}$/J (Jax stock number 005628) (Gorski et al., 2002), Dlx5/6 (Jax stock number 008199), CamKIIa (Dragatsis and Zeitlin, 2000), and Ppp1r2 (Belforte et al., 2010). The Ppp1r2 and the CamKIIa lines were kind gifts from Kazu Nakazawa at the National Institutes of Health and Ioannis Dragatsis at the University of Tennessee, respectively. We crossed each line to C57BL/6J to establish our colony before crossing to *Scn8a*$^{f/f}$ mice which are congenic on C57BL/6J (Jax Stock number 000664). The mice were maintained on a 12 h light/dark cycle. Food and water were available *ad libitum*. All experimental procedures were performed in accordance with the guidelines of Emory University and the University of California, Irvine Institutional Animal Care and Use Committees.

Genotyping of Scn8a conditional knockout mice

PCR identification of the *Scn8a* floxed allele was performed as previously described (Levin and Meisler, 2004) using the primer pair FloxF (5'-GTG TGT GAT TCT CAA CAG TGG GTT-3')/FloxR (5'-GTC TGT AAG AAG GCC TGA AAG TGA-3'). All Cre transgenes were identified using a primer pair located within the Cre transgene: CreF (5'-TGA CCC GGC AAA ACA GGT AGT TA-3')/CreR (5'-TTC-CCG-CAG-AAC-CTG-AAG-ATG-TT-3').

Flurothyl seizure induction

Flurothyl seizure induction was performed as described in Chapters 2 and 3.

EEG implantation recording and analysis

Continuous real-time video and EEG recordings were performed as described in Chapters 2 and 3 with the following modifications. To measure the progression of absence seizures in *Scn8a*$^{med/+}$ mice, EEG implantation surgery was performed on P14 mice. EEG recordings were performed for 2 hours per day so that pups could remain with the dam between recording periods. All recordings were performed between 11:00AM and 2:00PM in order to minimize possible circadian rhythm effects.

Immunohistochemistry

Immunohistochemistry was performed as previously described (Dutton et al., 2012; Papale et al., 2013) in order to determine the cell-type specificity of the Emx1 and Dlx5/6 *Cre* lines and to measure $Na_v1.6$ expression in cortical and thalamic interneuronal populations. Mice were deeply anesthetized with isoflurane and transcardially perfused with 4% PFA. Brains were post-fixed in paraformaldehyde (4%), cryopreserved in 30% sucrose, and 45 μm sections were cut on a cryostat (Leica, Germany). Coronal sections, 400 μm apart, from bregma − 0.46 mm to − 3.38 mm, were examined. Free-floating sections were washed in TBS/Triton-X and blocked in 2% avidin and then 2% biotin. Sections were then incubated with polyclonal rabbit anit-GAD67 (1:200, Millipore) or polyclonal rabbit anti-GluR2 (1:200, Millipore) and monoclonal mouse anti-GAD65/67 (1:100, Millipore). Sections were then incubated with polyclonal rabbit anti-*Scn8a* (1:200, Millipore) and monoclonal mouse anti-GAD65/67 (1:100, Millipore). After washing, sections were incubated in secondary antibodies; biotinylated anti-rabbit IgG (1:300, Vector Laboratories) and Alexa Fluor 555 anti-mouse IgG (1:1000, Invitrogen), followed by washing and

incubation in fluorescein avidin D (1:300, Vector Laboratories). Negative controls included sections that were not incubated with primary antibody, and sections from P2-3 neonatal mouse pups that do not express detectable levels of $Na_v1.6$. Sections were mounted and visualized using confocal microscopy (Carl Zeiss LSM 510 META). Cells were counted using lmaris software (Bitplane Scientific solutions) on images captured under 40 × and 10 × magnification. Results from three different animals were combined for the analysis of each sodium channel/cell-type combination.

Preparation of slices for electrophysiology

Slice preparation for electrophysiology were performed as described in Chapters 2 and 3.

Slice electrophysiology

Male WT or *Scn8a*$^{med/+}$ mice (P147-150) were anesthetized with pentobarbital sodium (i.p., 55 mg/kg) and the brain was quickly removed and placed in cold (~4 ^{o}C) oxygenated (95% O_2/5% CO_2) sucrose slicing solution containing (in mM): 234 sucrose, 11 glucose, 26 $NaHCO_3$, 2.5 KCl, 1.25 NaH_2PO_4, 10 $MgSO_4$, and 0.5 $CaCl_2$ (310 mOsm). Horizontal thalamic slices (250 mm thickness) containing nRT and VB were prepared as previously described (Huguenard and Prince, 1994) using a Leica VT1200 microtome (Leica Microsystems, Bannockburn, IL). Slices were incubated and continuously oxygenated in warm (~32^{o}C) artificial cerebrospinal fluid (ACSF) containing (in mM): 10 glucose, 26 $NaHCO_3$, 2.5 KCl, 1.25 $NaHPO_4$, 1 $MgSO_4$, 2 $CaCl_2$, and 126 NaCl (298 mOsm) for 1 hour and then transferred to room temperature (~21-23 ^{o}C) for at least 15 min prior to recording.

For current-clamp recordings, the pipette solution contained (in mM): 120 K-gluconate, 11 KCl, 1 $MgCl_2$, 1 $CaCl_2$, 10 HEPES, 1 EGTA, and pH was adjusted to 7.4 with KOH (290 mOsm).

Recordings were corrected for an estimated -15 mV liquid junction potential. I-V plots were constructed from a series of current steps in 20 pA increments from -140 to 140 pA from a holding potential of -75 mV.

Statistical analysis

All bar graphs indicate the mean and all error bars represent ± standard error of the mean (SEM). Statistical analyses were performed using Prism 6 (GraphPad Software Inc, La Jolla, CA). The Levene's test was used to assess for differences in the variance between groups, and the Shapiro-Wilk test was used to determine normality of continuous data sets. One-way analysis of variance (ANOVA) was used to evaluate seizure thresholds between groups of three or more. *Post-hoc* comparisons were performed using either the Dunnett's or Bonferroni test. The Student's two-tailed t test was used to analyze hippocampal bursting. The Mann-Whitney-U test was used to assess differences in seizure thresholds between two groups.

4.6. Acknowledgements

This research was also supported in part by the NINDS core facilities grant P30N5055077 to the Emory University Microscopy Core. We would like to thank Stacey Dutton for assistance with performing flurothyl seizure induction procedures. We would also like to thank Christian Gonzalez for assistance with immunohistochemistry.

CHAPTER 5

Overall Discussion and Conclusions

5.1. Overview

Voltage-gated sodium channels (VGSCs) are important regulators of neuronal excitability and are responsible for the initiation and propagation of action potentials in neurons. Disruptions in VGSC function can lead to a host of pathophysiological conditions (George, 2005; Mantegazza and Catterall, 2012). Most notably, mutations in the four CNS VGSCs, *SCN1A*, *SCN2A*, *SCN3A*, and *SCN8A*, are responsible for several types of idiopathic epilepsy. Among these, *SCN1A* mutations are well established as the major cause of DS and GEFS+, and many clinical features of these disorders are recapitulated in mouse models of *Scn1a* dysfunction. In contrast, mutations in *SCN8A* have been only recently discovered in patients with epileptic encephalopathy (Veeramah et al., 2012; Carvill et al., 2013). Moreover, clinical presentation in patients with *SCN8A* mutations contrasts with existing mouse models of *Scn8a* dysfunction, which exhibit resistance to induced seizures (Martin et al., 2007; Hawkins et al., 2011) yet paradoxically, exhibit SWDs, a hallmark of absence epilepsy (Papale et al., 2009).

The experiments described in this thesis aim to provide a more complete understanding of the role of *Scn8a* in epilepsy. In Chapter 2, we described the relationship between the development of seizure protection and *Scn8a* expression in the CNS as well as the effect on seizure phenotypes of selectively targeting *Scn8a* in the hippocampus of adult animals. Chapter 3 described the generation and initial characterization of a new mouse model of *Scn8a* dysfunction, revealing new aspects of *Scn8a* function on recessive seizure and behavioral phenotypes. In Chapter 4 we presented results from the use of a Cre/loxP strategy to investigate the role of *Scn8a* in different CNS cell types and we proposed a mechanism to explain the major seizure phenotypes observed in *Scn8a* mutant mice: seizure protection and absence seizure generation. Our primary findings are as follows:

1) The progression of *Scn8a* expression in early postnatal development is coincident with seizure resistance and the emergence of absence seizures.
2) Global or hippocampal-specific reduction of *Scn8a* expression in adult animals increases seizure resistance in multiple seizure and epilepsy models, highlighting the therapeutic potential for targeting *SCN8A*.
3) Heterozygous but not homozygous substitution mutations in the *Scn8a* gene confer seizure protection, while homozygous *Scn8a* mutant mice are susceptible to audiogenic seizures.
4) Reducing *Scn8a* expression in forebrain excitatory neurons increases seizure resistance while reducing *Scn8a* in inhibitory cells does not. In contrast, reduced *Scn8a* expression in inhibitory neurons, but not forebrain excitatory cells, is sufficient to generate spontaneous SWDs.
5) High levels of *Scn8a* expression were observed in nRT neurons. Also, deficits in tonic but not bursting outputs were observed in nRT neurons from *Scn8a*-deficient mice, implicating this nucleus in the generation of SWD.

Taken together, these findings provide additional mechanistic insight into the role of *Scn8a* in epilepsy, and importantly, provide genetic, developmental, anatomical and physiological rationale for selective targeting of *Scn8a* as a treatment for epilepsy. In this Discussion, I will provide partially overlapping frameworks to understand these results in the context of the VGSC field.

5.2. Reconciliation of Seizure Outcomes Associated with *Scn8a* Mutations

Heterozygous *Scn8a* mutations have been shown to confer seizure protection and are capable of increasing the lifespans of animals with mutations in *Scn1a* (Martin et al., 2007; Hawkins et al., 2011). In addition, we have found that heterozygous conditional inactivation of

Scn8a in forebrain excitatory neurons leads to increased seizure thresholds and that seizure thresholds are further increased following homozygous inactivation of *Scn8a* (Fig. 4.4). This result demonstrates that *Scn8a*-mediated seizure protection is dependent on excitatory neurons and that an inverse gene-dosage-dependent relationship exists between *Scn8a* expression in excitatory neurons and seizure resistance. In agreement with these results, increased seizure resistance was observed in mice that were heterozygous for the *Scn8a* mutations R1627H ($Scn8a^{RH/+}$) and medjo ($Scn8a^{RH/+}$); however, lower seizure latencies were seen in homozygous mutants (Fig. 3.5, 3.9). Furthermore, homozygous mutants appear to be susceptible to audiogenic seizures (Fig. 3.8, 3.9).

It remains to be determined why *Scn8a*-mediated seizure protection is lost at the homozygous level in the case of substitution mutations but not following homozygous deletion of *Scn8a* from excitatory neurons. We hypothesize that homozygous *Scn8a* mutations lead to reduced activity of forebrain inhibitory neurons, leading to reduced network inhibition, in addition to reduced excitability of forebrain excitatory neurons. In contrast, mice with homozygous conditional excitatory cell-specific *Scn8a* deletion, which does not affect interneuronal activity, retain normal inhibitory function thereby having the overall effect of reducing neuronal excitability and increasing seizure resistance. Although we did not detect colocalization between inhibitory cells and *Scn8a* in the rodent forebrain (Fig. 4.8), it is possible that *Scn8a* is expressed at a low, but functionally important level, which is below the threshold of detection using this technique. Evidence in support of our hypothesis is derived from preliminary *in vivo* electrophysiological investigations of $Scn8a^{RH/RH}$, $Scn8a^{RH/+}$, and WT interneuronal firing properties. In response to large depolarizing current injections, interneurons in the hippocampus of $Scn8a^{RH/RH}$ mice exhibit fatigue and produce significantly fewer action potentials than interneurons in $Scn8a^{RH/+}$ or WT littermates (Fig. 5.1). This loss of inhibitory neuronal output would be predicted to promote seizure activity. We therefore propose that mice carrying

homozygous *Scn8a* mutations experience a competition of effects on network excitability, decreased excitatory neuronal activity and decreased inhibitory neuronal excitability. This in turn leads to the complex seizure phenotypes observed at the homozygous level, including normal thresholds to pharmacologically and electrically-induced seizures (Fig. 3.5, 3.9), reduced tonic extension in response to proconvulsants (Fig. 3.5, 3.9), but susceptibility to audiogenic seizures (Fig. 3.8, 3.9). In the future, it would be interesting to determine if homozygous inhibitory neuronal-specific inactivation of *Scn8a* driven by the Dlx5/6-*Cre* line would lead to reduced seizure thresholds and susceptibility to audiogenic seizure.

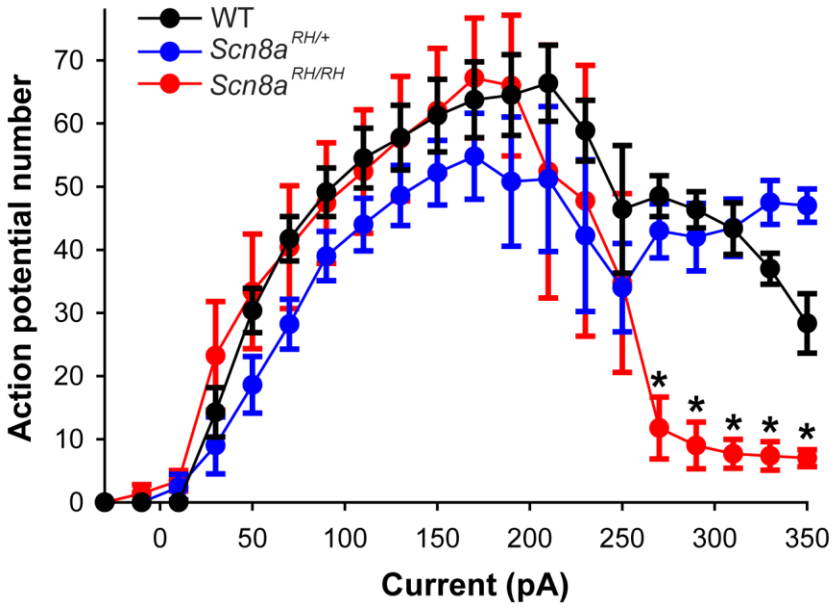

Figure 5.1. Homozygous *Scn8a*-R1627H mice exhibit deficits in interneuron firing in response to large depolarization

Current clamp recordings were performed on inhibitory interneurons in the CA3 region of the hippocampus in *Scn8a*$^{RH/RH}$, *Scn8a*$^{RH/+}$, and WT literates. The number of action potentials elicited in response to increasing current injections were analyzed. In response to high depolarization (> 275 pA), interneurons in *Scn8a*$^{RH/RH}$ animals fatigue and produce fewer APs than *Scn8a*$^{RH/+}$ or WT littermates (two-way ANOVA, Genotype X Current, Tukey *post-hoc* $*p < 0.05$ *Scn8a*$^{RH/RH}$ vs. *Scn8a*$^{RH/+}$ and WT; n = 5-8 per group). Error bars represent SEM. These experiments were performed by Karoni Dutt in the laboratory of Alan Goldin at the University of California, Irvine.

5.3. A Circuit Model of *SCN1A*-Epilepsy and Genetic Modification by *SCN8A* Mutations

SCN1A-derived epilepsies encompass a spectrum of phenotypes with overlapping clinical presentations that range in severity from relatively benign febrile seizures to the catastrophic DS (Harkin et al., 2007). Mouse models have been successfully used to demonstrate that *Scn1a* channels are highly expressed in GABAergic inhibitory neurons of the hippocampus and cortex and that loss of *Scn1a* activity reduces the excitability of these neurons (Yu et al., 2006; Ogiwara et al., 2007; Martin et al., 2010). These observations led to the hypothesis that loss of *Scn1a* causes reduced neuronal inhibition and thus increased risk of seizure generation (Yu et al., 2006; Ogiwara et al., 2007).

These findings are in stark contrast to emerging data on other VGSCs in epilepsy, including *SCN2A*, *SCN3A*, and *SCN8A*, which express predominantly gain-of-function substitution mutations (Kearney et al., 2001; Holland et al., 2008; Estacion et al., 2010; Veeramah et al., 2012; Lauxmann et al., 2013; Vanoye et al., 2013). In chapter 4, we demonstrated that loss of *Scn8a* from excitatory forebrain neurons increases seizure resistance (Fig. 4.2) and reduces hippocampal epileptiform bursting activity in the presence of high extracellular potassium (Fig. 4.3), while loss of *Scn8a* from interneurons did not lead to increased seizure resistance. These results indicate that reducing *Scn8a* activity increases seizure protection by decreasing the excitability of excitatory forebrain projection neurons. We speculate that loss of *Scn8a* leads to improved survival and increased seizure thresholds in models of GEFS+ and DS by normalizing neuronal excitability. Figure 5.2 illustrates our simplified model of loss of *Scn1a* leading to seizure generation and reversal of this phenotype by loss of *Scn8a*. It should be noted that this model only illustrates the putative effects of heterozygous loss- or reduction-of-function *Scn1a* and *Scn8a* mutations in forebrain networks.

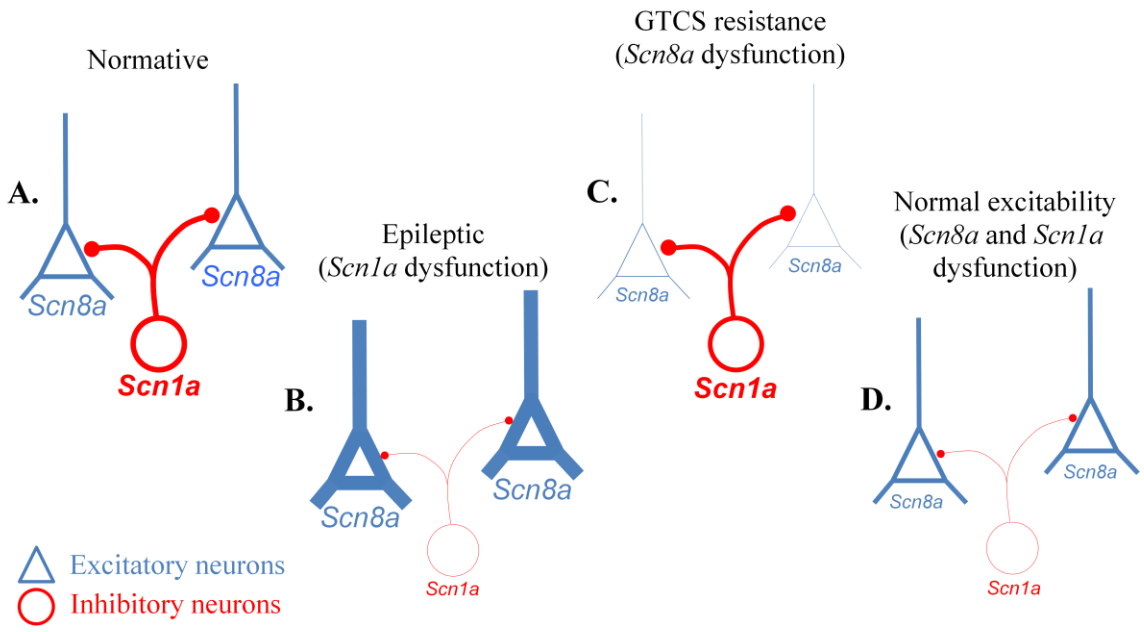

Figure 5.2 Loss of inhibition model of *Scn1a* dysfunction leading to generalized tonic-clonic epilepsy and reversal by loss of *Scn8a*

A-D. Illustrated are four hypothetical instances of cortical circuitry in *Scn1a* and *Scn8a*-deficient animals. Each example includes a cortical parvalbumin positive interneurons (red) synapsing onto two glutamatergic pyramidal neurons (blue). The thickness of the cell body and processes indicates the relative excitability of the cell type. The font size of the VGSC indicates the relative expression level of this channel. ***A.*** In a normal, non-epileptic brain sufficient *Scn1a* expression exists to support interneuronal excitability which suppresses network hyperexcitability. ***B.*** Loss of *Scn1a* expression leads to a reduction in interneuronal function and an overall increase in network activity. This loss of inhibition allows excitatory aspects of the network to enter into hyperexcitable epileptic states. ***C.*** Loss of *Scn8a* reduces the excitability of glutamatergic projection neurons leading to a general reduction in network excitability that inhibits seizure generation. ***D.*** Loss of both *Scn1a* and *Scn8a* produces opposing effects on network excitability that approximates the normative state.

5.4. Persistent Sodium Current: Unifying VGSC Epilepsy Mechanisms?

Cortical neurons exhibit a TTX-sensitive fast transient sodium current (I_{NaT}) and a low-voltage-activated, slow inactivating, persistent sodium current (I_{NaP}). I_{NaP} is implicated in boosting sub-threshold membrane depolarizations and responses to synaptic input (Deisz et al., 1991; Schwindt and Crill, 1995; Stuart and Sakmann, 1995; Lipowsky et al., 1996), while transient Na^+ currents are responsible for mediating the rising phase of the action potential. I_{NaP} has been demonstrated to strongly influence excitability and synaptic integration in many neuronal cell types (Chandler and Meves, 1966; Crill, 1996; Pennartz et al., 1997; Taddese and Bean, 2002; Baker et al., 2003). In heterologous expression systems, *Scn1a* as well as *Scn8a* have been found to produce a large I_{NaP} (Smith et al., 1998; Goldin, 1999), while many studies have demonstrated that *Scn8a* carries most (~70%) I_{NaP} in CNS neurons *in vivo* (Raman et al., 1997; Vega-Saenz de Miera et al., 1997; Maurice et al., 2001; Enomoto et al., 2007; Royeck et al., 2008; Osorio et al., 2010). The large contribution of *Scn8a* to I_{NaP} may distinguish this channel from *SCN1A* in regards to the effect of reduced channel activity on seizure susceptibility.

Gain of function mutations in *SCN2A* (Kearney et al., 2001; Liao et al., 2010a), *SCN3A* (Holland et al., 2008; Estacion et al., 2010), and *SCN8A* (Veeramah et al., 2012), identified in epileptic patients, were all found to increase I_{NaP}. While *Scn8a* is normally the primary VGSC responsible for I_{NaP} in CNS neurons, it seems that gain-of-function mutations in other VGSCs can alter these α subunits such that they aberrantly increase their contribution to subthreshold currents. This in turn leads to increased neuronal excitability and epilepsy.

5.5. A Circuit Model of *Scn8a*-Absence Epilepsy

Absence epilepsy is characterized by spontaneous generalized spike-and-wave discharges (SWDs) that are the consequence of aberrant oscillatory thalamocortical activity (Panayiotopoulos, 2001). Absence seizures result in temporary loss of awareness and can occur

hundreds of times per day, and in fact, absence seizures account for approximately 10% of all childhood seizures (Posner, 2008). These seizures represent a major health concern and are associated with reduced academic performance and attention, and increased accident risk, as well as affective and behavioral disorders (Vrielynck, 2013). We have previously reported that mice with *Scn8a* mutations exhibit SWDs (Papale et al., 2009).

In Chapter 4 we showed that inactivation of *Scn8a* in inhibitory neurons leads to spontaneous SWDs (Fig. 4.6). We also demonstrated that *Scn8a* is expressed in nRT neurites (Fig. 4.7) and that *Scn8a* deficient animals exhibit reduced tonic but not bursting outputs from nRT neurons (Fig. 4.8). These findings indicate that *Scn8a* is important for supporting the activity of the nRT and raise the possibility that loss of *Scn8a* from the nRT can lead to SWDs. What is less clear is how loss of *Scn8a* expression could lead to increased oscillations in the thalamocortical circuitry and hence SWD generation.

SWDs are the result of oscillatory activity between the cortex and thalamus which involves the interplay between reciprocally connected corticothalamic neurons (CT) and thalamocortical (TC) neurons, as well as GABAergic neurons of the thalamic reticular nucleus (nRT) which send inhibitory projections to thalamocortical cells and also back onto the nRT itself (Fig. 5.3*A*). nRT neurons produce high frequency bursts of activity that are capable of strongly inhibiting TC neurons during SWD generation. The strength of this input is highly related to the generation of thalamocortical oscillations as strong nRT-TC hyperpolarization is capable of deinactivating T-type Ca^{++} channels, leading to rebound bursts of TC activity once self-limiting nRT bursts terminate (von Krosigk et al., 1993; Warren et al., 1994; Huguenard, 1996; von Krosigk et al., 1999; Beenhakker and Huguenard, 2009). Excitatory feedback to the nRT then initiates another oscillation in the circuit.

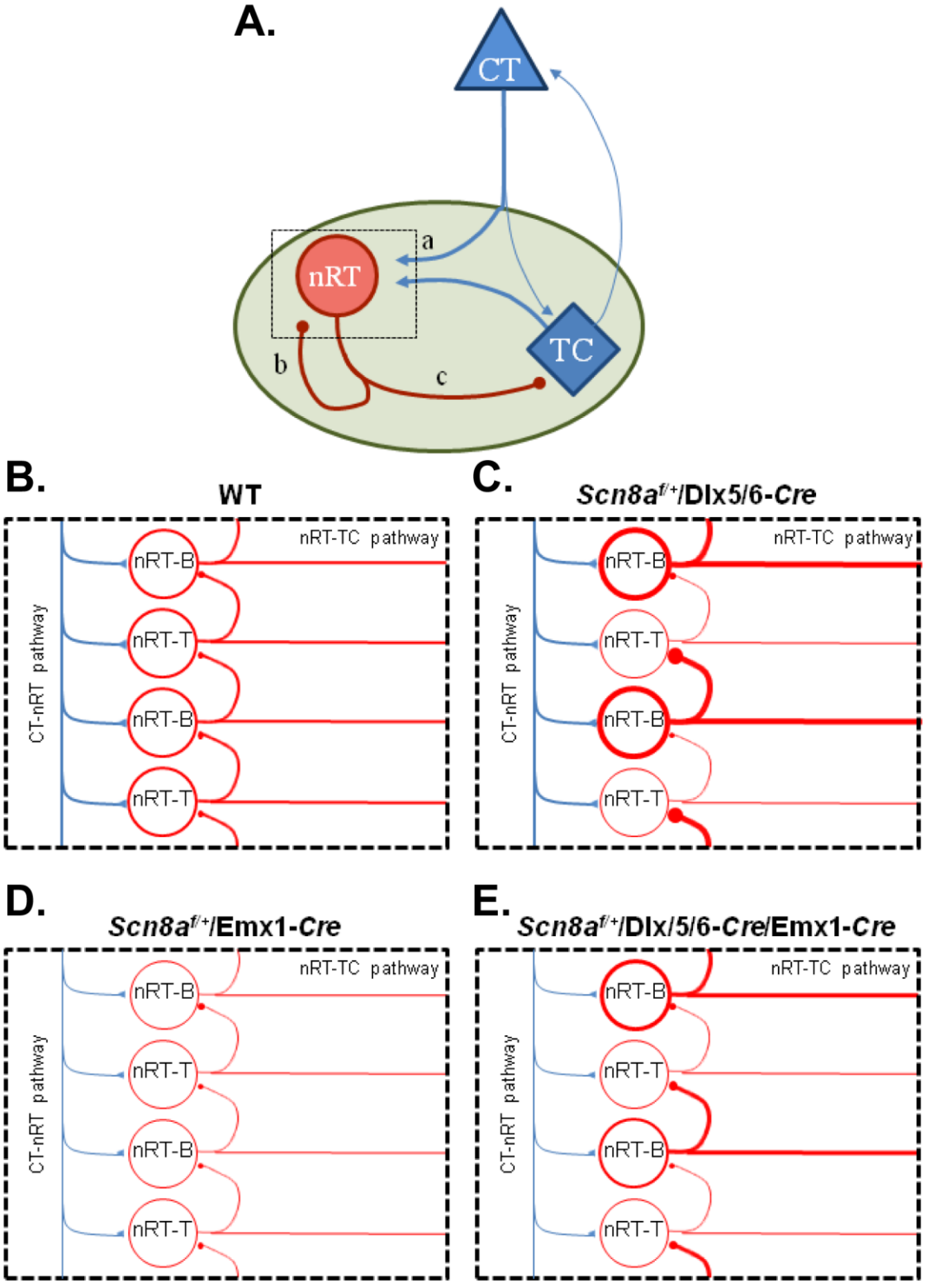
A.
CT
nRT
TC
a
b
c
B.
WT
nRT-TC pathway
CT-nRT pathway
nRT-B
nRT-T
nRT-B
nRT-T
C.
Scn8a f/+/Dlx5/6-Cre
nRT-TC pathway
CT-nRT pathway
nRT-B
nRT-T
nRT-B
nRT-T
D.
Scn8a f/+/Emx1-Cre
nRT-TC pathway
CT-nRT pathway
nRT-B
nRT-T
nRT-B
nRT-T
E.
Scn8a f/+/Dlx/5/6-Cre/Emx1-Cre
nRT-TC pathway
CT-nRT pathway
nRT-B
nRT-T
nRT-B
nRT-T

Figure 5.3. Thalamocortical circuit models of conditional cell-type specific inactivation of *Scn8a* leading to SWD generation

A. Schematic representation of thalamocortical circuitry. Red cells are inhibitory, blue cells are excitatory. CT represents excitatory corticothalamic neurons, TC represents excitatory thalamocortical neurons, nRT represents inhibitory thalamic reticular neurons. The thickness of projections indicates relative excitability. The green background indicates the thalamus. The nRT receives excitatory input from the CT and TC cells (***a***) and reentrant inhibition from the nRT itself (***b***). Strong bursts of inhibition from the nRT onto TC cells (***c***) are thought to drive thalamocortical oscillations by eliciting strong rebound bursts in TC neurons. ***B-E.*** Inset of ***A*** demonstrating intra-nRT circuitry following loss of *Scn8a* from different aspects of the thalamocortical loop. nRT-B represents nRT neurons that prefer bursting modes and nRT-T represents nRT neurons that prefer tonic modes of output. ***B.*** In WT animals, normal excitatory CT-nRT input as well as normal nRT-B and nRT-T output does not lead to SWD generation. ***C.*** Loss of *Scn8a* in the nRT specifically reduces the activity of nRT-T but not nRT-B neurons leading to a loss of inhibition at the nRT-B neurons. The resulting increase in nRT bursting outputs drive SWDs. ***D.*** Loss of CT *Scn8a* expression reduces excitatory input to the nRT which leads to reduced nRT output which inhibits SWD generation. ***E.*** Loss of *Scn8a* in both CT and nRT neurons leads to intermediate levels of nRT-B output which is sufficient to generate SWDs, but at a lower level than in ***C***.

Given that nRT bursting activity is a critical driver of thalamocortical oscillations and that *Scn8a*-deficiency leads to preserved nRT bursting but reduced tonic firing, we proposes two possible explanations for the role of reduced *Scn8a* activity in SWD generation. First, loss of *Scn8a* from the nRT might result in less tonic-firing which would then reduce inhibition to the nRT via recurrent connections (Fig. 5.3*C*). The resulting loss of inhibitory tone within the nRT would promote increased burst firing and SWD generation. Second, a related possibility is based on the observation that some nRT cells more readily fire bursts while others prefer tonic output modes (Contreras et al., 1992; Lee et al., 2007; Alberi et al., 2013). It is possible that interfering with tonic modes but not bursting modes of output, as a consequence of loss of *Scn8a* activity, causes tonically firing nRT neurons to enter into burst modes of output which would be predicted to increase SWD generation. Thus *Scn8a*-deficiency may specifically alter tonic but not bursting nRT cells which either pushes tonic bursting cells to enter into burst modes or leads to loss of tonic inhibition in the nRT which increases bursting activity.

Lastly, we observed lower SWD frequency in animals with *Scn8a* inactivation in both inhibitory and excitatory neurons (*Scn8a*$^{f/+}$/Dlx5/6-*Cre*/Emx1-*Cre*) when compared to animals with only inhibitory neuron inactivation (*Scn8a*$^{f/+}$/Dlx5/6-*Cre*). This finding is consistent with our proposed models, as loss of corticothalamic activity would partially disrupt the seizurogenic thalamocortical loop and would reduce excitatory input to the nRT leading to a reduction in nRT output (Fig. 5.3*E*). Thus in an animal carrying a mutation in *Scn8a*, thalamocortical oscillations may be driven by loss of inhibition at the nRT leading to increased nRT output and inhibited by reduced activity of the corticothalamic pathway. The net effect apparently favors oscillation of the thalamocortical loop as mice carrying *Scn8a* mutations experience spontaneous SWDs.

5.6. Therapies for VGSC-Derived Epilepsies

Most AEDs are only partially effective for the treatment of DS (Chiron and Dulac, 2011). Many studies have evaluated the effectiveness of different treatment options for DS and have found that the most effective drugs, such as stiripentol and clobazam, share enhancement of GABAergic neurotransmission as part of their mechanism of action. In contrast, AEDs that worsen DS, for example phenytoin, lamotrigine, and carbamazepine, often block VGSC activity (Guerrini et al., 1998). Interestingly, drugs that both reduce VGSC activity and enhance GABAergic neurotransmission, such as valproate, have intermediate effectiveness. This finding is consistent with the loss of inhibition model of DS, in which loss of *SCN1A* activity, predominantly in inhibitory interneurons, leads to reduced GABAergic neurotransmission. Thus, VGSC blockers that further decrease sodium currents will be expected to worsen the disorder, while enhancement of GABAergic neurotransmission will provide partial correction of inhibitory neuronal function.

While VGSC blockers are not effective for DS, they might be effective in other VGSC-derived epilepsies which involve gain-of-function mutations. As epilepsy mutations in the *SCN2A*, *SCN3A*, and *SCN8A* genes are most often gain-of-function (see Mechanisms of VGSCs in Epilepsy section), administration of phenytoin, lamotrigine, or carbamazepine may effectively normalize the activity of overactive VGSCs in these individuals with mutations in these genes.

Selective targeting of a specific VGSC isoform as a therapeutic strategy to compensate for the loss of another isoform has been explored using mouse models of VGSC dysfunction. Proof of principle of this approach was demonstrated by crossing *Scn1a* mutant mice to *Scn8a* mutant mice, leading to increased lifespan and seizure resistance (Martin et al., 2007; Hawkins et al., 2011). In a mouse model of temporal lobe epilepsy in which up regulation of *Scn8a* in entorhinal cortex was observed, partially selective inhibition of *Scn8a* by 4.9-anhydro-TTX was found to improve seizure outcomes (Hargus et al., 2011). In Chapter 2, we demonstrated that

specifically reducing *Scn8a* expression in the hippocampus is capable of increasing resistance to picrotoxin-induced seizures in WT mice (Fig. 2.6) and increasing latencies to flurothyl-induced seizures in WT and epileptic *Scn1a*$^{+/-}$ mice (Fig. 2.8). The injection of an shRNA to reduce *Scn8a* expression in a specific brain region in order to achieve seizure control may be effective in focal forms of epilepsy where reducing *Scn8a* expression at the site of seizure initiation might reduce the ability of this region to drive the spread of seizure activity to other regions.

Gene replacement has also been explored as a strategy to correct for loss of the *Scn1a* gene in epileptic *Scn1a*$^{+/-}$ mice. Proof of concept of gene replacement in a DS model was demonstrated using a transgenic mouse carrying a bacteria artificial chromosome (BAC) containing a full length *Scn1a* gene. Compensation for reduced *Scn1a* expression in *Scn1a*$^{+/-}$ mice by expression of the *Scn1a* BAC transgene increased the lifespan of these mice (Tang et al., 2009). Unfortunately, the large size of the *SCN1A* gene and lack of an appropriate delivery system makes this approach currently impractical as a therapeutic avenue.

It is unlikely that a single effective treatment for all VGSC epilepsies will be found. In the end, individualized approaches coupled with selective genetic and pharmacologic tools may be the most effective strategy. Along these lines, patient-derived neurons, using an induced pluiripotent stem cell approach, have been successfully generated from DS patients and used to probe disease mechanisms (see *Scn1a* Epilepsy Mechanisms section) (Liu et al., 2013). This approach in conjunction with isoform specific pharmacologic or genetic tools that are capable of altering VGSC expression levels or activity might facilitate *in vitro*, low risk, testing of patient-specific therapeutic strategies.

5.7. Concluding Remarks

Voltage gated sodium channels (VGSCs) are integral to the regulation of neuronal excitability. Alterations in the function of the CNS VGSCs are associated with susceptibility to

epilepsy as well as cognitive and behavioral impairments. Mice with mutations in the VGSC *Scn8a* exhibit increased resistance to induced seizures; however, paradoxically experience frequent spontaneous absence seizures. We have more fully characterized the development of *Scn8a* expression and key *Scn8a*-epilepsy phenotypes. We also provided mechanistic insight into the role of *Scn8a* in seizure protection, and also provided genetic, developmental, anatomical and physiological rationale for selectively targeting *Scn8a* as a treatment for epilepsy. We have generated a new mouse model of *Scn8a* dysfunction which has revealed new recessive phenotypes including loss of proconvulsant resistance and susceptibility to audiogenic seizure. Lastly, by specifically reducing *Scn8a* expression in discrete cell types, we have proposed a mechanism to explain both *Scn8a*-mediated seizure protection and *Scn8a*-absence epilepsy. These findings provide the foundation for future studies on the contribution of VGSCs to epilepsy and behavioral outcomes and for the development of improved therapies that target VGSCs.

REFERENCES

Alberi L, Lintas A, Kretz R, Schwaller B, Villa AE (2013) The calcium-binding protein parvalbumin modulates the firing 1 properties of the reticular thalamic nucleus bursting neurons. Journal of neurophysiology 109:2827-2841.

Aloisi F (2001) Immune function of microglia. Glia 36:165-179.

Anderson PA, Greenberg RM (2001) Phylogeny of ion channels: clues to structure and function. Comparative biochemistry and physiology Part B, Biochemistry & molecular biology 129:17-28.

Andrade DM, Paton T, Turnbull J, Marshall CR, Scherer SW, Minassian BA (2012) Mutation of the CLN6 gene in teenage-onset progressive myoclonus epilepsy. Pediatric neurology 47:205-208.

Armstrong CM, Bezanilla F (1973) Currents related to movement of the gating particles of the sodium channels. Nature 242:459-461.

Armstrong CM, Bezanilla F (1977) Inactivation of the sodium channel. II. Gating current experiments. The Journal of general physiology 70:567-590.

Baker MD, Chandra SY, Ding Y, Waxman SG, Wood JN (2003) GTP-induced tetrodotoxin-resistant Na+ current regulates excitability in mouse and rat small diameter sensory neurones. The Journal of physiology 548:373-382.

Bal T, von Krosigk M, McCormick DA (1995) Role of the ferret perigeniculate nucleus in the generation of synchronized oscillations in vitro. The Journal of physiology 483 (Pt 3):665-685.

Bamshad MJ, Ng SB, Bigham AW, Tabor HK, Emond MJ, Nickerson DA, Shendure J (2011) Exome sequencing as a tool for Mendelian disease gene discovery. Nature reviews Genetics 12:745-755.

Bartnik M, Chun-Hui Tsai A, Xia Z, Cheung SW, Stankiewicz P (2011) Disruption of the SCN2A and SCN3A genes in a patient with mental retardation, neurobehavioral and psychiatric abnormalities, and a history of infantile seizures. Clinical genetics 80:191-195.

Barton ME, Klein BD, Wolf HH, White HS (2001) Pharmacological characterization of the 6 Hz psychomotor seizure model of partial epilepsy. Epilepsy research 47:217-227.

Basel-Vanagaite L et al. (2013) Biallelic SZT2 mutations cause infantile encephalopathy with epilepsy and dysmorphic corpus callosum. American journal of human genetics 93:524-529.

Beckh S, Noda M, Lubbert H, Numa S (1989) Differential regulation of three sodium channel messenger RNAs in the rat central nervous system during development. The EMBO journal 8:3611-3616.

Beenhakker MP, Huguenard JR (2009) Neurons that fire together also conspire together: is normal sleep circuitry hijacked to generate epilepsy? Neuron 62:612-632.

Begley CE, Baker GA, Beghi E, Butler J, Chisholm D, Langfitt JT, Levy P, Pachlatko C, Wiebe S, Donaldson KL, Policy ICoH (2007) Cross-country measures for monitoring epilepsy care. Epilepsia 48:990-1001.

Belforte JE, Zsiros V, Sklar ER, Jiang Z, Yu G, Li Y, Quinlan EM, Nakazawa K (2010) Postnatal NMDA receptor ablation in corticolimbic interneurons confers schizophrenia-like phenotypes. Nature neuroscience 13:76-83.

Bender AC, Natola H, Ndong C, Holmes GL, Scott RC, Lenck-Santini PP (2013) Focal Scn1a knockdown induces cognitive impairment without seizures. Neurobiology of disease 54:297-307.

Beneski DA, Catterall WA (1980) Covalent labeling of protein components of the sodium channel with a photoactivable derivative of scorpion toxin. Proceedings of the National Academy of Sciences of the United States of America 77:639-643.

Berkovic SF, Heron SE, Giordano L, Marini C, Guerrini R, Kaplan RE, Gambardella A, Steinlein OK, Grinton BE, Dean JT, Bordo L, Hodgson BL, Yamamoto T, Mulley JC, Zara F, Scheffer IE (2004) Benign familial neonatal-infantile seizures: characterization of a new sodium channelopathy. Annals of neurology 55:550-557.

Bezanilla F, Armstrong CM (1977) Inactivation of the sodium channel. I. Sodium current experiments. The Journal of general physiology 70:549-566.

Black JA, Waxman SG (1996) Sodium channel expression: a dynamic process in neurons and non-neuronal cells. Developmental neuroscience 18:139-152.

Black JA, Sontheimer H, Waxman SG (1993) Spinal cord astrocytes in vitro: phenotypic diversity and sodium channel immunoreactivity. Glia 7:272-285.

Black JA, Liu S, Waxman SG (2009) Sodium channel activity modulates multiple functions in microglia. Glia 57:1072-1081.

Black JA, Newcombe J, Waxman SG (2010) Astrocytes within multiple sclerosis lesions upregulate sodium channel Nav1.5. Brain : a journal of neurology 133:835-846.

Black JA, Westenbroek R, Ransom BR, Catterall WA, Waxman SG (1994) Type II sodium channels in spinal cord astrocytes in situ: immunocytochemical observations. Glia 12:219-227.

Black JA, Westenbroek R, Minturn JE, Ransom BR, Catterall WA, Waxman SG (1995) Isoform-specific expression of sodium channels in astrocytes in vitro: immunocytochemical observations. Glia 14:133-144.

Blumenfeld H, Lampert A, Klein JP, Mission J, Chen MC, Rivera M, Dib-Hajj S, Brennan AR, Hains BC, Waxman SG (2009) Role of hippocampal sodium channel Nav1.6 in kindling epileptogenesis. Epilepsia 50:44-55.

Boiko T, Van Wart A, Caldwell JH, Levinson SR, Trimmer JS, Matthews G (2003) Functional specialization of the axon initial segment by isoform-specific sodium channel targeting.

The Journal of neuroscience : the official journal of the Society for Neuroscience 23:2306-2313.

Boiko T, Rasband MN, Levinson SR, Caldwell JH, Mandel G, Trimmer JS, Matthews G (2001) Compact myelin dictates the differential targeting of two sodium channel isoforms in the same axon. Neuron 30:91-104.

Brackenbury WJ, Yuan Y, O'Malley HA, Parent JM, Isom LL (2013) Abnormal neuronal patterning occurs during early postnatal brain development of Scn1b-null mice and precedes hyperexcitability. Proceedings of the National Academy of Sciences of the United States of America 110:1089-1094.

Brodie MJ, Shorvon SD, Canger R, Halasz P, Johannessen S, Thompson P, Wieser HG, Wolf P (1997) Commission on European Affairs: appropriate standards of epilepsy care across Europe.ILEA. Epilepsia 38:1245-1250.

Brown CW (1953) Properties and Alterations of Electrically-Induced Seizures in Mice. Epilepsia C2:127-138.

Browne TR, Holmes GL (2001) Epilepsy. The New England journal of medicine 344:1145-1151.

Browning RA (1986) Neuroanatomical localization of structures responsible for seizures in the GEPR: lesion studies. Life sciences 39:857-867.

Brunklaus A, Dorris L, Zuberi SM (2011) Comorbidities and predictors of health-related quality of life in Dravet syndrome. Epilepsia 52:1476-1482.

Burgess DL, Kohrman DC, Galt J, Plummer NW, Jones JM, Spear B, Meisler MH (1995) Mutation of a new sodium channel gene, Scn8a, in the mouse mutant 'motor endplate disease'. Nature genetics 10:461-465.

Caldwell JH, Schaller KL, Lasher RS, Peles E, Levinson SR (2000) Sodium channel Na(v)1.6 is localized at nodes of ranvier, dendrites, and synapses. Proceedings of the National Academy of Sciences of the United States of America 97:5616-5620.

Carvill GL et al. (2013) Targeted resequencing in epileptic encephalopathies identifies de novo mutations in CHD2 and SYNGAP1. Nature genetics 45:825-830.

Catterall WA (2000) From ionic currents to molecular mechanisms: the structure and function of voltage-gated sodium channels. Neuron 26:13-25.

Catterall WA, Kalume F, Oakley JC (2010) NaV1.1 channels and epilepsy. The Journal of physiology 588:1849-1859.

Catterall WA, Dib-Hajj S, Meisler MH, Pietrobon D (2008) Inherited neuronal ion channelopathies: new windows on complex neurological diseases. The Journal of neuroscience : the official journal of the Society for Neuroscience 28:11768-11777.

Celle ME, Cuoco C, Porta S, Gimelli G, Tassano E (2013) Interstitial 2q24.3 deletion including SCN2A and SCN3A genes in a patient with autistic features, psychomotor delay, microcephaly and no history of seizures. Gene.

Chanda B, Bezanilla F (2002) Tracking voltage-dependent conformational changes in skeletal muscle sodium channel during activation. The Journal of general physiology 120:629-645.

Chandler WK, Meves H (1966) Incomplete sodium inactivation in internally perfused giant axons from Loligo forbesi. The Journal of physiology 186:121P-122P.

Cheah CS, Yu FH, Westenbroek RE, Kalume FK, Oakley JC, Potter GB, Rubenstein JL, Catterall WA (2012) Specific deletion of NaV1.1 sodium channels in inhibitory interneurons causes seizures and premature death in a mouse model of Dravet syndrome. Proceedings of the National Academy of Sciences of the United States of America 109:14646-14651.

Chen C, Bharucha V, Chen Y, Westenbroek RE, Brown A, Malhotra JD, Jones D, Avery C, Gillespie PJ, 3rd, Kazen-Gillespie KA, Kazarinova-Noyes K, Shrager P, Saunders TL, Macdonald RL, Ransom BR, Scheuer T, Catterall WA, Isom LL (2002) Reduced sodium channel density, altered voltage dependence of inactivation, and increased susceptibility

to seizures in mice lacking sodium channel beta 2-subunits. Proceedings of the National Academy of Sciences of the United States of America 99:17072-17077.

Chen C, Westenbroek RE, Xu X, Edwards CA, Sorenson DR, Chen Y, McEwen DP, O'Malley HA, Bharucha V, Meadows LS, Knudsen GA, Vilaythong A, Noebels JL, Saunders TL, Scheuer T, Shrager P, Catterall WA, Isom LL (2004) Mice lacking sodium channel beta1 subunits display defects in neuronal excitability, sodium channel expression, and nodal architecture. The Journal of neuroscience : the official journal of the Society for Neuroscience 24:4030-4042.

Chen YH, Dale TJ, Romanos MA, Whitaker WR, Xie XM, Clare JJ (2000) Cloning, distribution and functional analysis of the type III sodium channel from human brain. The European journal of neuroscience 12:4281-4289.

Chiron C, Dulac O (2011) The pharmacologic treatment of Dravet syndrome. Epilepsia 52 Suppl 2:72-75.

Claes L, Del-Favero J, Ceulemans B, Lagae L, Van Broeckhoven C, De Jonghe P (2001) De novo mutations in the sodium-channel gene SCN1A cause severe myoclonic epilepsy of infancy. American journal of human genetics 68:1327-1332.

Claes LR, Deprez L, Suls A, Baets J, Smets K, Van Dyck T, Deconinck T, Jordanova A, De Jonghe P (2009) The SCN1A variant database: a novel research and diagnostic tool. Human mutation 30:E904-920.

Cloarec R et al. (2012) PRRT2 links infantile convulsions and paroxysmal dyskinesia with migraine. Neurology 79:2097-2103.

Contreras D, Curro Dossi R, Steriade M (1992) Bursting and tonic discharges in two classes of reticular thalamic neurons. Journal of neurophysiology 68:973-977.

Cooper DC, Chung S, Spruston N (2005) Output-mode transitions are controlled by prolonged inactivation of sodium channels in pyramidal neurons of subiculum. PLoS biology 3:e175.

Craner MJ, Damarjian TG, Liu S, Hains BC, Lo AC, Black JA, Newcombe J, Cuzner ML, Waxman SG (2005) Sodium channels contribute to microglia/macrophage activation and function in EAE and MS. Glia 49:220-229.

Crill WE (1996) Persistent sodium current in mammalian central neurons. Annual review of physiology 58:349-362.

Deisz RA, Fortin G, Zieglgansberger W (1991) Voltage dependence of excitatory postsynaptic potentials of rat neocortical neurons. Journal of neurophysiology 65:371-382.

Dhamija R, Wirrell E, Falcao G, Kirmani S, Wong-Kisiel LC (2013) Novel de novo SCN2A Mutation in a Child With Migrating Focal Seizures of Infancy. Pediatric neurology.

Dickie MM (1965) Jolting. Mouse News Lett 32:44.

Distler MG, Gorfinkle N, Papale LA, Wuenschell GE, Termini J, Escayg A, Winawer MR, Palmer AA (2013) Glyoxalase 1 and its substrate methylglyoxal are novel regulators of seizure susceptibility. Epilepsia 54:649-657.

Doherty D, Bamshad MJ (2012) Exome sequencing to find rare variants causing neurologic diseases. Neurology 79:396-397.

Dragatsis I, Zeitlin S (2000) CaMKIIalpha-Cre transgene expression and recombination patterns in the mouse brain. Genesis 26:133-135.

Duflocq A, Le Bras B, Bullier E, Couraud F, Davenne M (2008) Nav1.1 is predominantly expressed in nodes of Ranvier and axon initial segments. Molecular and cellular neurosciences 39:180-192.

Dutton SB, Makinson CD, Papale LA, Shankar A, Balakrishnan B, Nakazawa K, Escayg A (2012) Preferential inactivation of Scn1a in parvalbumin interneurons increases seizure susceptibility. Neurobiology of disease 49C:211-220.

Ebach K, Joos H, Doose H, Stephani U, Kurlemann G, Fiedler B, Hahn A, Hauser E, Hundt K, Holthausen H, Muller U, Neubauer BA (2005) SCN1A mutation analysis in myoclonic astatic epilepsy and severe idiopathic generalized epilepsy of infancy with generalized tonic-clonic seizures. Neuropediatrics 36:210-213.

Elo JM, Yadavalli SS, Euro L, Isohanni P, Gotz A, Carroll CJ, Valanne L, Alkuraya FS, Uusimaa J, Paetau A, Caruso EM, Pihko H, Ibba M, Tyynismaa H, Suomalainen A (2012) Mitochondrial phenylalanyl-tRNA synthetase mutations underlie fatal infantile Alpers encephalopathy. Human molecular genetics 21:4521-4529.

Enomoto A, Han JM, Hsiao CF, Chandler SH (2007) Sodium currents in mesencephalic trigeminal neurons from Nav1.6 null mice. Journal of neurophysiology 98:710-719.

Epi KC et al. (2013) De novo mutations in epileptic encephalopathies. Nature 501:217-221.

Escayg A, Goldin AL (2010) Sodium channel SCN1A and epilepsy: mutations and mechanisms. Epilepsia 51:1650-1658.

Escayg A, MacDonald BT, Meisler MH, Baulac S, Huberfeld G, An-Gourfinkel I, Brice A, LeGuern E, Moulard B, Chaigne D, Buresi C, Malafosse A (2000) Mutations of SCN1A, encoding a neuronal sodium channel, in two families with GEFS+2. Nature genetics 24:343-345.

Estacion M, Gasser A, Dib-Hajj SD, Waxman SG (2010) A sodium channel mutation linked to epilepsy increases ramp and persistent current of Nav1.3 and induces hyperexcitability in hippocampal neurons. Experimental neurology 224:362-368.

Feng L, Li AP, Wang MP, Sun DN, Wang YL, Long LL, Xiao B (2013) Plasticity at axon initial segment of hippocampal CA3 neurons in rat after status epilepticus induced by lithium-pilocarpine. Acta neurochirurgica.

Fujiwara T, Sugawara T, Mazaki-Miyazaki E, Takahashi Y, Fukushima K, Watanabe M, Hara K, Morikawa T, Yagi K, Yamakawa K, Inoue Y (2003) Mutations of sodium channel alpha subunit type 1 (SCN1A) in intractable childhood epilepsies with frequent generalized tonic-clonic seizures. Brain : a journal of neurology 126:531-546.

Genton P, Velizarova R, Dravet C (2011) Dravet syndrome: the long-term outcome. Epilepsia 52 Suppl 2:44-49.

George AL, Jr. (2005) Inherited disorders of voltage-gated sodium channels. The Journal of clinical investigation 115:1990-1999.

Goldin AL (1991) Expression of ion channels by injection of mRNA into Xenopus oocytes. Methods in cell biology 36:487-509.

Goldin AL (1999) Diversity of mammalian voltage-gated sodium channels. Annals of the New York Academy of Sciences 868:38-50.

Goldin AL (2001) Resurgence of sodium channel research. Annual review of physiology 63:871-894.

Goldin AL, Barchi RL, Caldwell JH, Hofmann F, Howe JR, Hunter JC, Kallen RG, Mandel G, Meisler MH, Netter YB, Noda M, Tamkun MM, Waxman SG, Wood JN, Catterall WA (2000) Nomenclature of voltage-gated sodium channels. Neuron 28:365-368.

Goldschen-Ohm MP, Capes DL, Oelstrom KM, Chanda B (2013) Multiple pore conformations driven by asynchronous movements of voltage sensors in a eukaryotic sodium channel. Nature communications 4:1350.

Gong B, Rhodes KJ, Bekele-Arcuri Z, Trimmer JS (1999) Type I and type II Na(+) channel alpha-subunit polypeptides exhibit distinct spatial and temporal patterning, and

association with auxiliary subunits in rat brain. The Journal of comparative neurology 412:342-352.

Gorski JA, Talley T, Qiu M, Puelles L, Rubenstein JL, Jones KR (2002) Cortical excitatory neurons and glia, but not GABAergic neurons, are produced in the Emx1-expressing lineage. The Journal of neuroscience : the official journal of the Society for Neuroscience 22:6309-6314.

Guerrini R, Dravet C, Genton P, Belmonte A, Kaminska A, Dulac O (1998) Lamotrigine and seizure aggravation in severe myoclonic epilepsy. Epilepsia 39:508-512.

Hamann M, Meisler MH, Richter A (2003) Motor disturbances in mice with deficiency of the sodium channel gene Scn8a show features of human dystonia. Experimental neurology 184:830-838.

Han S, Yu FH, Schwartz MD, Linton JD, Bosma MM, Hurley JB, Catterall WA, de la Iglesia HO (2012a) Na(V)1.1 channels are critical for intercellular communication in the suprachiasmatic nucleus and for normal circadian rhythms. Proceedings of the National Academy of Sciences of the United States of America 109:E368-377.

Han S, Tai C, Westenbroek RE, Yu FH, Cheah CS, Potter GB, Rubenstein JL, Scheuer T, de la Iglesia HO, Catterall WA (2012b) Autistic-like behaviour in Scn1a+/- mice and rescue by enhanced GABA-mediated neurotransmission. Nature 489:385-390.

Hargus NJ, Nigam A, Bertram EH, 3rd, Patel MK (2013) Evidence for a role of Nav1.6 in facilitating increases in neuronal hyperexcitability during epileptogenesis. Journal of neurophysiology 110:1144-1157.

Hargus NJ, Merrick EC, Nigam A, Kalmar CL, Baheti AR, Bertram EH, 3rd, Patel MK (2011) Temporal lobe epilepsy induces intrinsic alterations in Na channel gating in layer II medial entorhinal cortex neurons. Neurobiology of disease 41:361-376.

Harkin LA et al. (2007) The spectrum of SCN1A-related infantile epileptic encephalopathies. Brain : a journal of neurology 130:843-852.

Hawkins NA, Martin MS, Frankel WN, Kearney JA, Escayg A (2011) Neuronal voltage-gated ion channels are genetic modifiers of generalized epilepsy with febrile seizures plus. Neurobiology of disease 41:655-660.

Heldt SA, Stanek L, Chhatwal JP, Ressler KJ (2007) Hippocampus-specific deletion of BDNF in adult mice impairs spatial memory and extinction of aversive memories. Mol Psychiatry 12:656-670.

Herlenius E, Heron SE, Grinton BE, Keay D, Scheffer IE, Mulley JC, Berkovic SF (2007) SCN2A mutations and benign familial neonatal-infantile seizures: the phenotypic spectrum. Epilepsia 48:1138-1142.

Heron SE, Crossland KM, Andermann E, Phillips HA, Hall AJ, Bleasel A, Shevell M, Mercho S, Seni MH, Guiot MC, Mulley JC, Berkovic SF, Scheffer IE (2002) Sodium-channel defects in benign familial neonatal-infantile seizures. Lancet 360:851-852.

Heron SE, Smith KR, Bahlo M, Nobili L, Kahana E, Licchetta L, Oliver KL, Mazarib A, Afawi Z, Korczyn A, Plazzi G, Petrou S, Berkovic SF, Scheffer IE, Dibbens LM (2012) Missense mutations in the sodium-gated potassium channel gene KCNT1 cause severe autosomal dominant nocturnal frontal lobe epilepsy. Nature genetics 44:1188-1190.

Hille B (1971) The permeability of the sodium channel to organic cations in myelinated nerve. The Journal of general physiology 58:599-619.

Hille B (1972) The permeability of the sodium channel to metal cations in myelinated nerve. The Journal of general physiology 59:637-658.

Hille B (1975) Ionic selectivity, saturation, and block in sodium channels. A four-barrier model. The Journal of general physiology 66:535-560.

Hille B (2001) Ion Channels of Excitable Membranes, Third Edition. Sunderland, MA: Sinauer Associates, Inc.

Hodgkin AL, Huxley AF (1952a) The dual effect of membrane potential on sodium conductance in the giant axon of Loligo. The Journal of physiology 116:497-506.

Hodgkin AL, Huxley AF (1952b) The components of membrane conductance in the giant axon of Loligo. The Journal of physiology 116:473-496.

Hodgkin AL, Huxley AF (1952c) Currents carried by sodium and potassium ions through the membrane of the giant axon of Loligo. The Journal of physiology 116:449-472.

Hodgkin AL, Huxley AF (1952d) A quantitative description of membrane current and its application to conduction and excitation in nerve. The Journal of physiology 117:500-544.

Holland KD, Kearney JA, Glauser TA, Buck G, Keddache M, Blankston JR, Glaaser IW, Kass RS, Meisler MH (2008) Mutation of sodium channel SCN3A in a patient with cryptogenic pediatric partial epilepsy. Neuroscience letters 433:65-70.

Hsu D (2007) The dentate gyrus as a filter or gate: a look back and a look ahead. Prog Brain Res 163:601-613.

Hu W, Tian C, Li T, Yang M, Hou H, Shu Y (2009) Distinct contributions of Na(v)1.6 and Na(v)1.2 in action potential initiation and backpropagation. Nature neuroscience 12:996-1002.

Huguenard JR (1996) Low-threshold calcium currents in central nervous system neurons. Annual review of physiology 58:329-348.

Huguenard JR, Prince DA (1994) Intrathalamic rhythmicity studied in vitro: nominal T-current modulation causes robust antioscillatory effects. The Journal of neuroscience : the official journal of the Society for Neuroscience 14:5485-5502.

Isom LL, De Jongh KS, Catterall WA (1994) Auxiliary subunits of voltage-gated ion channels. Neuron 12:1183-1194.

Isom LL, Ragsdale DS, De Jongh KS, Westenbroek RE, Reber BF, Scheuer T, Catterall WA (1995) Structure and function of the beta 2 subunit of brain sodium channels, a transmembrane glycoprotein with a CAM motif. Cell 83:433-442.

Isom LL, De Jongh KS, Patton DE, Reber BF, Offord J, Charbonneau H, Walsh K, Goldin AL, Catterall WA (1992) Primary structure and functional expression of the beta 1 subunit of the rat brain sodium channel. Science 256:839-842.

Ito S, Ogiwara I, Yamada K, Miyamoto H, Hensch TK, Osawa M, Yamakawa K (2012) Mouse with Na(v)1.1 haploinsufficiency, a model for Dravet syndrome, exhibits lowered sociability and learning impairment. Neurobiology of disease 49C:29-40.

Jang MA, Woo HI, Kim JW, Lee J, Ki CS (2013) Identification of DCX gene mutation in lissencephaly spectrum with subcortical band heterotopia using whole exome sequencing. Pediatric neurology 48:411-414.

Jiang YH et al. (2013) Detection of Clinically Relevant Genetic Variants in Autism Spectrum Disorder by Whole-Genome Sequencing. American journal of human genetics.

Kazen-Gillespie KA, Ragsdale DS, D'Andrea MR, Mattei LN, Rogers KE, Isom LL (2000) Cloning, localization, and functional expression of sodium channel beta1A subunits. The Journal of biological chemistry 275:1079-1088.

Kearney JA, Plummer NW, Smith MR, Kapur J, Cummins TR, Waxman SG, Goldin AL, Meisler MH (2001) A gain-of-function mutation in the sodium channel gene Scn2a results in seizures and behavioral abnormalities. Neuroscience 102:307-317.

Kearney JA, Buchner DA, De Haan G, Adamska M, Levin SI, Furay AR, Albin RL, Jones JM, Montal M, Stevens MJ, Sprunger LK, Meisler MH (2002) Molecular and pathological

effects of a modifier gene on deficiency of the sodium channel Scn8a (Na(v)1.6). Human molecular genetics 11:2765-2775.

Kesner RP (1966) Subcortical mechanisms of audiogenic seizures. Experimental neurology 15:192-205.

Kim DY, Gersbacher MT, Inquimbert P, Kovacs DM (2011) Reduced sodium channel Na(v)1.1 levels in BACE1-null mice. The Journal of biological chemistry 286:8106-8116.

Kjeldsen MJ, Kyvik KO, Christensen K, Friis ML (2001) Genetic and environmental factors in epilepsy: a population-based study of 11900 Danish twin pairs. Epilepsy research 44:167-178.

Klein BD, Fu YH, Ptacek LJ, White HS (2004) c-Fos immunohistochemical mapping of the audiogenic seizure network and tonotopic neuronal hyperexcitability in the inferior colliculus of the Frings mouse. Epilepsy research 62:13-25.

Kohrman DC, Harris JB, Meisler MH (1996a) Mutation detection in the med and medJ alleles of the sodium channel Scn8a. Unusual splicing due to a minor class AT-AC intron. The Journal of biological chemistry 271:17576-17581.

Kohrman DC, Smith MR, Goldin AL, Harris J, Meisler MH (1996b) A missense mutation in the sodium channel Scn8a is responsible for cerebellar ataxia in the mouse mutant jolting. The Journal of neuroscience : the official journal of the Society for Neuroscience 16:5993-5999.

Korotzer AR, Cotman CW (1992) Voltage-gated currents expressed by rat microglia in culture. Glia 6:81-88.

Kress GJ, Dowling MJ, Eisenman LN, Mennerick S (2010) Axonal sodium channel distribution shapes the depolarized action potential threshold of dentate granule neurons. Hippocampus 20:558-571.

Kuo CC, Bean BP (1994) Na+ channels must deactivate to recover from inactivation. Neuron 12:819-829.

Kwon J, Pierson M (1997) Fos-immunoreactive responses in inferior colliculi of rats with experimental audiogenic seizure susceptibility. Epilepsy research 27:89-99.

Lacroix JJ, Campos FV, Frezza L, Bezanilla F (2013) Molecular bases for the asynchronous activation of sodium and potassium channels required for nerve impulse generation. Neuron 79:651-657.

Laedermann CJ, Syam N, Pertin M, Decosterd I, Abriel H (2013) beta1- and beta3- voltage-gated sodium channel subunits modulate cell surface expression and glycosylation of Nav1.7 in HEK293 cells. Frontiers in cellular neuroscience 7:137.

Lauxmann S, Boutry-Kryza N, Rivier C, Mueller S, Hedrich UB, Maljevic S, Szepetowski P, Lerche H, Lesca G (2013) An SCN2A mutation in a family with infantile seizures from Madagascar reveals an increased subthreshold Na(+) current. Epilepsia 54:e117-121.

Le Gal La Salle G, Naquet R (1990) Audiogenic seizures evoked in DBA/2 mice induce c-fos oncogene expression into subcortical auditory nuclei. Brain research 518:308-312.

Lee SH, Govindaiah G, Cox CL (2007) Heterogeneity of firing properties among rat thalamic reticular nucleus neurons. The Journal of physiology 582:195-208.

Lemke JR et al. (2012) Targeted next generation sequencing as a diagnostic tool in epileptic disorders. Epilepsia 53:1387-1398.

Levin SI, Meisler MH (2004) Floxed allele for conditional inactivation of the voltage-gated sodium channel Scn8a (NaV1.6). Genesis 39:234-239.

Li BM, Liu XR, Yi YH, Deng YH, Su T, Zou X, Liao WP (2011) Autism in Dravet syndrome: prevalence, features, and relationship to the clinical characteristics of epilepsy and mental retardation. Epilepsy & behavior : E&B 21:291-295.

Liao Y, Anttonen AK, Liukkonen E, Gaily E, Maljevic S, Schubert S, Bellan-Koch A, Petrou S, Ahonen VE, Lerche H, Lehesjoki AE (2010a) SCN2A mutation associated with neonatal epilepsy, late-onset episodic ataxia, myoclonus, and pain. Neurology 75:1454-1458.

Liao Y, Deprez L, Maljevic S, Pitsch J, Claes L, Hristova D, Jordanova A, Ala-Mello S, Bellan-Koch A, Blazevic D, Schubert S, Thomas EA, Petrou S, Becker AJ, De Jonghe P, Lerche H (2010b) Molecular correlates of age-dependent seizures in an inherited neonatal-infantile epilepsy. Brain : a journal of neurology 133:1403-1414.

Liautard C, Scalmani P, Carriero G, de Curtis M, Franceschetti S, Mantegazza M (2013) Hippocampal hyperexcitability and specific epileptiform activity in a mouse model of Dravet syndrome. Epilepsia 54:1251-1261.

Lindgren AM, Hoyos T, Talkowski ME, Hanscom C, Blumenthal I, Chiang C, Ernst C, Pereira S, Ordulu Z, Clericuzio C, Drautz JM, Rosenfeld JA, Shaffer LG, Velsher L, Pynn T, Vermeesch J, Harris DJ, Gusella JF, Liao EC, Morton CC (2013) Haploinsufficiency of KDM6A is associated with severe psychomotor retardation, global growth restriction, seizures and cleft palate. Human genetics 132:537-552.

Lipowsky R, Gillessen T, Alzheimer C (1996) Dendritic Na+ channels amplify EPSPs in hippocampal CA1 pyramidal cells. Journal of neurophysiology 76:2181-2191.

Liu Y, Lopez-Santiago LF, Yuan Y, Jones JM, Zhang H, O'Malley HA, Patino GA, O'Brien JE, Rusconi R, Gupta A, Thompson RC, Natowicz MR, Meisler MH, Isom LL, Parent JM (2013) Dravet syndrome patient-derived neurons suggest a novel epilepsy mechanism. Annals of neurology 74:128-139.

Lorincz A, Nusser Z (2008) Cell-type-dependent molecular composition of the axon initial segment. The Journal of neuroscience : the official journal of the Society for Neuroscience 28:14329-14340.

Lorincz A, Nusser Z (2010) Molecular identity of dendritic voltage-gated sodium channels. Science 328:906-909.

Loscher W (2002) Current status and future directions in the pharmacotherapy of epilepsy. Trends in pharmacological sciences 23:113-118.

Lossin C (2009) A catalog of SCN1A variants. Brain & development 31:114-130.

Mackenzie FE, Parker A, Parkinson NJ, Oliver PL, Brooker D, Underhill P, Lukashkina VA, Lukashkin AN, Holmes C, Brown SD (2009) Analysis of the mouse mutant Cloth-ears shows a role for the voltage-gated sodium channel Scn8a in peripheral neural hearing loss. Genes, brain, and behavior 8:699-713.

Mahoney K, Moore SJ, Buckley D, Alam M, Parfrey P, Penney S, Merner N, Hodgkinson K, Young TL (2009) Variable neurologic phenotype in a GEFS+ family with a novel mutation in SCN1A. Seizure : the journal of the British Epilepsy Association 18:492-497.

Manolio TA et al. (2009) Finding the missing heritability of complex diseases. Nature 461:747-753.

Mantegazza M, Catterall WA (2012) Voltage-Gated Na+ Channels: Structure, Function, and Pathophysiology. In: Jasper's Basic Mechanisms of the Epilepsies, 4th Edition (Noebels JL, Avoli M, Rogawski MA, Olsen RW, Delgado-Escueta AV, eds). Bethesda (MD).

Marini C, Mei D, Temudo T, Ferrari AR, Buti D, Dravet C, Dias AI, Moreira A, Calado E, Seri S, Neville B, Narbona J, Reid E, Michelucci R, Sicca F, Cross HJ, Guerrini R (2007) Idiopathic epilepsies with seizures precipitated by fever and SCN1A abnormalities. Epilepsia 48:1678-1685.

Marti-Masso JF, Bergareche A, Makarov V, Ruiz-Martinez J, Gorostidi A, de Munain AL, Poza JJ, Striano P, Buxbaum JD, Paisan-Ruiz C (2013) The ACMSD gene, involved in tryptophan metabolism, is mutated in a family with cortical myoclonus, epilepsy, and parkinsonism. Journal of molecular medicine 91:1399-1406.

Martin MS, Tang B, Papale LA, Yu FH, Catterall WA, Escayg A (2007) The voltage-gated sodium channel Scn8a is a genetic modifier of severe myoclonic epilepsy of infancy. Human molecular genetics 16:2892-2899.

Martin MS, Dutt K, Papale LA, Dube CM, Dutton SB, de Haan G, Shankar A, Tufik S, Meisler MH, Baram TZ, Goldin AL, Escayg A (2010) Altered function of the SCN1A voltage-gated sodium channel leads to gamma-aminobutyric acid-ergic (GABAergic) interneuron abnormalities. The Journal of biological chemistry 285:9823-9834.

Maurice N, Tkatch T, Meisler M, Sprunger LK, Surmeier DJ (2001) D1/D5 dopamine receptor activation differentially modulates rapidly inactivating and persistent sodium currents in prefrontal cortex pyramidal neurons. The Journal of neuroscience : the official journal of the Society for Neuroscience 21:2268-2277.

McDonell LM et al. (2013) Mutations in STAMBP, encoding a deubiquitinating enzyme, cause microcephaly-capillary malformation syndrome. Nature genetics 45:556-562.

McKinney BC, Chow CY, Meisler MH, Murphy GG (2008) Exaggerated emotional behavior in mice heterozygous null for the sodium channel Scn8a (Nav1.6). Genes, brain, and behavior 7:629-638.

Miyoshi H, Blomer U, Takahashi M, Gage FH, Verma IM (1998) Development of a self-inactivating lentivirus vector. J Virol 72:8150-8157.

Monory K et al. (2006) The endocannabinoid system controls key epileptogenic circuits in the hippocampus. Neuron 51:455-466.

Morgan K, Stevens EB, Shah B, Cox PJ, Dixon AK, Lee K, Pinnock RD, Hughes J, Richardson PJ, Mizuguchi K, Jackson AP (2000) beta 3: an additional auxiliary subunit of the voltage-sensitive sodium channel that modulates channel gating with distinct kinetics. Proceedings of the National Academy of Sciences of the United States of America 97:2308-2313.

Mulley JC, Hodgson B, McMahon JM, Iona X, Bellows S, Mullen SA, Farrell K, Mackay M, Sadleir L, Bleasel A, Gill D, Webster R, Wirrell EC, Harbord M, Sisodiya S, Andermann E, Kivity S, Berkovic SF, Scheffer IE, Dibbens LM (2013) Role of the sodium channel SCN9A in genetic epilepsy with febrile seizures plus and Dravet syndrome. Epilepsia 54:e122-126.

Murdock DR, Clark GD, Bainbridge MN, Newsham I, Wu YQ, Muzny DM, Cheung SW, Gibbs RA, Ramocki MB (2011) Whole-exome sequencing identifies compound heterozygous mutations in WDR62 in siblings with recurrent polymicrogyria. American journal of medical genetics Part A 155A:2071-2077.

Nakamura K et al. (2013) De Novo mutations in GNAO1, encoding a Galphao subunit of heterotrimeric G proteins, cause epileptic encephalopathy. American journal of human genetics 93:496-505.

Need AC, Shashi V, Hitomi Y, Schoch K, Shianna KV, McDonald MT, Meisler MH, Goldstein DB (2012) Clinical application of exome sequencing in undiagnosed genetic conditions. Journal of medical genetics 49:353-361.

Noda M, Ikeda T, Kayano T, Suzuki H, Takeshima H, Kurasaki M, Takahashi H, Numa S (1986) Existence of distinct sodium channel messenger RNAs in rat brain. Nature 320:188-192.

Noebels JL (2003) Exploring new gene discoveries in idiopathic generalized epilepsy. Epilepsia 44 Suppl 2:16-21.

Norenberg W, Illes P, Gebicke-Haerter PJ (1994) Sodium channel in isolated human brain macrophages (microglia). Glia 10:165-172.

O'Brien JE, Meisler MH (2013) Sodium channel SCN8A (Nav1.6): properties and de novo mutations in epileptic encephalopathy and intellectual disability. Frontiers in genetics 4:213.

Ogiwara I, Nakayama T, Yamagata T, Ohtani H, Mazaki E, Tsuchiya S, Inoue Y, Yamakawa K (2012) A homozygous mutation of voltage-gated sodium channel beta(I) gene SCN1B in a patient with Dravet syndrome. Epilepsia 53:e200-203.

Ogiwara I, Iwasato T, Miyamoto H, Iwata R, Yamagata T, Mazaki E, Yanagawa Y, Tamamaki N, Hensch TK, Itohara S, Yamakawa K (2013) Nav1.1 haploinsufficiency in excitatory neurons ameliorates seizure-associated sudden death in a mouse model of Dravet syndrome. Human molecular genetics.

Ogiwara I, Miyamoto H, Morita N, Atapour N, Mazaki E, Inoue I, Takeuchi T, Itohara S, Yanagawa Y, Obata K, Furuichi T, Hensch TK, Yamakawa K (2007) Nav1.1 localizes to axons of parvalbumin-positive inhibitory interneurons: a circuit basis for epileptic seizures in mice carrying an Scn1a gene mutation. The Journal of neuroscience : the official journal of the Society for Neuroscience 27:5903-5914.

Ogiwara I, Ito K, Sawaishi Y, Osaka H, Mazaki E, Inoue I, Montal M, Hashikawa T, Shike T, Fujiwara T, Inoue Y, Kaneda M, Yamakawa K (2009) De novo mutations of voltage-gated sodium channel alphaII gene SCN2A in intractable epilepsies. Neurology 73:1046-1053.

Osorio N, Cathala L, Meisler MH, Crest M, Magistretti J, Delmas P (2010) Persistent Nav1.6 current at axon initial segments tunes spike timing of cerebellar granule cells. The Journal of physiology 588:651-670.

Panayiotopoulos CP (2001) Treatment of typical absence seizures and related epileptic syndromes. Paediatric drugs 3:379-403.

Papale LA, Paul KN, Sawyer NT, Manns JR, Tufik S, Escayg A (2010) Dysfunction of the Scn8a voltage-gated sodium channel alters sleep architecture, reduces diurnal corticosterone levels, and enhances spatial memory. The Journal of biological chemistry 285:16553-16561.

Papale LA, Makinson CD, Christopher Ehlen J, Tufik S, Decker MJ, Paul KN, Escayg A (2013) Altered sleep regulation in a mouse model of SCN1A-derived genetic epilepsy with febrile seizures plus (GEFS+). Epilepsia 54:625-634.

Papale LA, Beyer B, Jones JM, Sharkey LM, Tufik S, Epstein M, Letts VA, Meisler MH, Frankel WN, Escayg A (2009) Heterozygous mutations of the voltage-gated sodium channel SCN8A are associated with spike-wave discharges and absence epilepsy in mice. Human molecular genetics 18:1633-1641.

Patino GA, Brackenbury WJ, Bao Y, Lopez-Santiago LF, O'Malley HA, Chen C, Calhoun JD, Lafreniere RG, Cossette P, Rouleau GA, Isom LL (2011) Voltage-gated Na+ channel beta1B: a secreted cell adhesion molecule involved in human epilepsy. The Journal of neuroscience : the official journal of the Society for Neuroscience 31:14577-14591.

Patino GA, Claes LR, Lopez-Santiago LF, Slat EA, Dondeti RS, Chen C, O'Malley HA, Gray CB, Miyazaki H, Nukina N, Oyama F, De Jonghe P, Isom LL (2009) A functional null mutation of SCN1B in a patient with Dravet syndrome. The Journal of neuroscience : the official journal of the Society for Neuroscience 29:10764-10778.

Patton DE, Goldin AL (1991) A voltage-dependent gating transition induces use-dependent block by tetrodotoxin of rat IIA sodium channels expressed in Xenopus oocytes. Neuron 7:637-647.

Payandeh J, Scheuer T, Zheng N, Catterall WA (2011) The crystal structure of a voltage-gated sodium channel. Nature 475:353-358.

Paz JT, Bryant AS, Peng K, Fenno L, Yizhar O, Frankel WN, Deisseroth K, Huguenard JR (2011) A new mode of corticothalamic transmission revealed in the Gria4(-/-) model of absence epilepsy. Nature neuroscience 14:1167-1173.

Pellow S, Chopin P, File SE, Briley M (1985) Validation of open:closed arm entries in an elevated plus-maze as a measure of anxiety in the rat. Journal of neuroscience methods 14:149-167.

Pennartz CM, Bierlaagh MA, Geurtsen AM (1997) Cellular mechanisms underlying spontaneous firing in rat suprachiasmatic nucleus: involvement of a slowly inactivating component of sodium current. Journal of neurophysiology 78:1811-1825.

Pfeifer A, Brandon EP, Kootstra N, Gage FH, Verma IM (2001) Delivery of the Cre recombinase by a self-deleting lentiviral vector: efficient gene targeting in vivo. Proc Natl Acad Sci U S A 98:11450-11455.

Plummer NW, McBurney MW, Meisler MH (1997) Alternative splicing of the sodium channel SCN8A predicts a truncated two-domain protein in fetal brain and non-neuronal cells. The Journal of biological chemistry 272:24008-24015.

Posner E (2008) Absence seizures in children. Clinical evidence 2008.

Poulton C, Oegema R, Heijsman D, Hoogeboom J, Schot R, Stroink H, Willemsen MA, Verheijen FW, van de Spek P, Kremer A, Mancini GM (2013) Progressive cerebellar atrophy and polyneuropathy: expanding the spectrum of PNKP mutations. Neurogenetics 14:43-51.

Qin N, D'Andrea MR, Lubin ML, Shafaee N, Codd EE, Correa AM (2003) Molecular cloning and functional expression of the human sodium channel beta1B subunit, a novel splicing variant of the beta1 subunit. European journal of biochemistry / FEBS 270:4762-4770.

Raman IM, Sprunger LK, Meisler MH, Bean BP (1997) Altered subthreshold sodium currents and disrupted firing patterns in Purkinje neurons of Scn8a mutant mice. Neuron 19:881-891.

Rauch A et al. (2012) Range of genetic mutations associated with severe non-syndromic sporadic intellectual disability: an exome sequencing study. Lancet 380:1674-1682.

Ritchie JM (1987) Voltage-gated cation and anion channels in mammalian Schwann cells and astrocytes. Journal de physiologie 82:248-257.

Rogawski MA, Loscher W (2004) The neurobiology of antiepileptic drugs. Nature reviews Neuroscience 5:553-564.

Rosker C, Lohberger B, Hofer D, Steinecker B, Quasthoff S, Schreibmayer W (2007) The TTX metabolite 4,9-anhydro-TTX is a highly specific blocker of the Na(v1.6) voltage-dependent sodium channel. American journal of physiology Cell physiology 293:C783-789.

Royeck M, Horstmann MT, Remy S, Reitze M, Yaari Y, Beck H (2008) Role of axonal NaV1.6 sodium channels in action potential initiation of CA1 pyramidal neurons. Journal of neurophysiology 100:2361-2380.

Rush AM, Dib-Hajj SD, Waxman SG (2005) Electrophysiological properties of two axonal sodium channels, Nav1.2 and Nav1.6, expressed in mouse spinal sensory neurones. The Journal of physiology 564:803-815.

Samoriski GM, Piekut DT, Applegate CD (1998) Regional analysis of the spatial patterns of Fos induction in brain following flurothyl kindling. Neuroscience 84:1209-1222.

Sawyer NT, Papale LA, Eliason J, Neigh GN, Escayg A (2013) Scn8a voltage-gated sodium channel mutation alters seizure and anxiety responses to acute stress. Psychoneuroendocrinology.

Schauf CL (1987) Zonisamide enhances slow sodium inactivation in Myxicola. Brain research 413:185-188.

Scheffer IE, Berkovic SF (1997) Generalized epilepsy with febrile seizures plus. A genetic disorder with heterogeneous clinical phenotypes. Brain : a journal of neurology 120 (Pt 3):479-490.

Scheffer IE, Harkin LA, Grinton BE, Dibbens LM, Turner SJ, Zielinski MA, Xu R, Jackson G, Adams J, Connellan M, Petrou S, Wellard RM, Briellmann RS, Wallace RH, Mulley JC, Berkovic SF (2007) Temporal lobe epilepsy and GEFS+ phenotypes associated with SCN1B mutations. Brain : a journal of neurology 130:100-109.

Schmidtmayer J, Jacobsen C, Miksch G, Sievers J (1994) Blood monocytes and spleen macrophages differentiate into microglia-like cells on monolayers of astrocytes: membrane currents. Glia 12:259-267.

Schmutz M, Brugger F, Gentsch C, McLean MJ, Olpe HR (1994) Oxcarbazepine: preclinical anticonvulsant profile and putative mechanisms of action. Epilepsia 35 Suppl 5:S47-50.

Schwindt PC, Crill WE (1995) Amplification of synaptic current by persistent sodium conductance in apical dendrite of neocortical neurons. Journal of neurophysiology 74:2220-2224.

Shi X, Yasumoto S, Nakagawa E, Fukasawa T, Uchiya S, Hirose S (2009) Missense mutation of the sodium channel gene SCN2A causes Dravet syndrome. Brain & development 31:758-762.

Singh NA, Pappas C, Dahle EJ, Claes LR, Pruess TH, De Jonghe P, Thompson J, Dixon M, Gurnett C, Peiffer A, White HS, Filloux F, Leppert MF (2009) A role of SCN9A in human epilepsies, as a cause of febrile seizures and as a potential modifier of Dravet syndrome. PLoS genetics 5:e1000649.

Siqueira SR, Alves B, Malpartida HM, Teixeira MJ, Siqueira JT (2009) Abnormal expression of voltage-gated sodium channels Nav1.7, Nav1.3 and Nav1.8 in trigeminal neuralgia. Neuroscience 164:573-577.

Smith MR, Smith RD, Plummer NW, Meisler MH, Goldin AL (1998) Functional analysis of the mouse Scn8a sodium channel. The Journal of neuroscience : the official journal of the Society for Neuroscience 18:6093-6102.

Snyder-Keller AM, Pierson MG (1992) Audiogenic seizures induce c-fos in a model of developmental epilepsy. Neuroscience letters 135:108-112.

Sprunger LK, Escayg A, Tallaksen-Greene S, Albin RL, Meisler MH (1999) Dystonia associated with mutation of the neuronal sodium channel Scn8a and identification of the modifier locus Scnm1 on mouse chromosome 3. Human molecular genetics 8:471-479.

Steinlein OK (2004) Genes and mutations in human idiopathic epilepsy. Brain & development 26:213-218.

Stuart G, Sakmann B (1995) Amplification of EPSPs by axosomatic sodium channels in neocortical pyramidal neurons. Neuron 15:1065-1076.

Sugawara T, Tsurubuchi Y, Agarwala KL, Ito M, Fukuma G, Mazaki-Miyazaki E, Nagafuji H, Noda M, Imoto K, Wada K, Mitsudome A, Kaneko S, Montal M, Nagata K, Hirose S, Yamakawa K (2001) A missense mutation of the Na+ channel alpha II subunit gene Na(v)1.2 in a patient with febrile and afebrile seizures causes channel dysfunction. Proceedings of the National Academy of Sciences of the United States of America 98:6384-6389.

Sun W, Wagnon JL, Mahaffey CL, Briese M, Ule J, Frankel WN (2013) Aberrant sodium channel activity in the complex seizure disorder of Celf4 mutant mice. The Journal of physiology 591:241-255.

Sundaram SK, Chugani HT, Tiwari VN, Huq AH (2013) SCN2A mutation is associated with infantile spasms and bitemporal glucose hypometabolism. Pediatric neurology 49:46-49.

Taddese A, Bean BP (2002) Subthreshold sodium current from rapidly inactivating sodium channels drives spontaneous firing of tuberomammillary neurons. Neuron 33:587-600.

Taglialatela M, Ongini E, Brown AM, Di Renzo G, Annunziato L (1996) Felbamate inhibits cloned voltage-dependent Na+ channels from human and rat brain. European journal of pharmacology 316:373-377.

Talkowski ME et al. (2011) Assessment of 2q23.1 microdeletion syndrome implicates MBD5 as a single causal locus of intellectual disability, epilepsy, and autism spectrum disorder. American journal of human genetics 89:551-563.

Tamkun MM, Catterall WA (1981) Reconstitution of the voltage-sensitive sodium channel of rat brain from solubilized components. The Journal of biological chemistry 256:11457-11463.

Tang B, Dutt K, Papale L, Rusconi R, Shankar A, Hunter J, Tufik S, Yu FH, Catterall WA, Mantegazza M, Goldin AL, Escayg A (2009) A BAC transgenic mouse model reveals neuron subtype-specific effects of a Generalized Epilepsy with Febrile Seizures Plus (GEFS+) mutation. Neurobiology of disease 35:91-102.

Taverna S, Mantegazza M, Franceschetti S, Avanzini G (1998) Valproate selectively reduces the persistent fraction of Na+ current in neocortical neurons. Epilepsy research 32:304-308.

Taverna S, Sancini G, Mantegazza M, Franceschetti S, Avanzini G (1999) Inhibition of transient and persistent Na+ current fractions by the new anticonvulsant topiramate. The Journal of pharmacology and experimental therapeutics 288:960-968.

Touma M, Joshi M, Connolly MC, Grant PE, Hansen AR, Khwaja O, Berry GT, Kinney HC, Poduri A, Agrawal PB (2013) Whole genome sequencing identifies SCN2A mutation in monozygotic twins with Ohtahara syndrome and unique neuropathologic findings. Epilepsia 54:e81-85.

Trudeau MM, Dalton JC, Day JW, Ranum LP, Meisler MH (2006) Heterozygosity for a protein truncation mutation of sodium channel SCN8A in a patient with cerebellar atrophy, ataxia, and mental retardation. Journal of medical genetics 43:527-530.

Uebachs M, Albus C, Opitz T, Isom L, Niespodziany I, Wolff C, Beck H (2012) Loss of beta1 accessory Na+ channel subunits causes failure of carbamazepine, but not of lacosamide,

in blocking high-frequency firing via differential effects on persistent Na+ currents. Epilepsia 53:1959-1967.

Van den Berg RJ, Kok P, Voskuyl RA (1993) Valproate and sodium currents in cultured hippocampal neurons. Experimental brain research Experimentelle Hirnforschung Experimentation cerebrale 93:279-287.

Van Wart A, Trimmer JS, Matthews G (2007) Polarized distribution of ion channels within microdomains of the axon initial segment. The Journal of comparative neurology 500:339-352.

Vanoye CG, Gurnett CA, Holland KD, George AL, Jr., Kearney JA (2013) Novel SCN3A Variants Associated with Focal Epilepsy in Children. Neurobiology of disease.

Veeramah KR, O'Brien JE, Meisler MH, Cheng X, Dib-Hajj SD, Waxman SG, Talwar D, Girirajan S, Eichler EE, Restifo LL, Erickson RP, Hammer MF (2012) De novo pathogenic SCN8A mutation identified by whole-genome sequencing of a family quartet affected by infantile epileptic encephalopathy and SUDEP. American journal of human genetics 90:502-510.

Veeramah KR, Johnstone L, Karafet TM, Wolf D, Sprissler R, Salogiannis J, Barth-Maron A, Greenberg ME, Stuhlmann T, Weinert S, Jentsch TJ, Pazzi M, Restifo LL, Talwar D, Erickson RP, Hammer MF (2013) Exome sequencing reveals new causal mutations in children with epileptic encephalopathies. Epilepsia 54:1270-1281.

Vega-Saenz de Miera EC, Rudy B, Sugimori M, Llinas R (1997) Molecular characterization of the sodium channel subunits expressed in mammalian cerebellar Purkinje cells. Proceedings of the National Academy of Sciences of the United States of America 94:7059-7064.

von Krosigk M, Bal T, McCormick DA (1993) Cellular mechanisms of a synchronized oscillation in the thalamus. Science 261:361-364.

von Krosigk M, Monckton JE, Reiner PB, McCormick DA (1999) Dynamic properties of corticothalamic excitatory postsynaptic potentials and thalamic reticular inhibitory postsynaptic potentials in thalamocortical neurons of the guinea-pig dorsal lateral geniculate nucleus. Neuroscience 91:7-20.

Vrielynck P (2013) Current and emerging treatments for absence seizures in young patients. Neuropsychiatric disease and treatment 9:963-975.

Wagnon JL, Mahaffey CL, Sun W, Yang Y, Chao HT, Frankel WN (2011) Etiology of a genetically complex seizure disorder in Celf4 mutant mice. Genes, brain, and behavior 10:765-777.

Wagnon JL, Briese M, Sun W, Mahaffey CL, Curk T, Rot G, Ule J, Frankel WN (2012) CELF4 regulates translation and local abundance of a vast set of mRNAs, including genes associated with regulation of synaptic function. PLoS genetics 8:e1003067.

Wallace RH, Wang DW, Singh R, Scheffer IE, George AL, Jr., Phillips HA, Saar K, Reis A, Johnson EW, Sutherland GR, Berkovic SF, Mulley JC (1998) Febrile seizures and generalized epilepsy associated with a mutation in the Na+-channel beta1 subunit gene SCN1B. Nature genetics 19:366-370.

Wang Y, Zhang J, Li X, Ji J, Yang F, Wan C, Feng G, Wan P, He L, He G (2008) SCN8A as a novel candidate gene associated with bipolar disorder in the Han Chinese population. Progress in neuro-psychopharmacology & biological psychiatry 32:1902-1904.

Wang Y, Zhang J, Liu B, Shao L, Wei Z, Li X, Ji J, Yang F, Wang T, Liu J, Wan C, Li B, Xu Y, Feng G, He L, He G (2010) Genetic polymorphisms in the SCN8A gene are associated with suicidal behavior in psychiatric disorders in the Chinese population. The world journal of biological psychiatry : the official journal of the World Federation of Societies of Biological Psychiatry 11:956-963.

Warren RA, Agmon A, Jones EG (1994) Oscillatory synaptic interactions between ventroposterior and reticular neurons in mouse thalamus in vitro. Journal of neurophysiology 72:1993-2003.

Wasserman D, Geijer T, Rozanov V, Wasserman J (2005) Suicide attempt and basic mechanisms in neural conduction: relationships to the SCN8A and VAMP4 genes. American journal of medical genetics Part B, Neuropsychiatric genetics : the official publication of the International Society of Psychiatric Genetics 133B:116-119.

Waxman SG, Kocsis JD, Black JA (1994) Type III sodium channel mRNA is expressed in embryonic but not adult spinal sensory neurons, and is reexpressed following axotomy. Journal of neurophysiology 72:466-470.

Westenbroek RE, Merrick DK, Catterall WA (1989) Differential subcellular localization of the RI and RII Na+ channel subtypes in central neurons. Neuron 3:695-704.

Whitaker WR, Faull RL, Waldvogel HJ, Plumpton CJ, Emson PC, Clare JJ (2001) Comparative distribution of voltage-gated sodium channel proteins in human brain. Brain research Molecular brain research 88:37-53.

Willott JF, Lu SM (1980) Midbrain pathways of audiogenic seizures in DBA/2 mice. Experimental neurology 70:288-299.

Woodruff-Pak DS, Green JT, Levin SI, Meisler MH (2006) Inactivation of sodium channel Scn8A (Na-sub(v)1.6) in Purkinje neurons impairs learning in Morris water maze and delay but not trace eyeblink classical conditioning. Behavioral neuroscience 120:229-240.

Xie X, Dale TJ, John VH, Cater HL, Peakman TC, Clare JJ (2001) Electrophysiological and pharmacological properties of the human brain type IIA Na+ channel expressed in a stable mammalian cell line. Pflugers Archiv : European journal of physiology 441:425-433.

Yang S, Xiao Y, Kang D, Liu J, Li Y, Undheim EA, Klint JK, Rong M, Lai R, King GF (2013) Discovery of a selective NaV1.7 inhibitor from centipede venom with analgesic efficacy exceeding morphine in rodent pain models. Proceedings of the National Academy of Sciences of the United States of America 110:17534-17539.

Yu EJ, Ko SH, Lenkowski PW, Pance A, Patel MK, Jackson AP (2005) Distinct domains of the sodium channel beta3-subunit modulate channel-gating kinetics and subcellular location. The Biochemical journal 392:519-526.

Yu FH, Catterall WA (2004) The VGL-chanome: a protein superfamily specialized for electrical signaling and ionic homeostasis. Science's STKE : signal transduction knowledge environment 2004:re15.

Yu FH, Mantegazza M, Westenbroek RE, Robbins CA, Kalume F, Burton KA, Spain WJ, McKnight GS, Scheuer T, Catterall WA (2006) Reduced sodium current in GABAergic interneurons in a mouse model of severe myoclonic epilepsy in infancy. Nature neuroscience 9:1142-1149.

Yu FH, Westenbroek RE, Silos-Santiago I, McCormick KA, Lawson D, Ge P, Ferriera H, Lilly J, DiStefano PS, Catterall WA, Scheuer T, Curtis R (2003) Sodium channel beta4, a new disulfide-linked auxiliary subunit with similarity to beta2. The Journal of neuroscience : the official journal of the Society for Neuroscience 23:7577-7585.

Zheng QY, Johnson KR, Erway LC (1999) Assessment of hearing in 80 inbred strains of mice by ABR threshold analyses. Hearing research 130:94-107.

Zhou W, Goldin AL (2004) Use-dependent potentiation of the Nav1.6 sodium channel. Biophysical journal 87:3862-3872.

I was born not knowing

and have only had a little time to change that here and there.

- Richard Feynman